Fyzikální vlastnosti materiálů

FX001

1. Vazba v pevné látce, elastické a tepelné vlastnosti materiálů
2. Elektrické vlastnosti materiálů
3. Optické vlastnosti materiálů
4. Magnetické vlastnosti materiálů
5. Supravodiče a grafen

Fyzikální vlastnosti materiálů

3. Optické vlastnosti materiálů

a) Optická odezva materiálů – Maxwellovy rovnice, Laplaceova transformace, materiálové vztahy a odezvové funkce, komplexní vodivost a dielektrická funkce, index lomu.

b) Rovinná vlna v materiálu – komplexní vlnový vektor, Poyntingův vektor, intenzita, absorbovaná energie.

c) Elektromagnetická vlna v materiálu a na rozhraní – okrajové podmínky na rozhraní, přenosové matice, efektivní indexy lomu pro šikmý dopad.

d) Kramersovy-Kronigovy relace – odezvové funkce v komplexní rovině, kuzalita odezvy, Kramersovy-Kronigovy relace pro odezvové funkce a reflektivitu.

e) Absorpce mřížky – Lorentzův model pro polární krystaly, spektrální závislosti, závislost na hmotnostech atomů a tuhosti vazeb, nepolární krystaly – vícefononová absorpce.

f) Odezva volných nositelů náboje – Drudeův model, plazmová frekvence, spektrální závislosti, elementární kovy.

g) Optická odezva vázaných elektronů – mezipásové přechody, sdružená hustota stavů, nízkorozměrné heterostruktury.

h) Propustná oblast – oblast mezi kmity mříže a elektronovou absorpcí, optická skla, tavený křemen, diamant, safír, materiály pro optická vlákna

i) Odezva v rtg oblasti – index lomu, absorpční hrany

Optické obory frekvencí

obor	f (Hz)	λ (μm)	1/λ (cm^{-1})	ħω (eV)
Rádiové mikrovlny	3×10^{11}	1000	10	0.0012
FIR	1.5×10^{13}	20	500	0.062
MIR	1.2×10^{14}	2.5	4000	0.5
NIR	3.7×10^{14}	0.8	12500	1.55
VIS	7.5×10^{14}	0.4	25000	3.1
UV	1.7×10^{15}	0.18	55000	6.8
VUV	3×10^{16}	0.01	10^{6}	125
rtg				

Odezvové funkce

$$\sigma(\omega) = -\mathrm{i}\omega\epsilon_0(\epsilon(\omega) - 1)$$

Vztah mezi vodivostí a dielektrickou funkcí

$$\epsilon(\omega) = 1 + \mathrm{i}\frac{\sigma(\omega)}{\omega\epsilon_0}.$$

$$(N + \mathrm{i}K)^2 = \epsilon_1 + \mathrm{i}\epsilon_2,$$

$$\epsilon_1 = N^2 - K^2, \quad \epsilon_2 = 2NK.$$

Vztah mezi dielektrickou funkcí a komplexním indexem lomu

$$N = \sqrt{\frac{\sqrt{\epsilon_1^2 + \epsilon_2^2} + \epsilon_1}{2}}, \quad K = \sqrt{\frac{\sqrt{\epsilon_1^2 + \epsilon_2^2} - \epsilon_1}{2}}$$

Odezvové funkce

Kramersovy-Kronigovy relace

$$\chi_{\mathrm{r}}(\omega_0) = \frac{2}{\pi}\mathrm{P}\int_0^\infty \frac{\omega\chi_{\mathrm{i}}(\omega)}{\omega^2-\omega_0^2}\,\mathrm{d}\omega$$

and

$$\chi_{\mathrm{i}}(\omega_0) = -\frac{2\omega_0}{\pi}\mathrm{P}\int_0^\infty \frac{\chi_{\mathrm{r}}(\omega)}{\omega^2-\omega_0^2}\,\mathrm{d}\omega$$

$$\ln r_{\mathrm{c}}(\omega) = \ln\sqrt{R(\omega)} + \mathrm{i}\phi(\omega)$$

$$\phi(\omega_0) = -\frac{2\omega_0}{\pi}\mathrm{P}\int_0^\infty \frac{\ln\sqrt{R(\omega)} - \ln\sqrt{R(\omega_0)}}{\omega^2-\omega_0^2}\,\mathrm{d}\omega$$

Formalismus přenosových matic

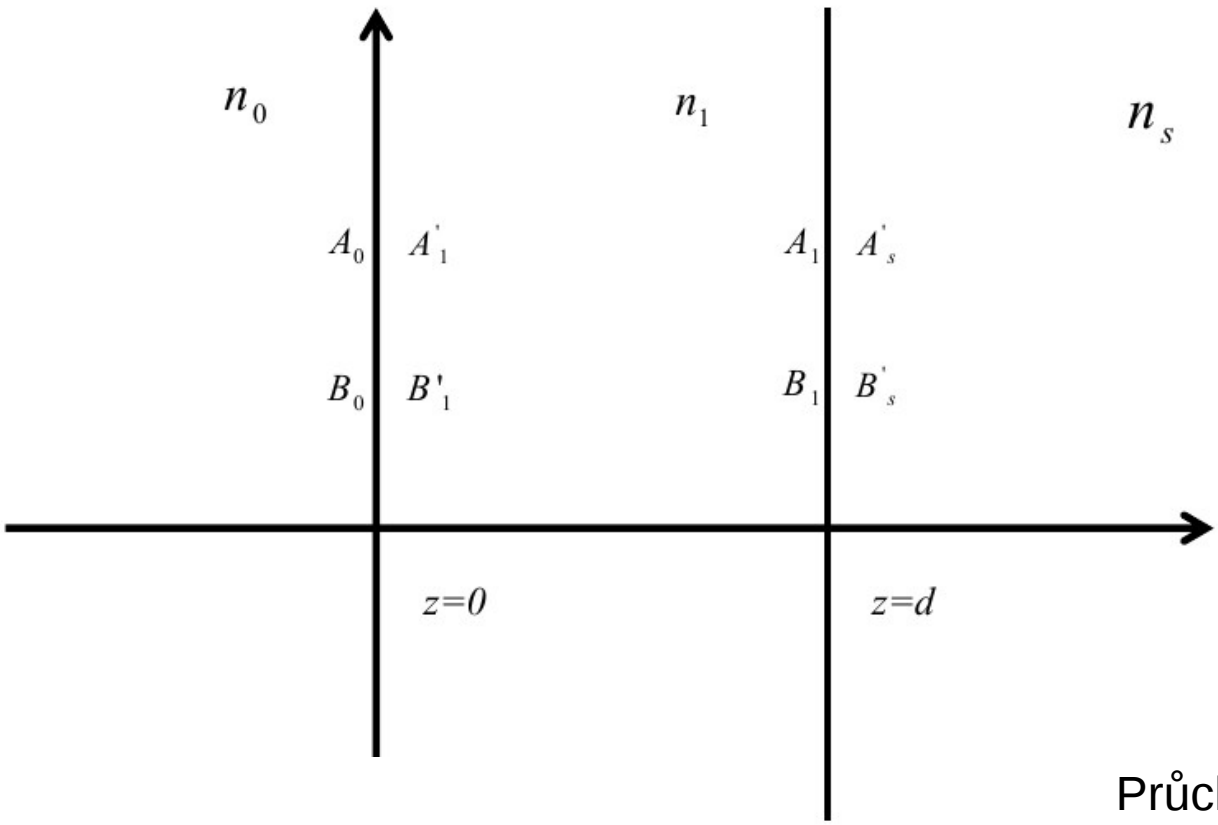

Průchod homogenním prostředím je popsán maticí P

$$E_p = E_p(z)e^{-jk_x x},$$

$$E_p(z) = A(z) + B(z) = Ae^{-jk_z z} + Be^{jk_z z}$$

$$\phi = k_z d$$

$$\begin{pmatrix} A'_1 \\ B'_1 \end{pmatrix} = \begin{pmatrix} e^{j\phi_1} & 0 \\ 0 & e^{-j\phi_1} \end{pmatrix} = P_1 \begin{pmatrix} A_1 \\ B_1 \end{pmatrix}$$

$$\phi = k_{1z} d = \frac{2\pi d}{\lambda} n_1 \cos\theta_1$$

Formalismus přenosových matic

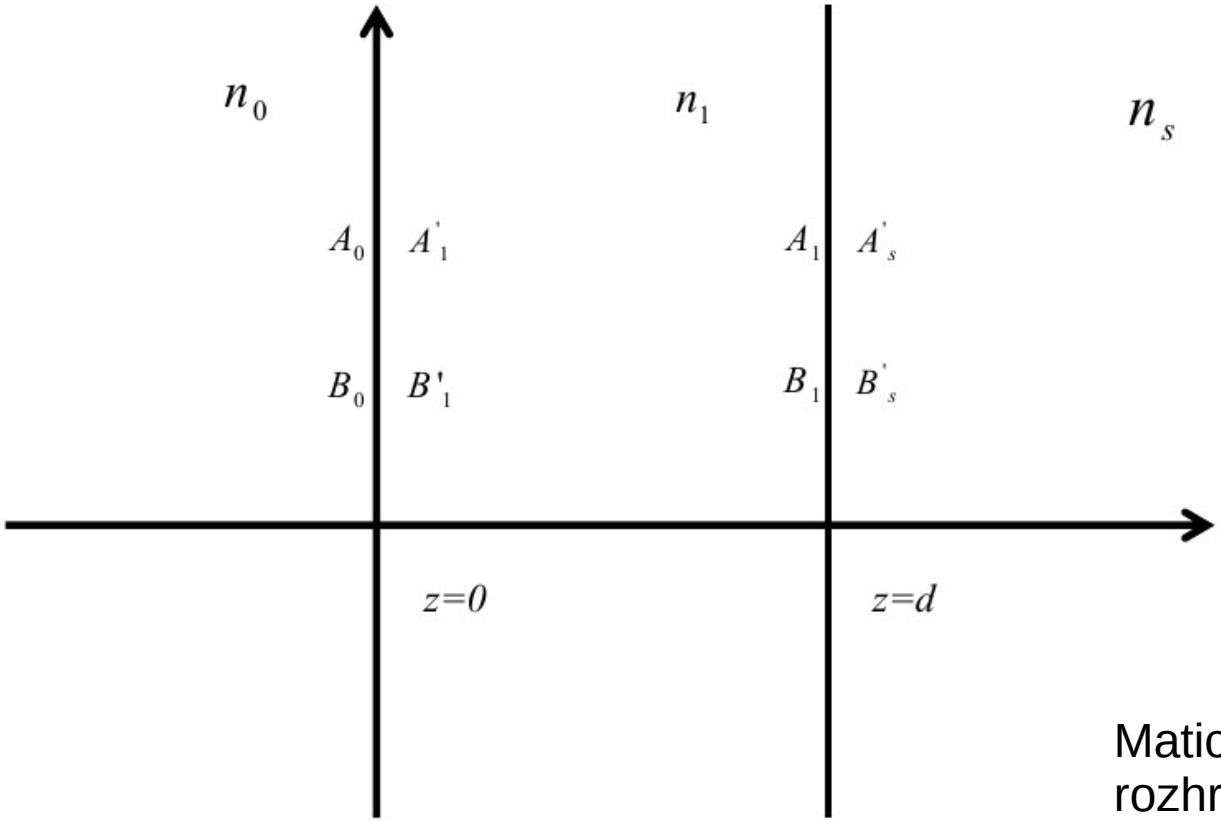

Matice D popisují podmínky na rozhraní dvou prostředí

$$E_p(z) = A(z) + B(z) = Ae^{-jk_z z} + Be^{jk_z z}$$

$$\begin{pmatrix} A_0 \\ B_0 \end{pmatrix} = D_0^{-1} D_1 \begin{pmatrix} A'_1 \\ B'_1 \end{pmatrix} \equiv D_{01} \begin{pmatrix} A'_1 \\ B'_1 \end{pmatrix}$$

$$D_i = \begin{cases} \begin{pmatrix} 1 & 1 \\ \sqrt{\frac{\varepsilon_i}{\mu_i}} \cos\theta_i & -\sqrt{\frac{\varepsilon_i}{\mu_i}} \cos\theta_i \end{pmatrix} & \text{for TE wave} \\ \begin{pmatrix} \cos\theta_i & \cos\theta_i \\ \sqrt{\frac{\varepsilon_i}{\mu_i}} & -\sqrt{\frac{\varepsilon_i}{\mu_i}} \end{pmatrix} & \text{for TM wave} \end{cases}$$

s-polarizace

p-polarizace

Formalismus přenosových matic

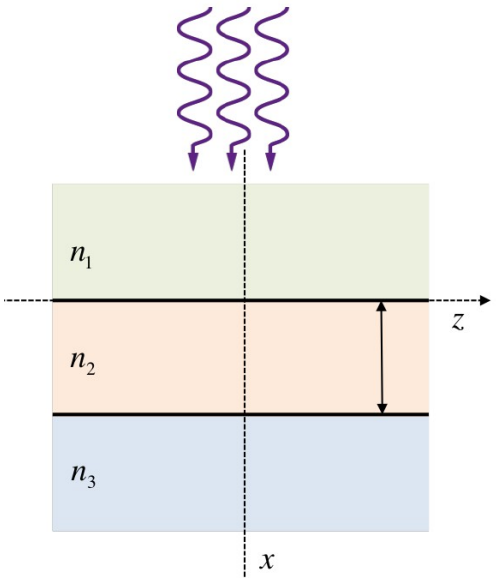

Podrobnější odvození pro s-polarizaci – šíření podél osy x

$$E(x)=\begin{cases} E_1 e^{ik_{1x}x}+E'_1 e^{-ik_{1x}x}, & x<0 \\ E_2 e^{ik_{2x}x}+E'_2 e^{-ik_{2x}x}, & 0<x<d \\ E_3 e^{ik_{3x}(x-d)}+E'_3 e^{-ik_{3x}(x-d)}, & x>d \end{cases}$$

$$\vec{E}_{1\|}=\vec{E}_{1\|} \Rightarrow E_{1y}+E'_{1y}=E_{2y}+E'_{2y}$$

$$H_{1\|}=H_{2\|} \Rightarrow H_{1z}+H'_{1z}=H_{2z}+H'_{2z} \Rightarrow n_1\cos\theta_1 E_{1y}-n_1\cos\theta_1 E'_{1y}=n_2\cos\theta_2 E_{2y}-n_2\cos\theta_2 E'_{2y}$$

$$\begin{pmatrix} 1 & 1 \\ n_1\cos\theta_1 & -n_1\cos\theta_1 \end{pmatrix}\begin{pmatrix} E_{1y} \\ E'_{1y} \end{pmatrix}=\begin{pmatrix} 1 & 1 \\ n_2\cos\theta_2 & -n_2\cos\theta_2 \end{pmatrix}\begin{pmatrix} E_{2y} \\ E'_{2y} \end{pmatrix} \Rightarrow D_1\begin{pmatrix} E_{1y} \\ E'_{1y} \end{pmatrix}=D_2\begin{pmatrix} E_{2y} \\ E'_{2y} \end{pmatrix}$$

$$D_2^{-1}D_1\begin{pmatrix} E_{1y} \\ E'_{1y} \end{pmatrix}=\begin{pmatrix} E_{2y} \\ E'_{2y} \end{pmatrix} \Rightarrow D_{12}\begin{pmatrix} E_{1y} \\ E'_{1y} \end{pmatrix}=\begin{pmatrix} E_{2y} \\ E'_{2y} \end{pmatrix}$$

Formalismus přenosových matic

$$D_2^{-1} D_1 \begin{pmatrix} E_{1y} \\ E'_{1y} \end{pmatrix} = \begin{pmatrix} E_{2y} \\ E'_{2y} \end{pmatrix} \Rightarrow D_{12} \begin{pmatrix} E_{1y} \\ E'_{1y} \end{pmatrix} = \begin{pmatrix} E_{2y} \\ E'_{2y} \end{pmatrix}$$

$$D_{12} = D_2^{-1} D_1 = \begin{pmatrix} 1 & 1 \\ n_2 \cos\theta_2 & -n_2 \cos\theta_2 \end{pmatrix}^{-1} \begin{pmatrix} 1 & 1 \\ n_1 \cos\theta_1 & -n_1 \cos\theta_1 \end{pmatrix} = \begin{pmatrix} \frac{1}{2} & \frac{1}{2n_2 \cos\theta_2} \\ \frac{1}{2} & -\frac{1}{2n_2 \cos\theta_2} \end{pmatrix} \begin{pmatrix} 1 & 1 \\ n_1 \cos\theta_1 & -n_1 \cos\theta_1 \end{pmatrix}$$

$$D_{12} = \begin{pmatrix} \frac{n_2 \cos\theta_2 + n_1 \cos\theta_1}{2n_2 \cos\theta_2} & \frac{n_2 \cos\theta_2 - n_1 \cos\theta_1}{2n_2 \cos\theta_2} \\ \frac{n_2 \cos\theta_2 - n_1 \cos\theta_1}{2n_2 \cos\theta_2} & \frac{n_2 \cos\theta_2 + n_1 \cos\theta_1}{2n_2 \cos\theta_2} \end{pmatrix}$$

Formalismus přenosových matic

Pro systém s jednou vrstvou

$$\begin{pmatrix} A_0 \\ B_0 \end{pmatrix} = D_0^{-1} D_1 P_1 D_1^{-1} D_s \begin{pmatrix} A'_s \\ B'_s \end{pmatrix} = M \begin{pmatrix} A'_s \\ B'_s \end{pmatrix}$$

Obecný mnohovrstevný systém – každá vrstva je popsána součinem tří matic $D_n P_n D_n^{-1}$

Celek je popsán maticí M = součin všech jednotlivých matic

Koeficienty Odrazivosti *r* a propustnosti *t*

$$\begin{cases} r = \dfrac{B_0}{A_0}, \\ t = \dfrac{A'_s}{A_0}. \end{cases}$$

Vyjádření pomocí prvků matice *M*

$$\begin{cases} r = \dfrac{M_{21}}{M_{11}}, \\ t = \dfrac{1}{M_{11}}. \end{cases}$$

Odrazivost systému $R=|r|^2=|M_{21}/M_{11}|^2$

Multivrstva – kolmá odrazivost

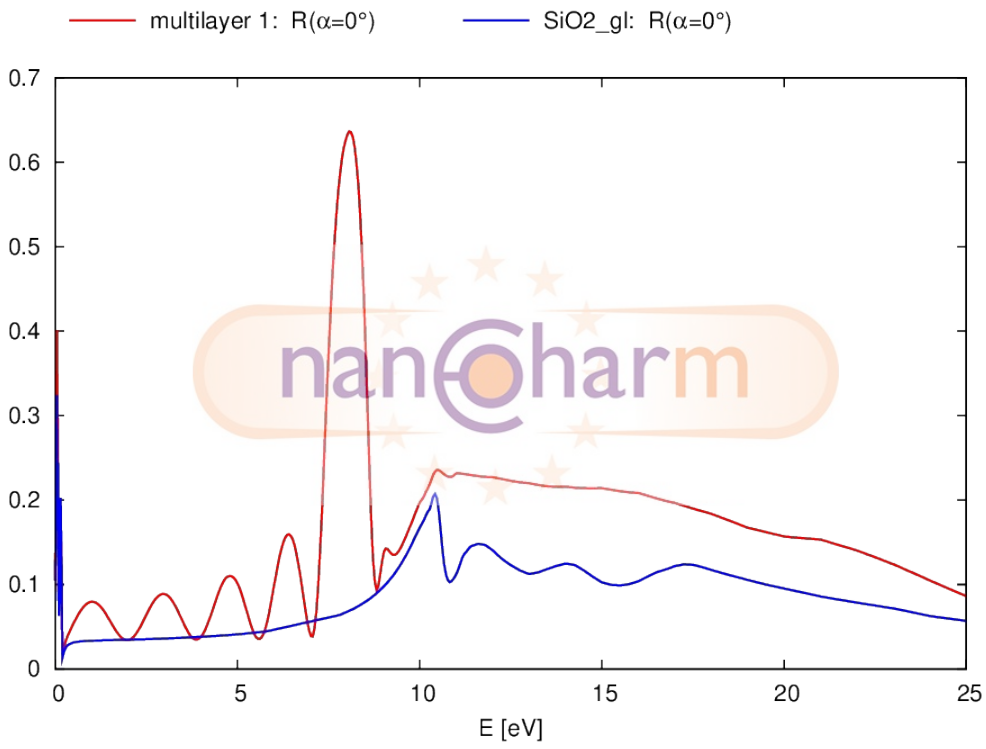

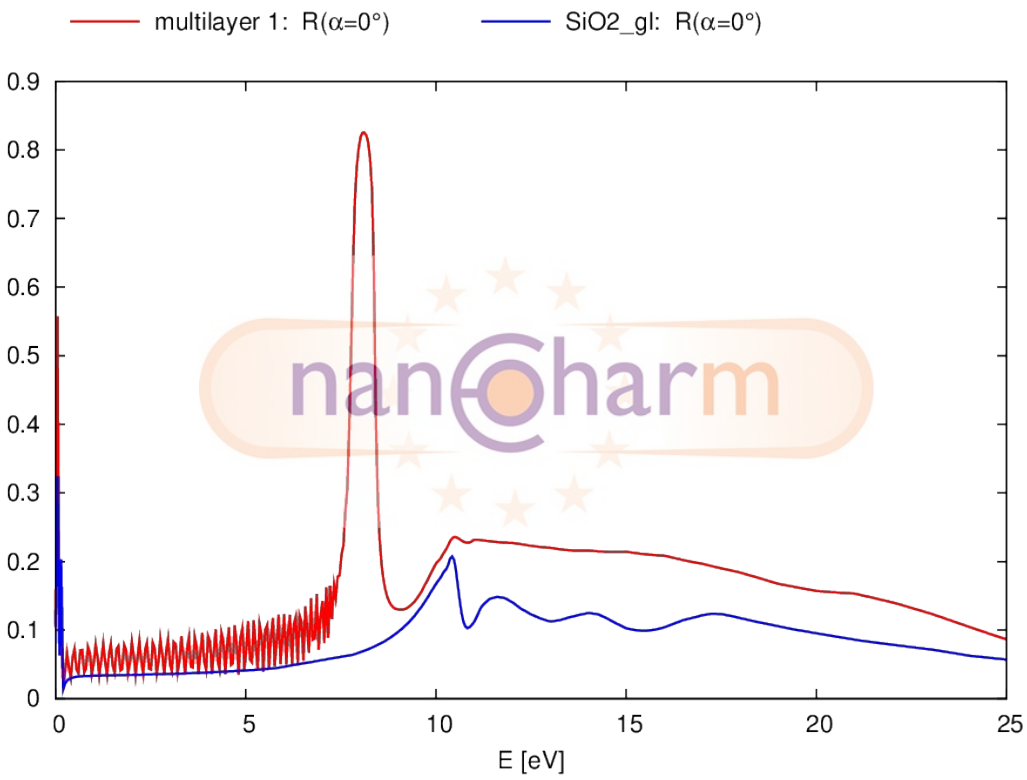

(SiO_2 20nm/Al_2O_3 20nm)x5

(SiO_2 20nm/Al_2O_3 20nm)x50

Multivrstva – kolmá odrazivost

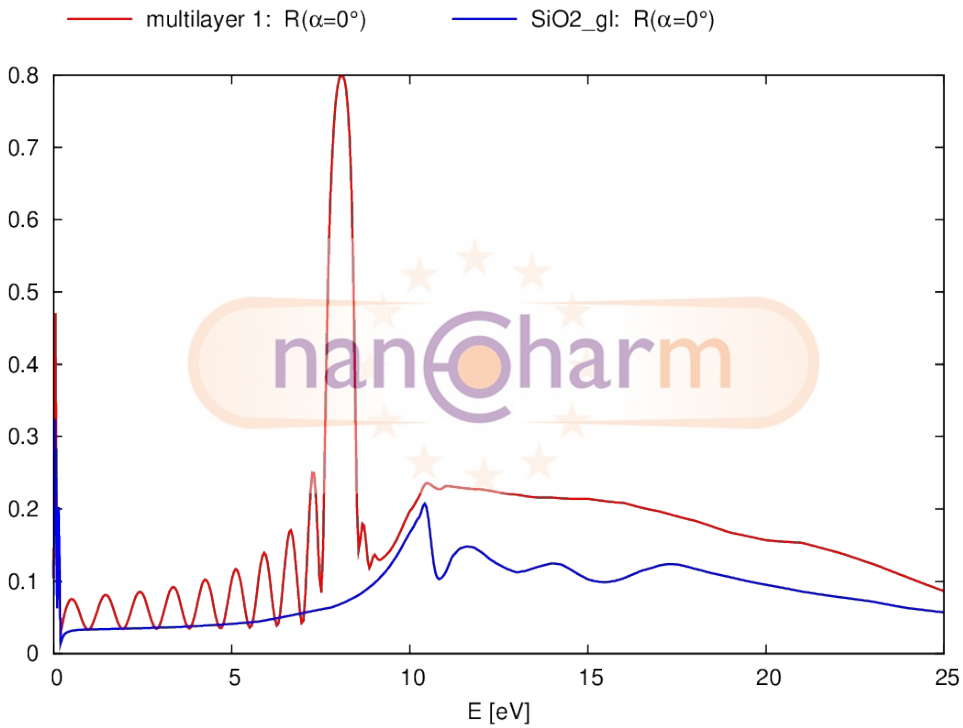

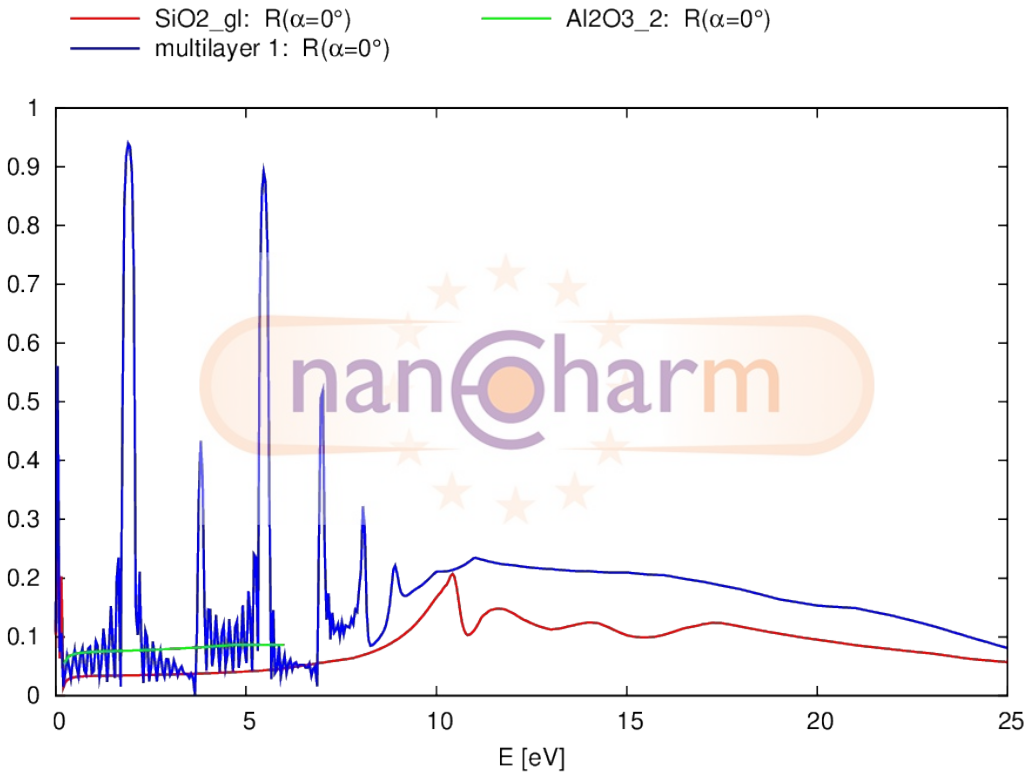

(SiO_2 20nm/Al_2O_3 20nm)x10

(SiO_2 100nm/Al_2O_3 100nm)x10

Lorentzův model

$$\epsilon(\omega) = 1 + \frac{Ne^2}{\epsilon_0 m}\frac{1}{\omega_0^2 - \omega^2 - \mathrm{i}\omega/\tau} = 1 + \frac{Ne^2}{\epsilon_0 m}\frac{\omega_0^2 - \omega^2}{(\omega_0^2 - \omega^2)^2 + \omega^2/\tau^2} + \mathrm{i}\frac{Ne^2}{\epsilon_0 m}\frac{\omega/\tau}{(\omega_0^2 - \omega^2)^2 + \omega^2/\tau^2}$$

$$\epsilon(\omega) = 1 + \frac{F}{\omega_0^2 - \omega^2 - \mathrm{i}\omega/\tau} = 1 + F\frac{\omega_0^2 - \omega^2}{(\omega_0^2 - \omega^2)^2 + \omega^2/\tau^2} + \mathrm{i}F\frac{\omega/\tau}{(\omega_0^2 - \omega^2)^2 + \omega^2/\tau^2}$$

$$F = \frac{Ne^2}{\epsilon_0 m}$$

$$\sigma(\omega) = -\mathrm{i}\omega\epsilon_0(\epsilon(\omega) - 1) = \frac{-\mathrm{i}\omega\epsilon_0 F}{\omega_0^2 - \omega^2 - \mathrm{i}\omega/\tau} = \epsilon_0 F\frac{\omega^2/\tau}{(\omega_0^2 - \omega^2)^2 + \omega^2/\tau^2} - \mathrm{i}\omega\epsilon_0 F\frac{\omega_0^2 - \omega^2}{(\omega_0^2 - \omega^2)^2 + \omega^2/\tau^2}$$

$$\epsilon(0) = 1 + \frac{F}{\omega_0^2},\ \epsilon(\infty) = 1$$

$$\epsilon_1(\omega_{LO}) = 0, \quad \frac{F}{\omega_0^2 - \omega_{LO}^2} + 1 = 0, \quad \omega_{LO}^2 \approx \omega_0^2 + F$$

Pří LO frekvence je reálná část dielektrické funkce rovna nule

$$\frac{\omega_{LO}^2}{\omega_0^2} = \frac{\epsilon(0)}{\epsilon(\infty)}.$$

Lorentzův model

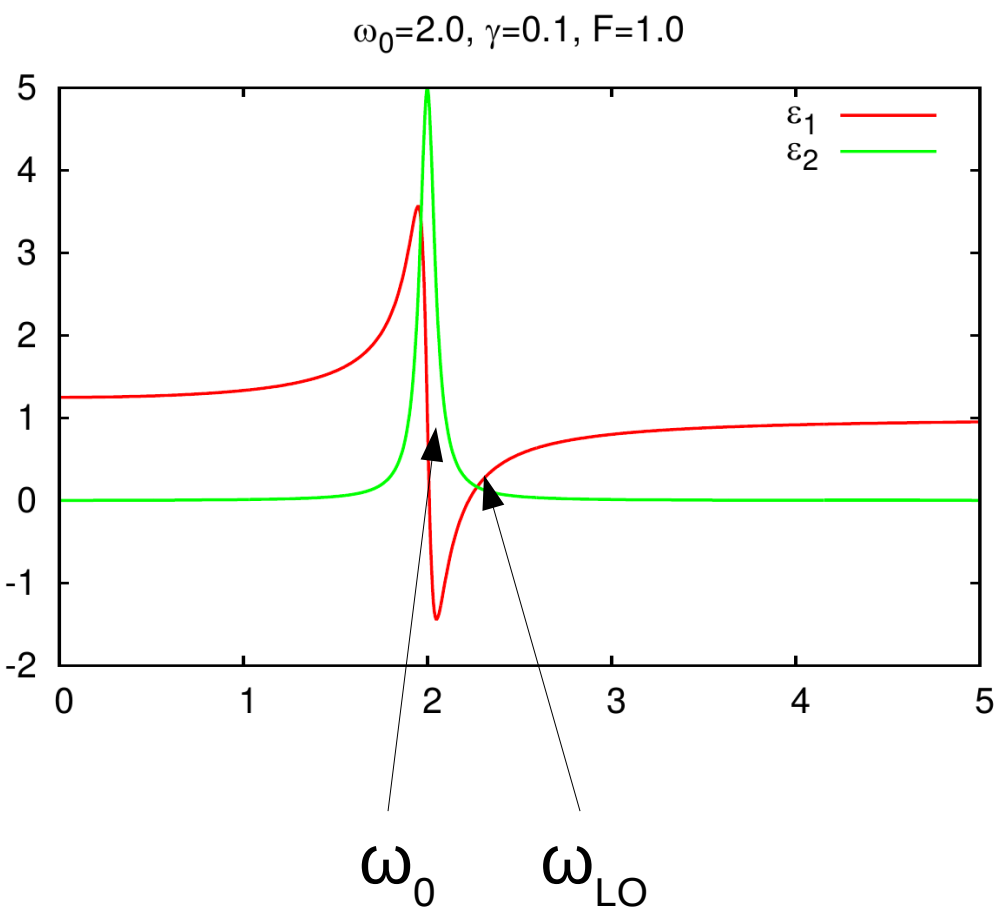

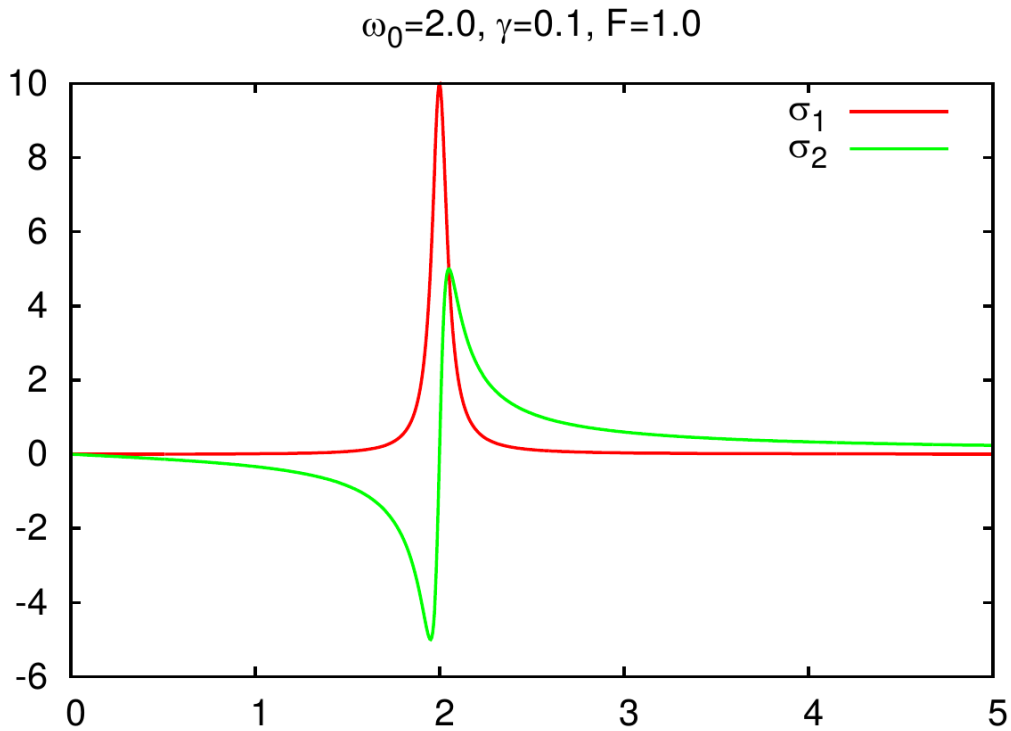

Lorentzův model

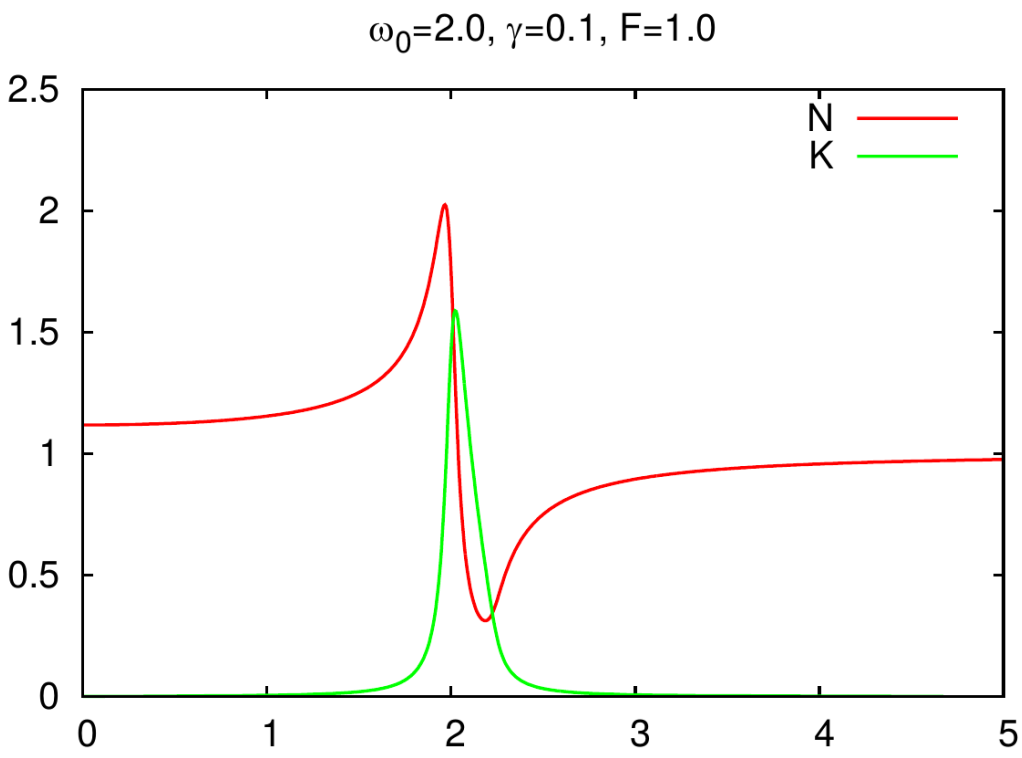

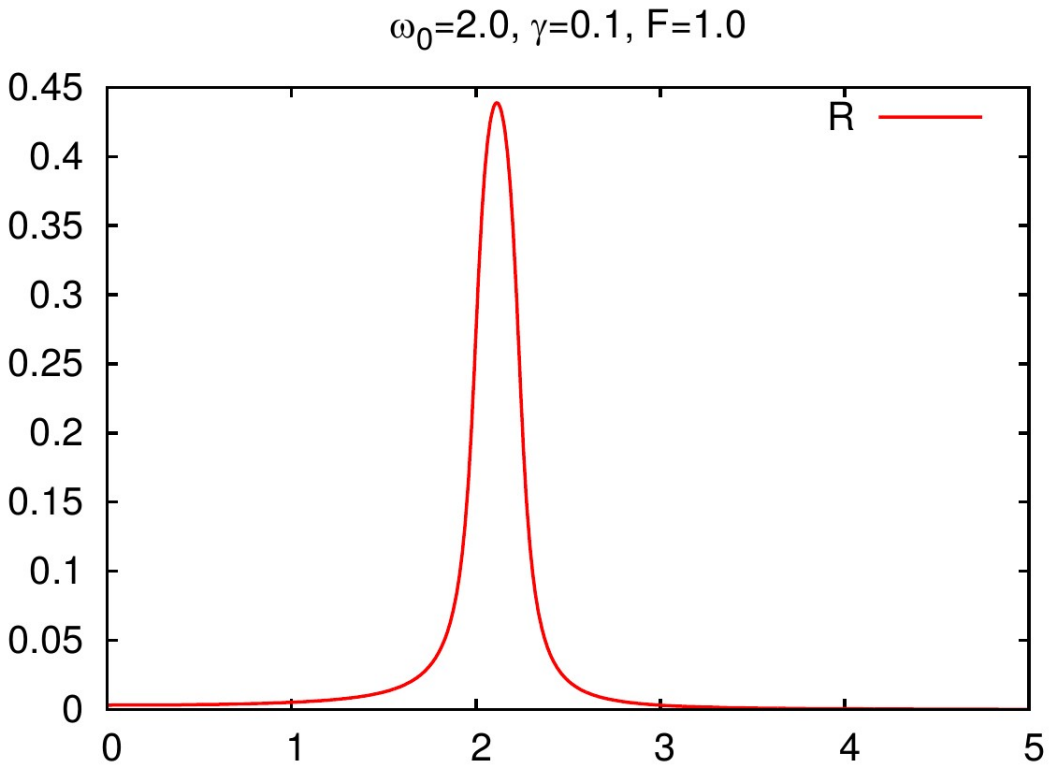

Lorentzův model

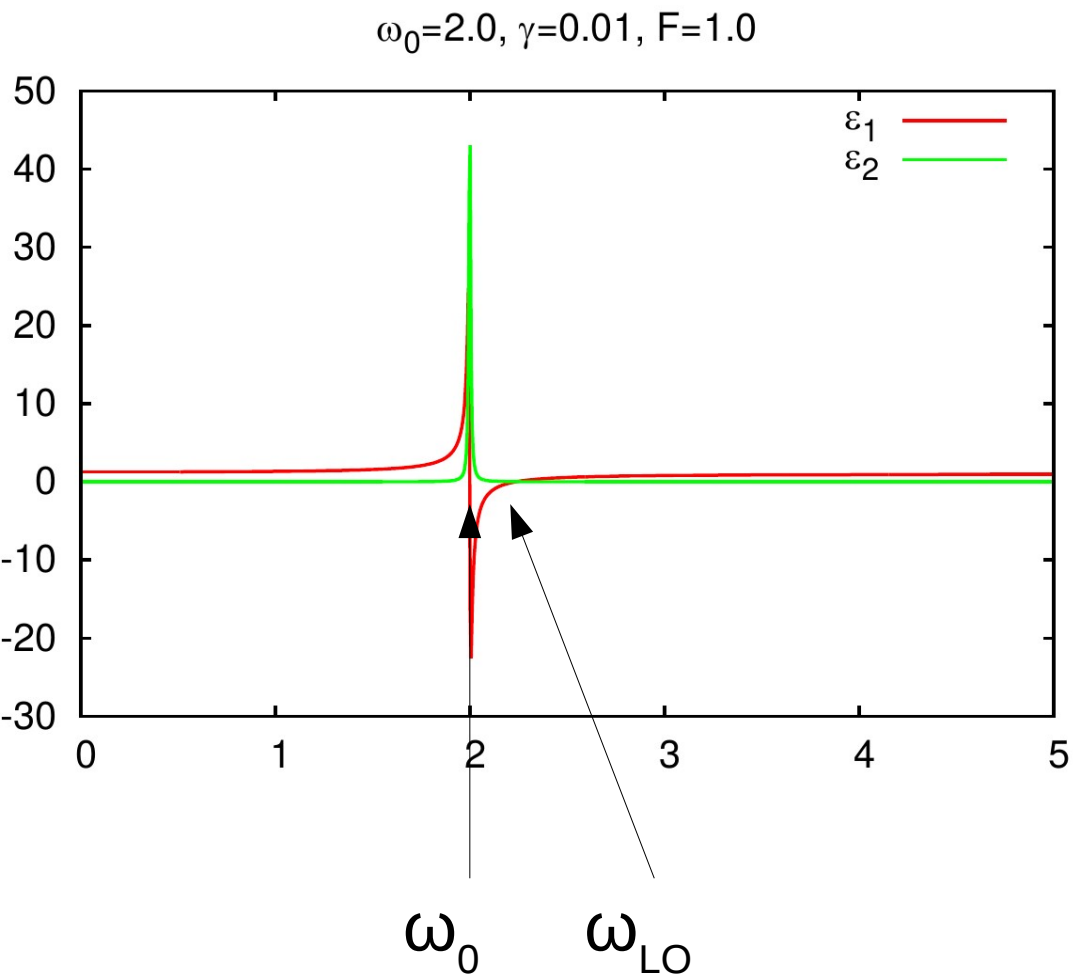

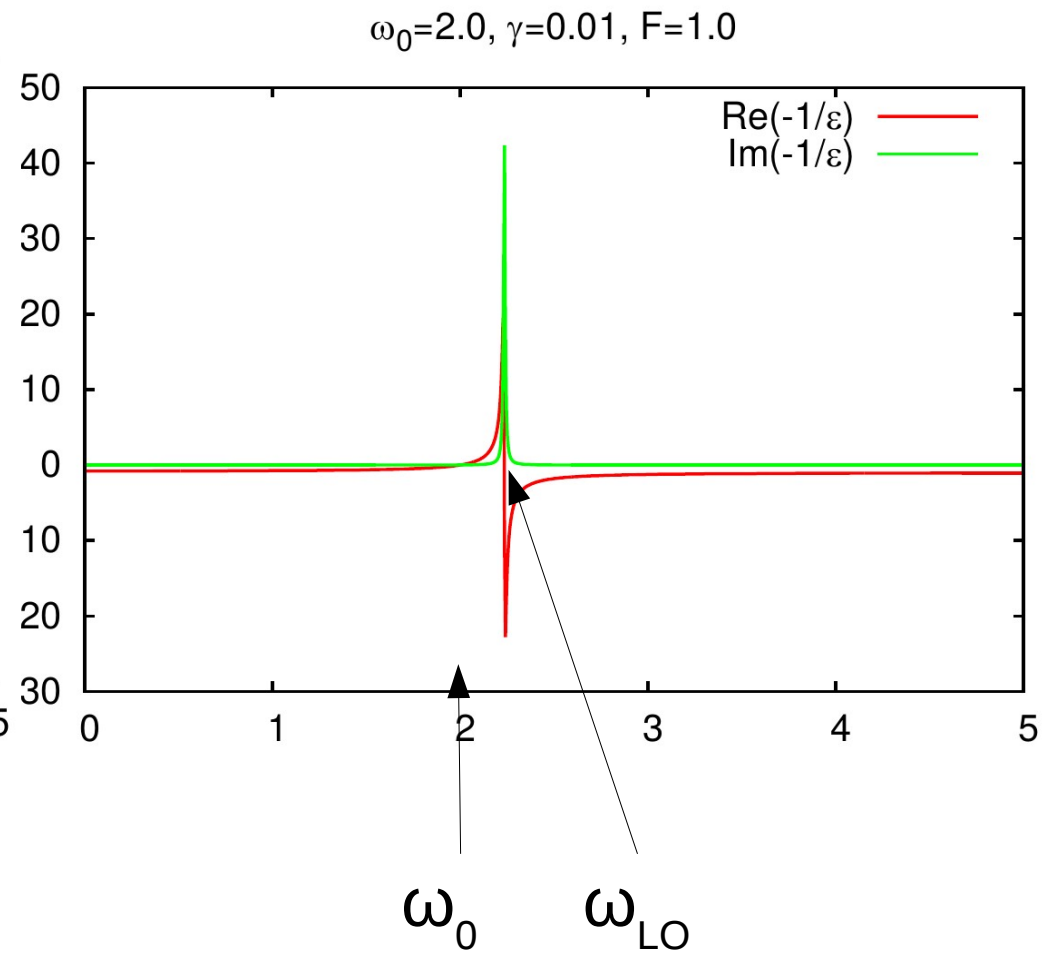

Lorentzův model

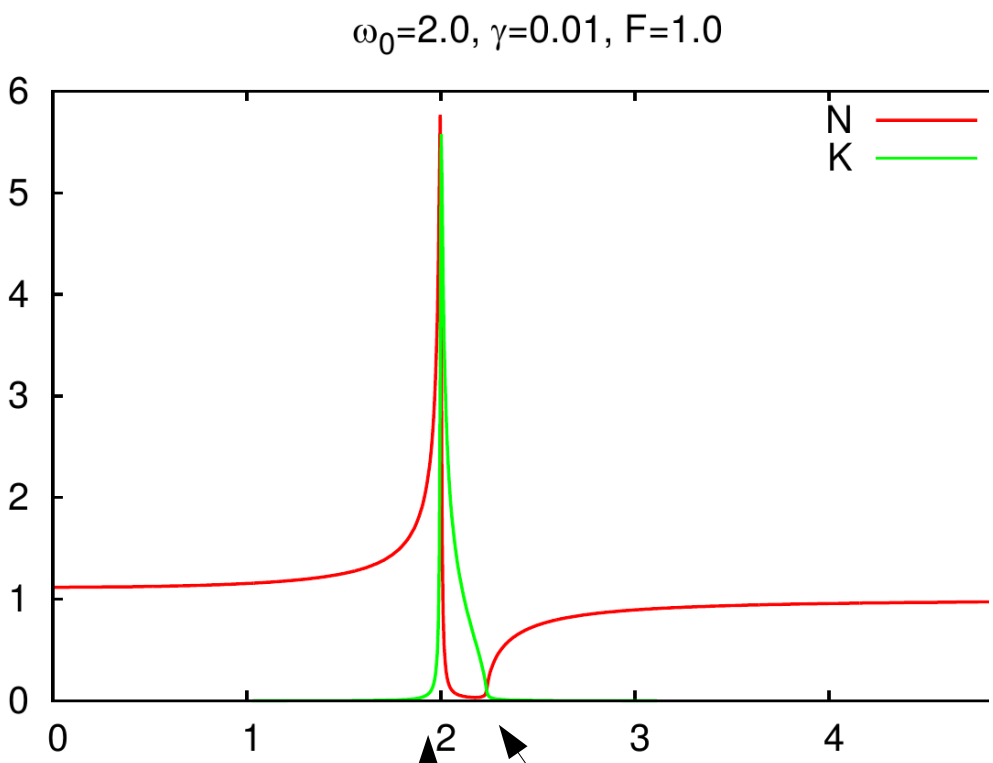

ω_0 $\omega_{LO}=\sqrt{\omega^2_0+F}$

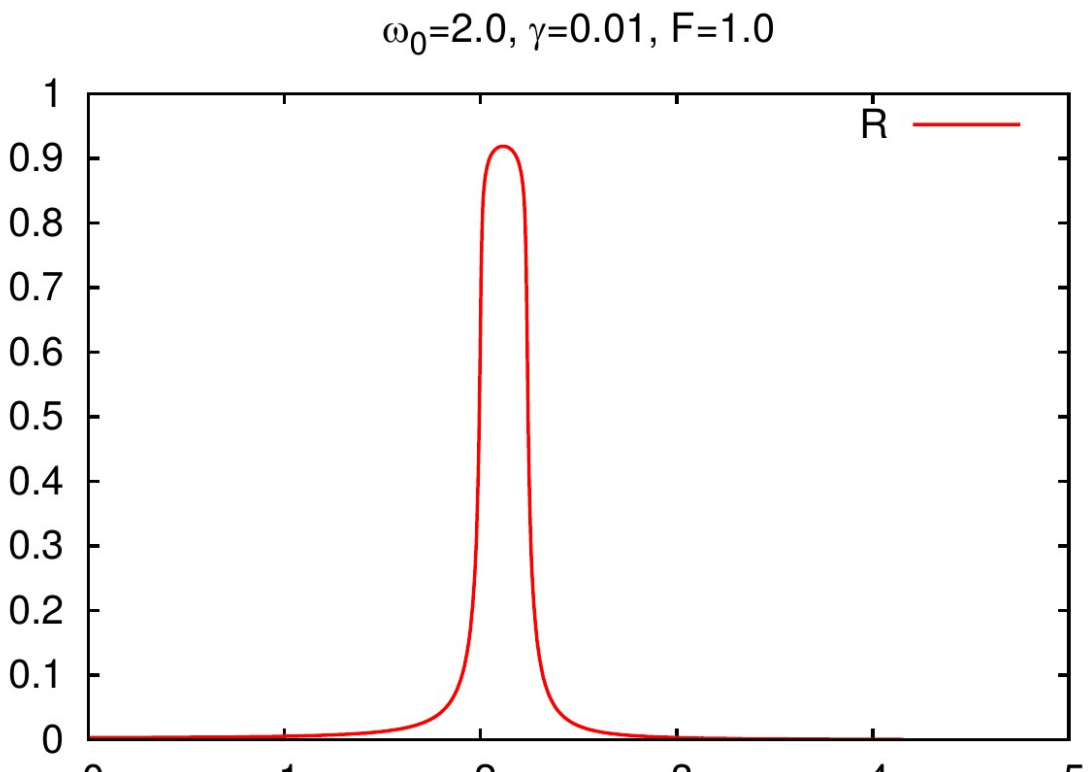

ω_0 ω_{LO}

Lorentzův model

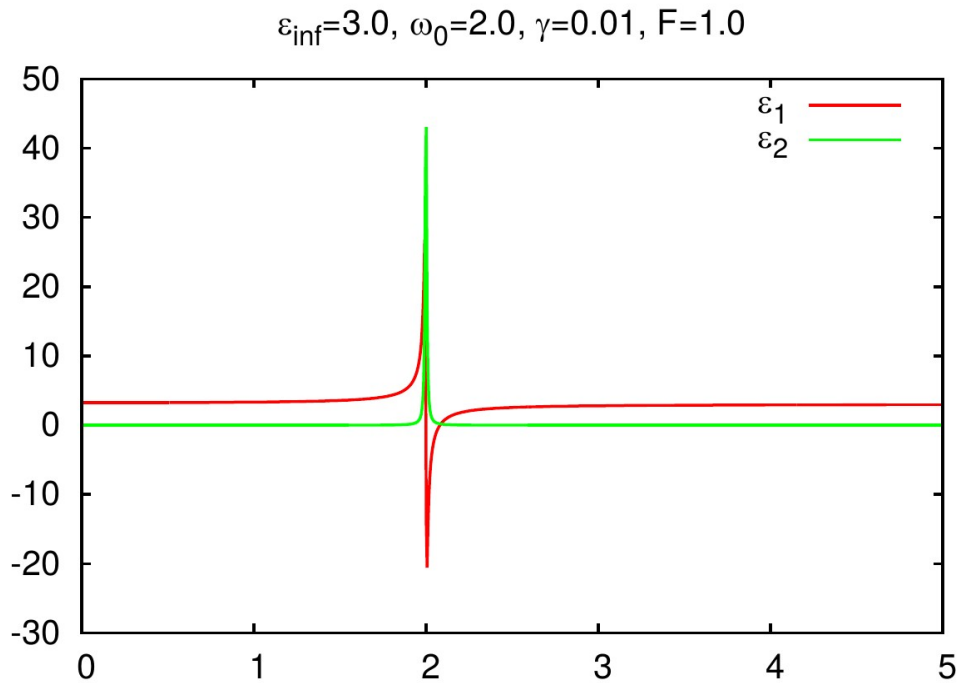

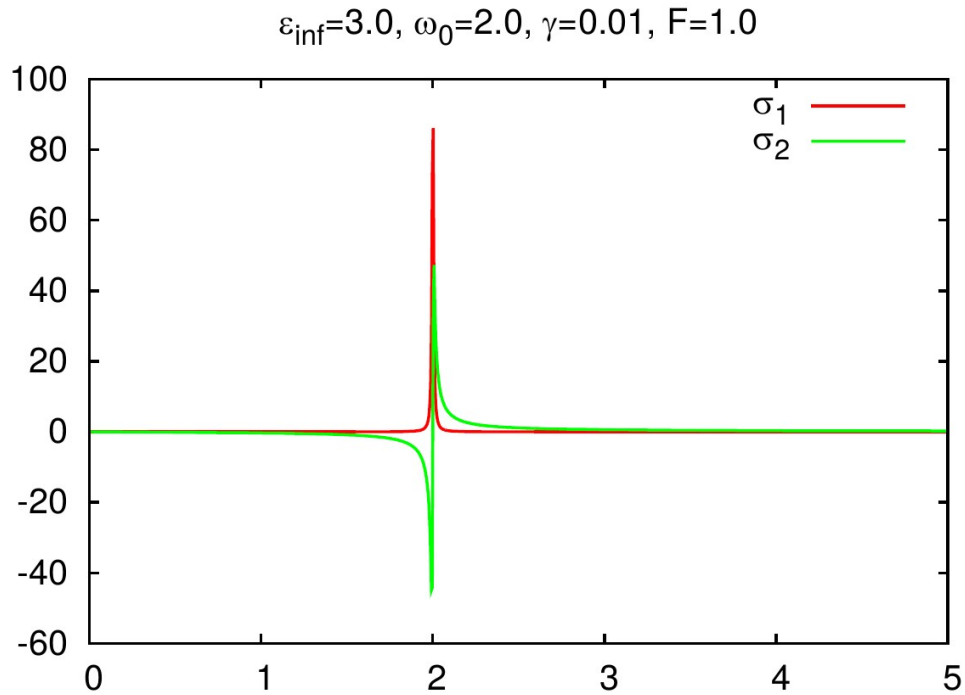

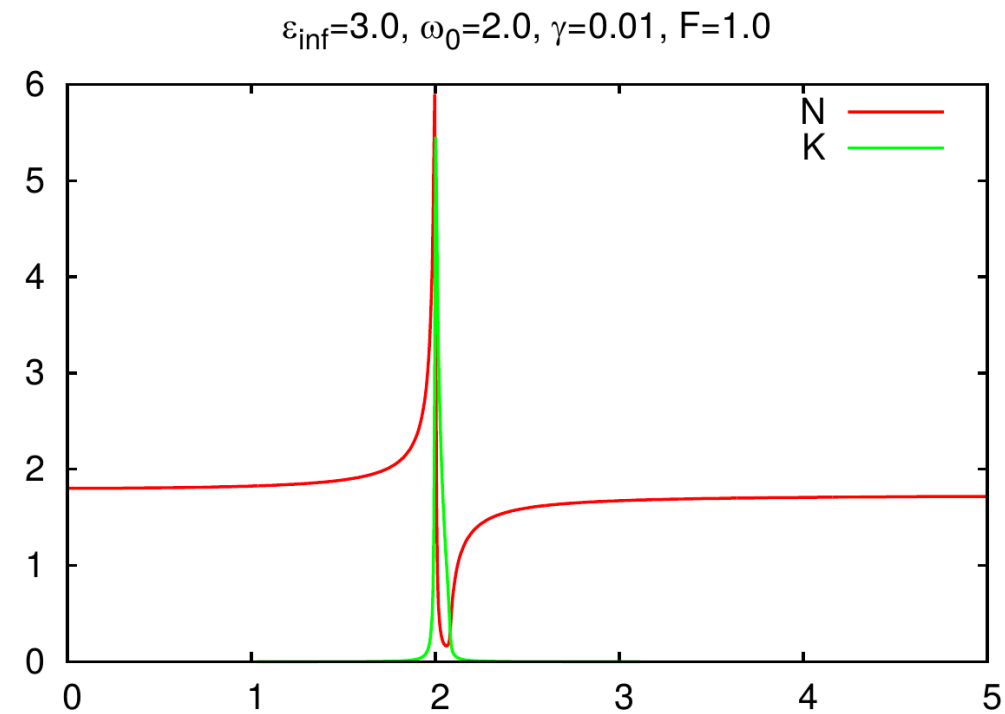

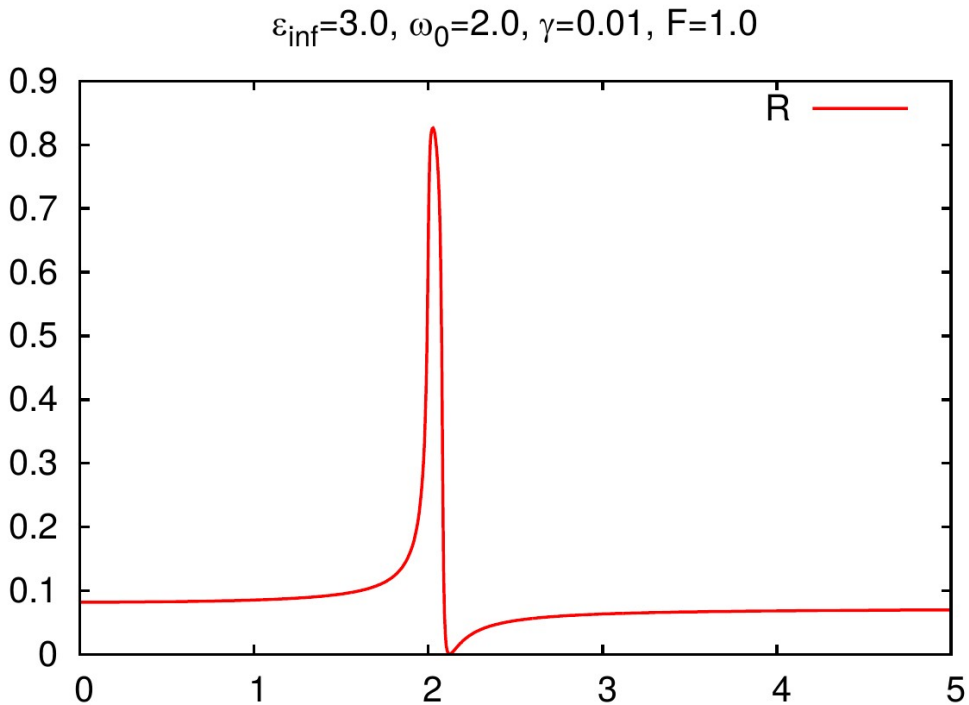

Odrazivost krystalického α-SiO_2

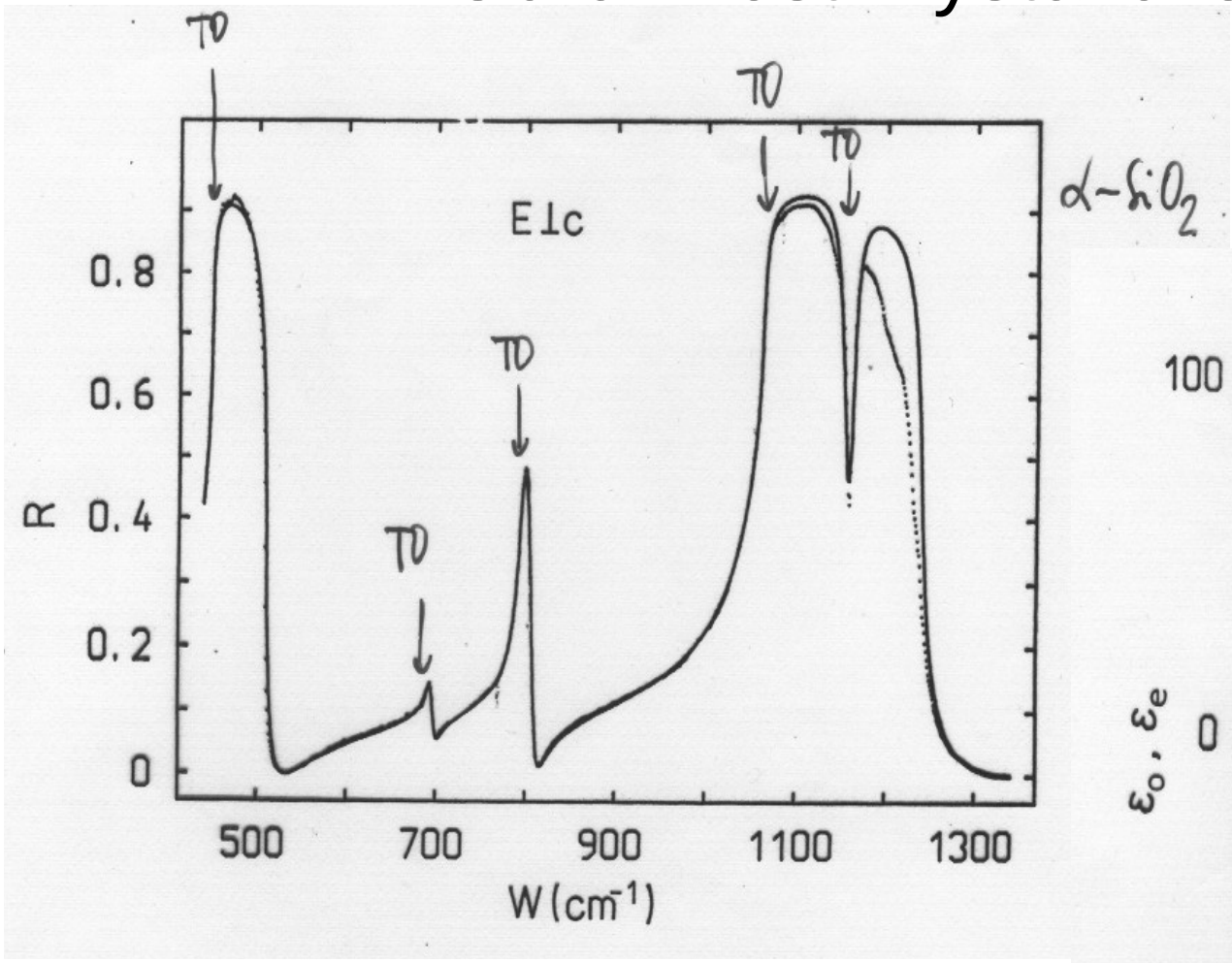

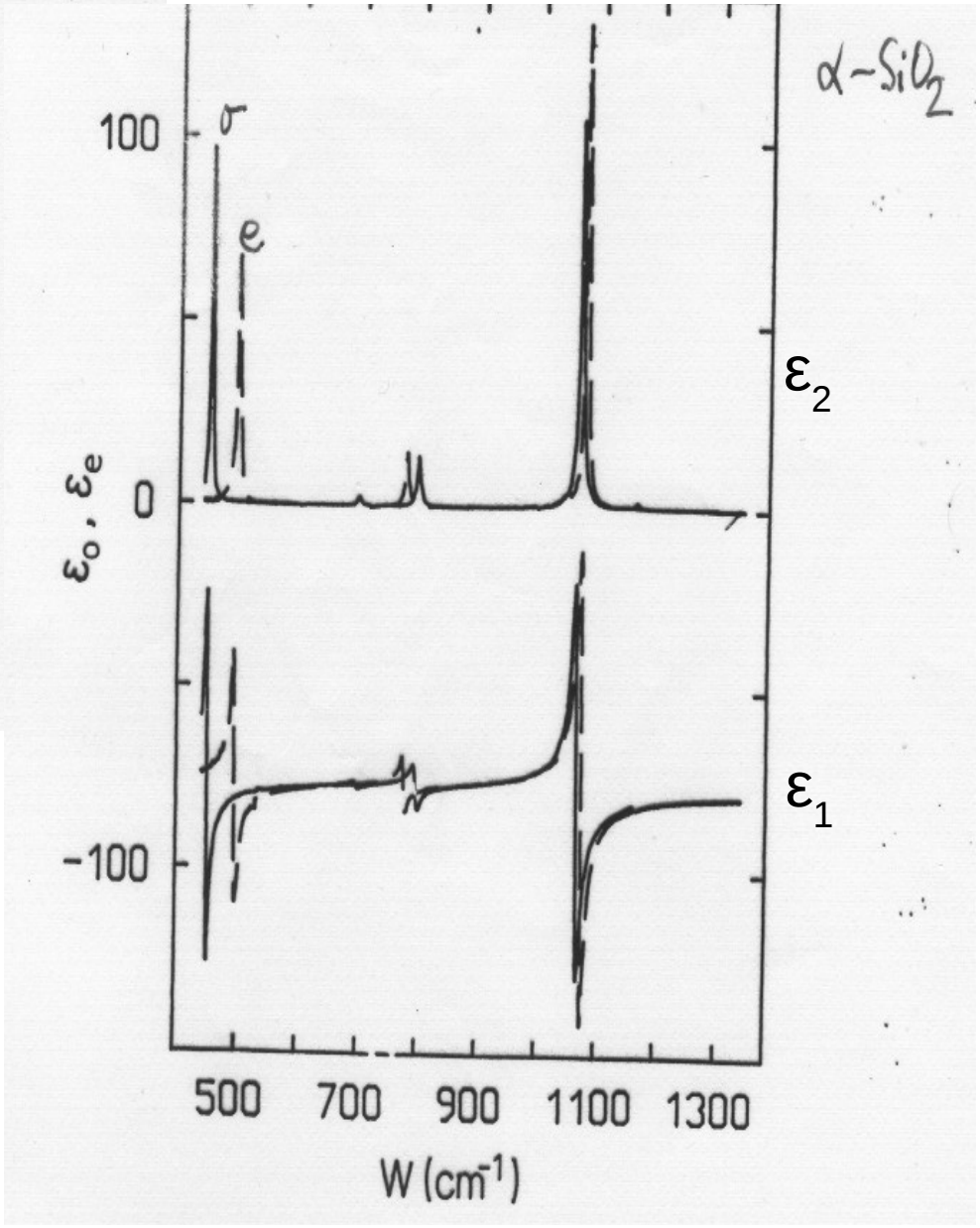

J. Humlíček

Odrazivost GaAs

fotonová disperze ω=ck
c=300000 km/s

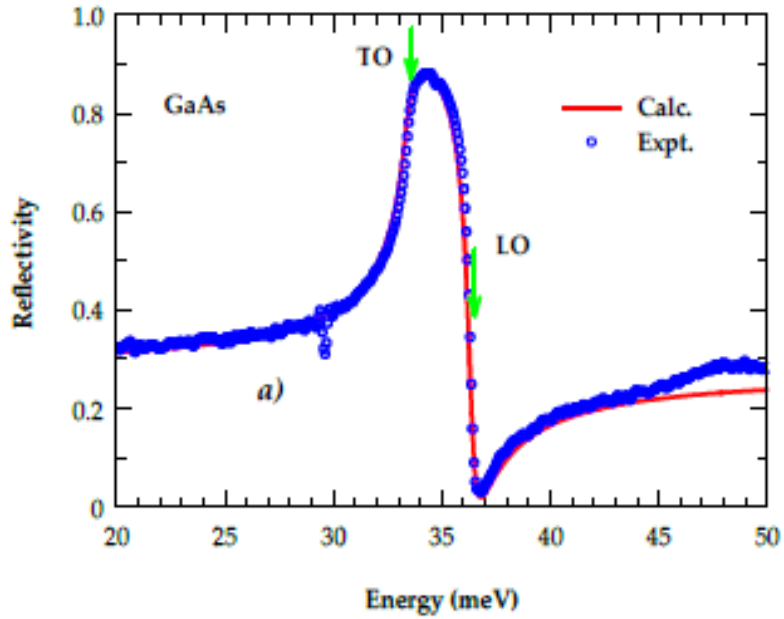

Figure 2a: Comparison of the experimental FIR reflectivity spectra for GaAs represented by blue color open circles (○) with the best fit simulated reflectivity results shown by red color solid line (—) using a classical Drude-Lorentz model (Eq. 3) with parameter values from Table 1 b) – green colored vertical arrows are used to represent TO and LO modes.

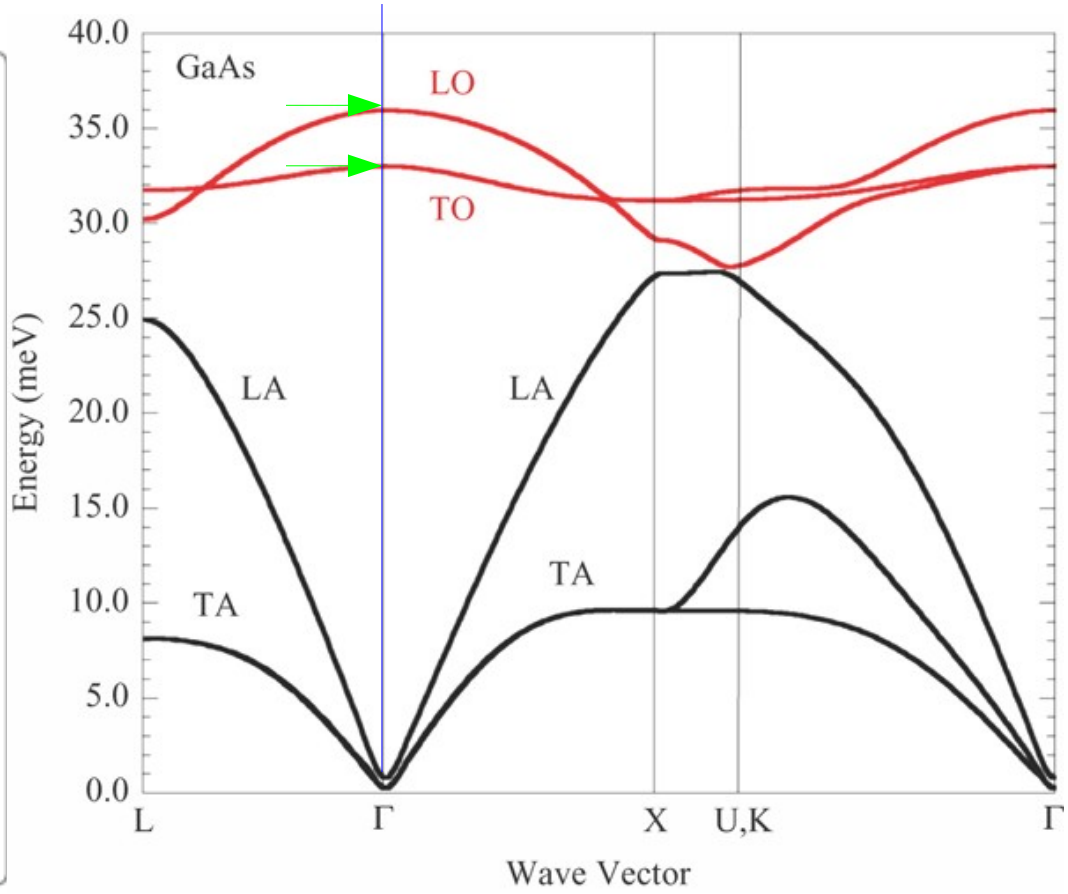

fononová disperze ω=vk
pro akustické fonony v≈1km/s

Frekvence oscilátoru je rovna frekvenci optických fononů v bodě Γ

Dielektrická funkce krystalického α-SiO_2 a amorfního v-SiO_2

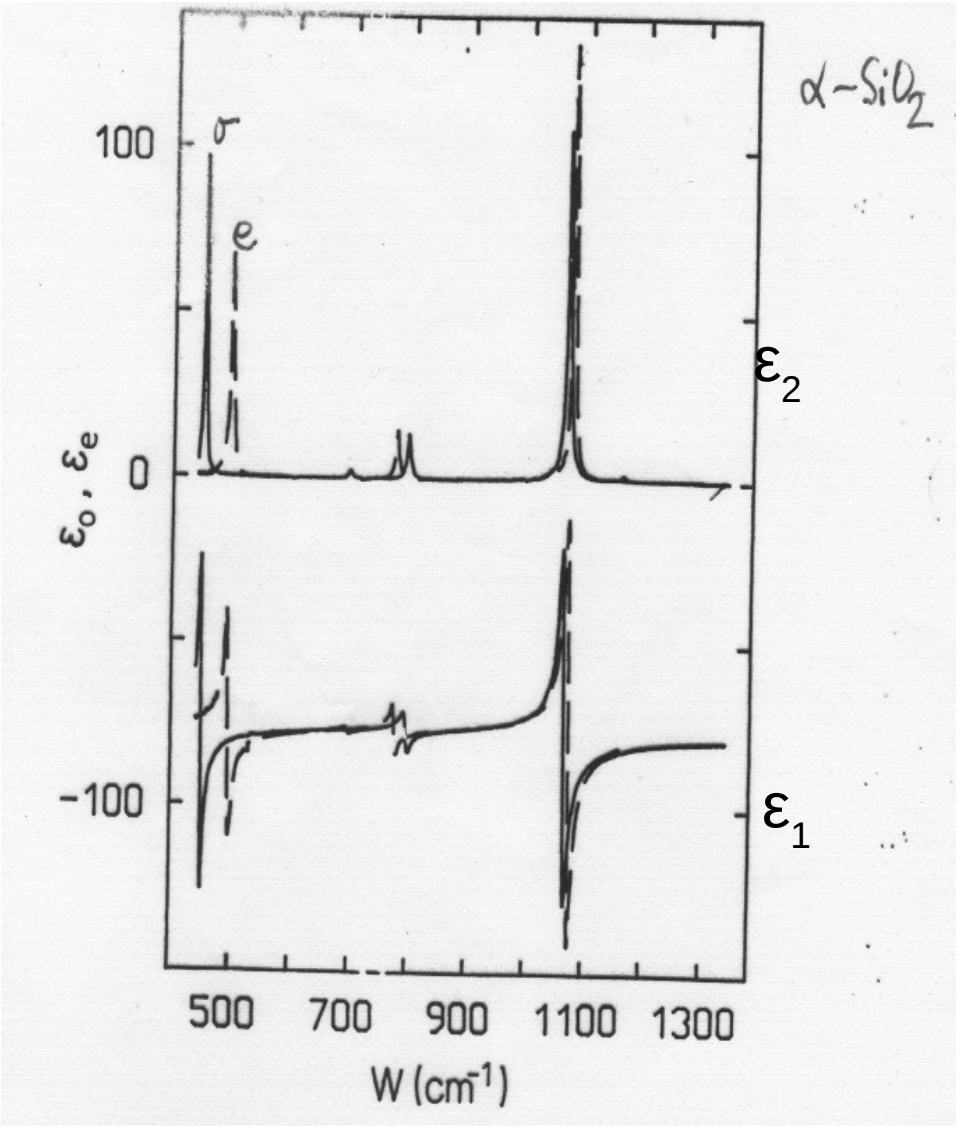

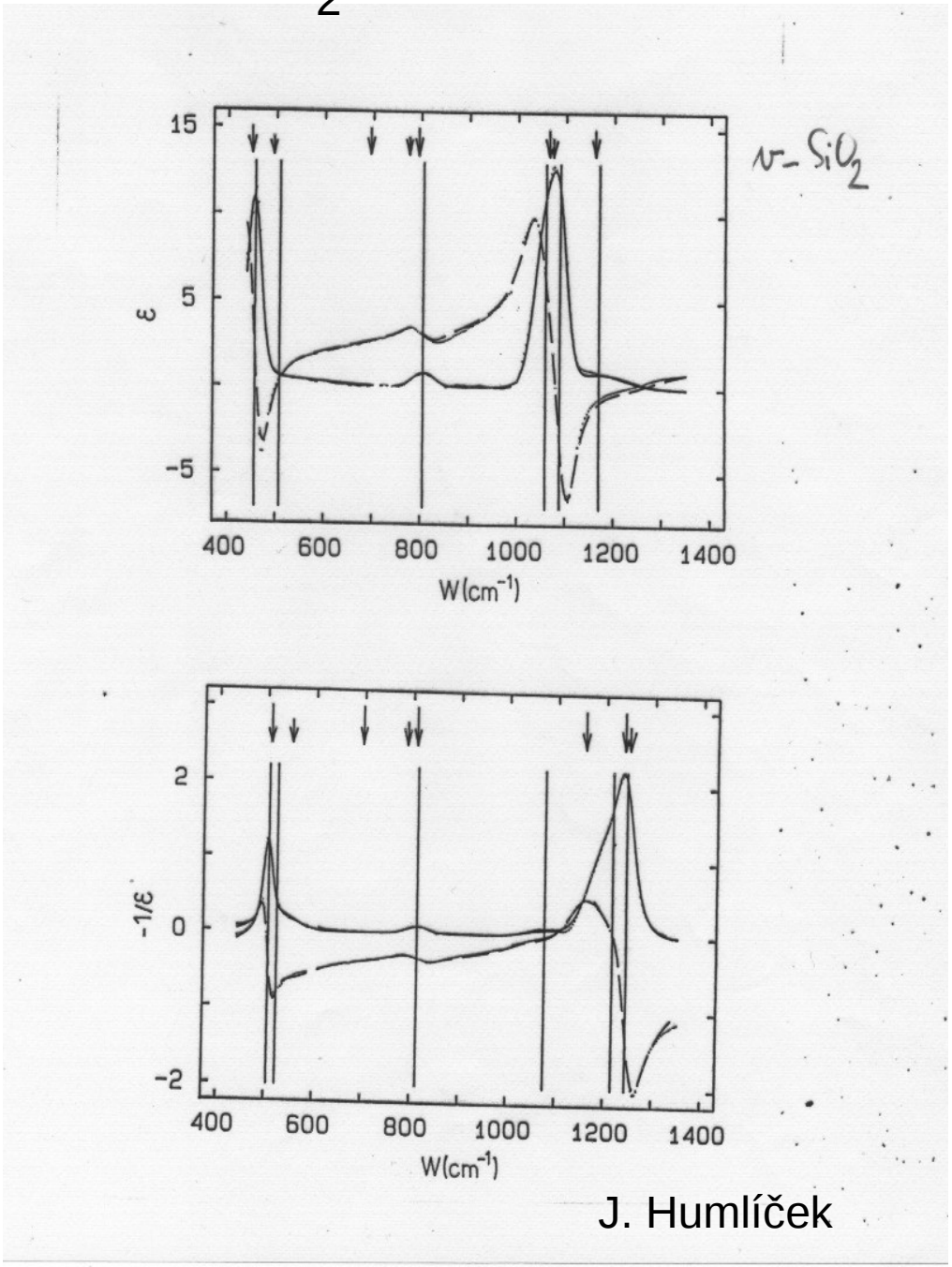

J. Humlíček

Index lomu amorfního SiO_2 skla

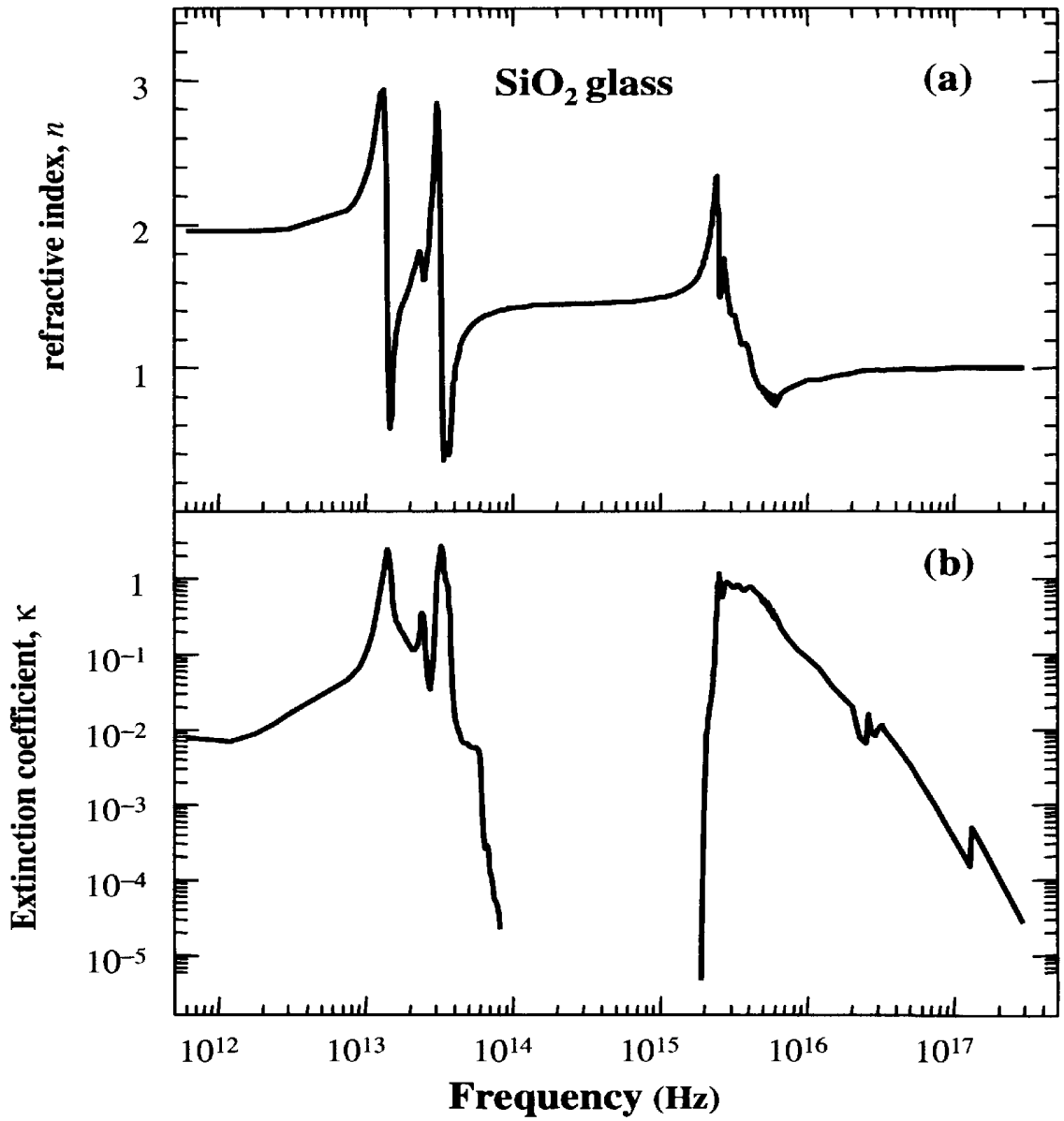

M. Fox: Optical properties of solids, Oxford university press, 2001.

$SrTiO_3$ – měření a fit Lorentzovým modelem

TO
530 cm-1 ... 16 THz

LO
470 cm-1 ... 14 THz
780 cm-1 ... 23 THz

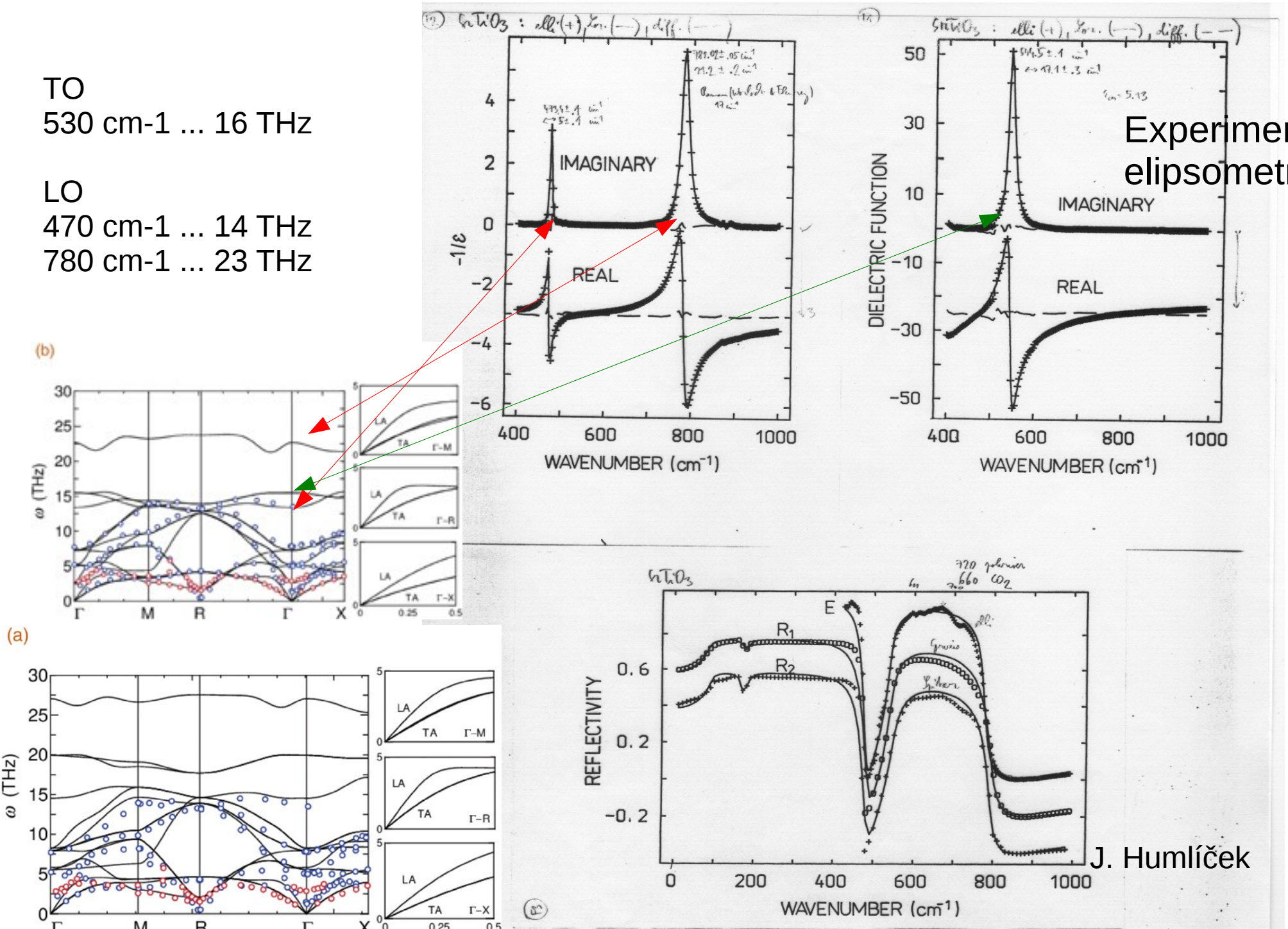

Experiment: elipsometrie

J. Humlíček

GaP disperzni relace polaritonu

GaP

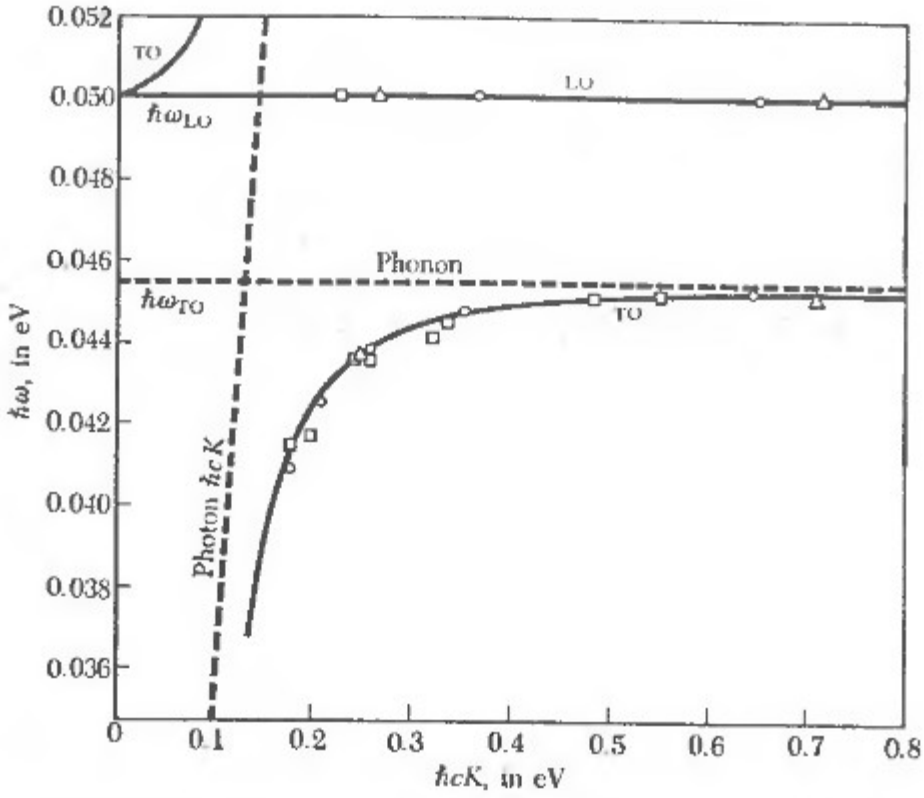

Drudeho model

$$\sigma(\omega) = -nev_0/E = \frac{\sigma_0}{1 - \mathrm{i}\omega\tau} = \frac{\sigma_0}{1+\omega^2\tau^2} + \mathrm{i}\frac{\sigma_0\omega\tau}{1+\omega^2\tau^2}$$

$$\sigma_0 = \frac{Ne^2\tau}{m}$$ Stejnosměrná vodivost

$$\epsilon(\omega) = 1 - \frac{Ne^2}{\epsilon_0 m}\frac{1}{\omega^2 + \mathrm{i}\omega/\tau} = 1 - \frac{Ne^2\tau}{\epsilon_0 m}\frac{1}{\omega(\mathrm{i}+\omega\tau)} = 1 - \frac{\omega_P^2\tau}{\omega(\mathrm{i}+\omega\tau)} = 1 - \frac{\sigma_0}{\epsilon_0\omega}\frac{1}{\mathrm{i}+\omega\tau}$$

$$\epsilon(\omega) = 1 - \frac{\omega_P^2\tau^2}{1+\omega^2\tau^2} + \mathrm{i}\frac{\omega_P^2\tau/\omega}{1+\omega^2\tau^2} = 1 - \frac{\sigma_0}{\epsilon_0}\frac{\tau}{1+\omega^2\tau^2} + \mathrm{i}\frac{\sigma_0}{\epsilon_0\omega}\frac{1}{1+\omega^2\tau^2}$$

$$\sigma_0 = \frac{Ne^2\tau}{m} = \epsilon_0\omega_P^2\tau$$

$$\epsilon_1(\omega_L) = 0,\ \omega_L = \sqrt{\omega_P^2 - 1/\tau^2} \approx \omega_P$$ LO frekvence je rovna plazmové frekvenci

$$\sigma(0) = \sigma_0.\ \sigma_1(1/\tau) = \sigma_2(1/\tau) = \sigma_0/2.$$ Stejnosměrná vodivost

Drudeho model

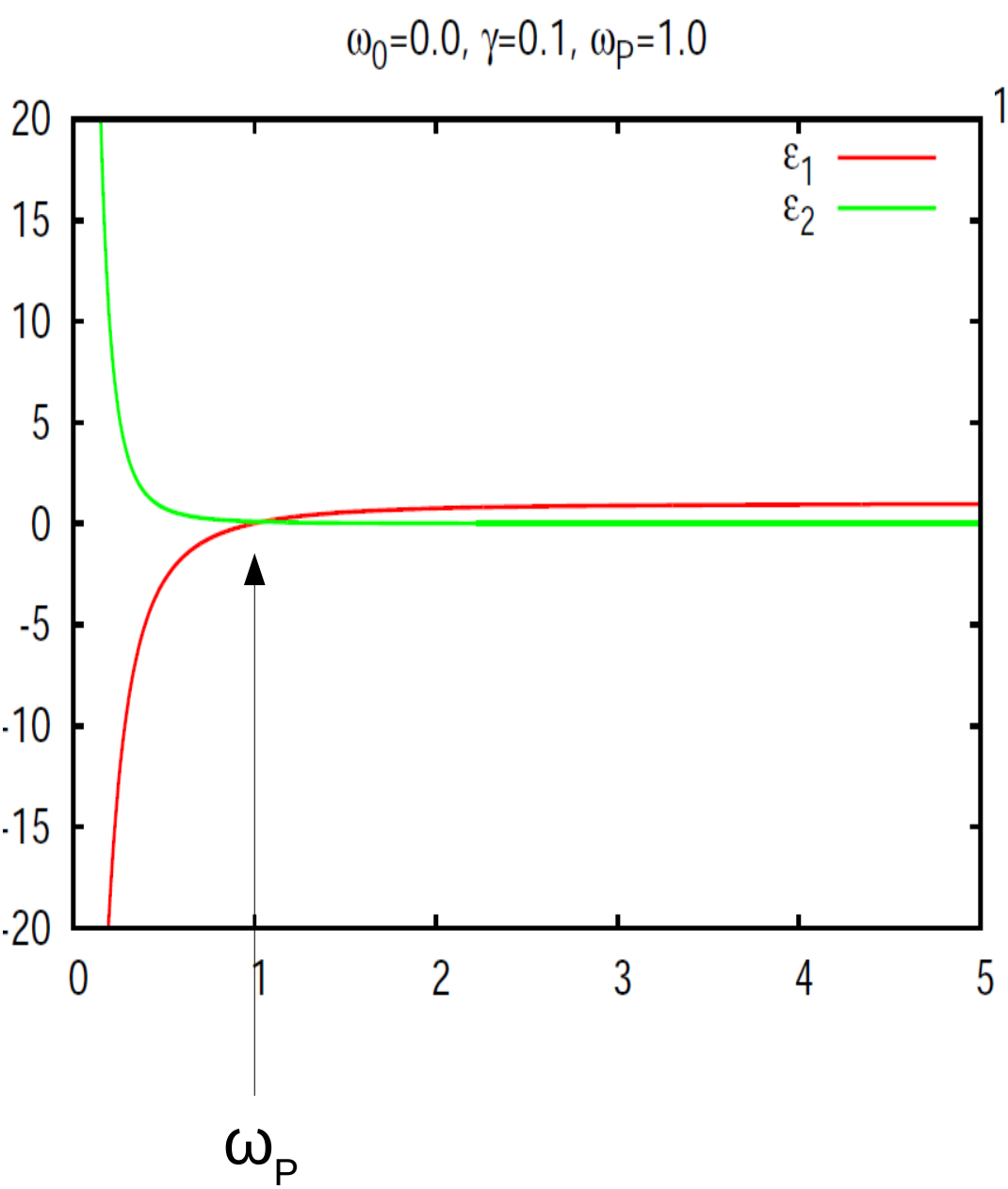

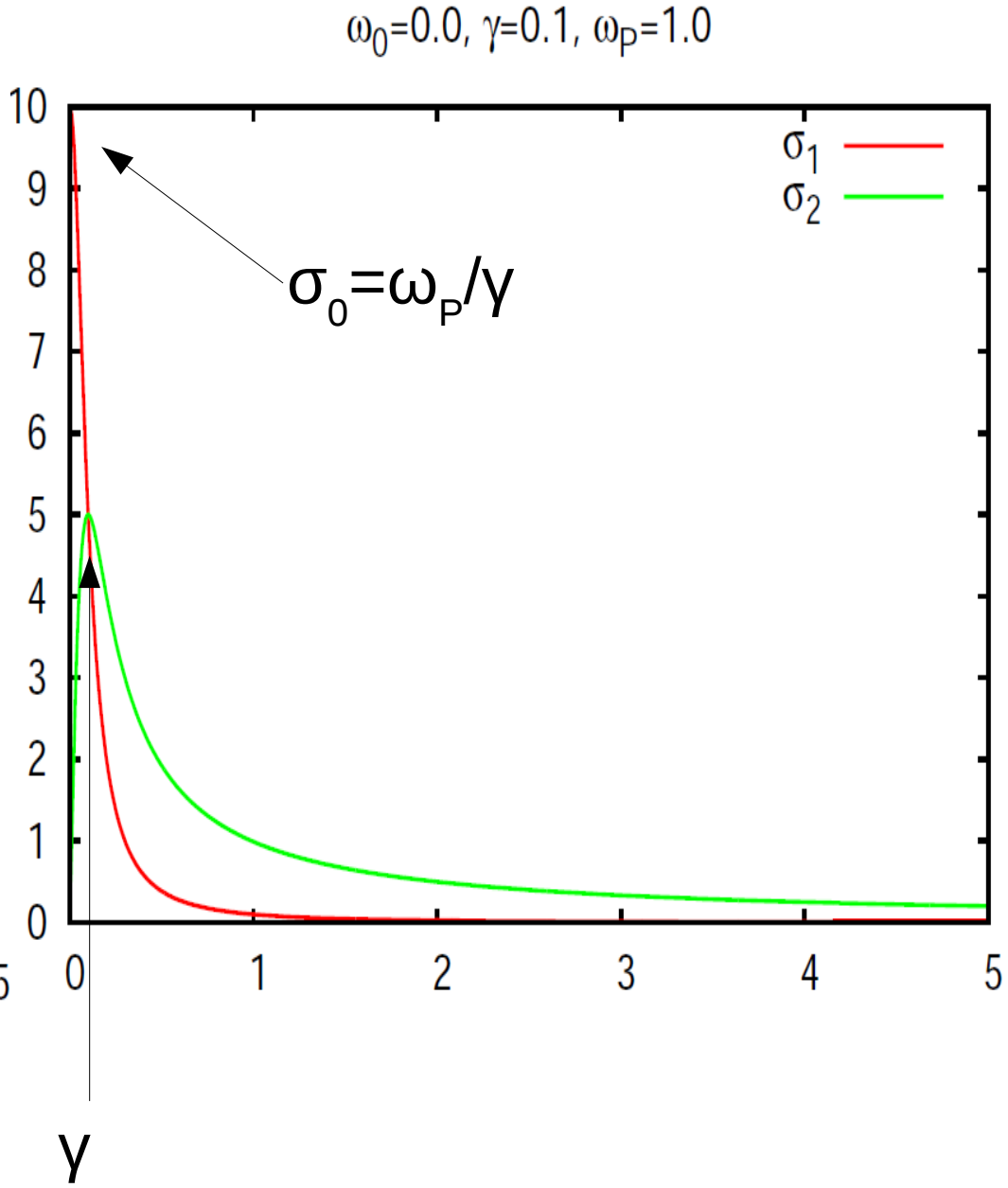

Drudeho model

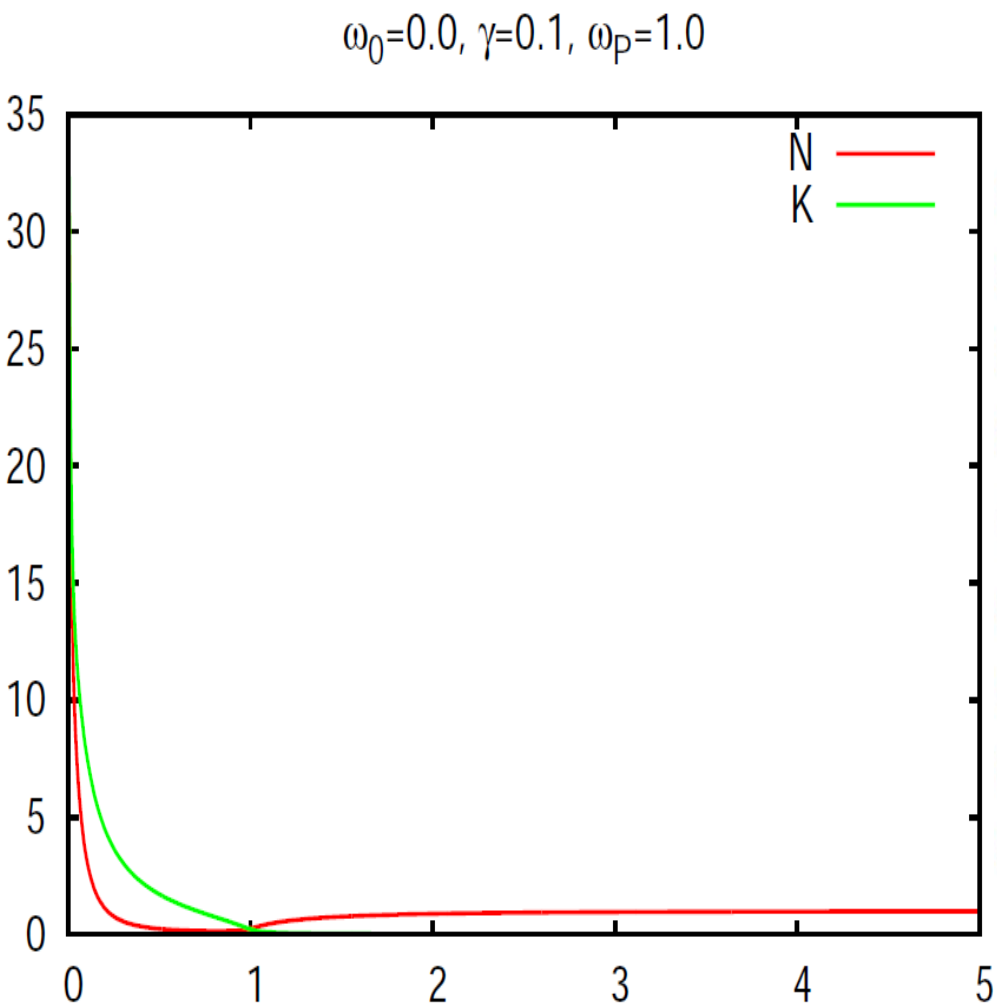

ω_P

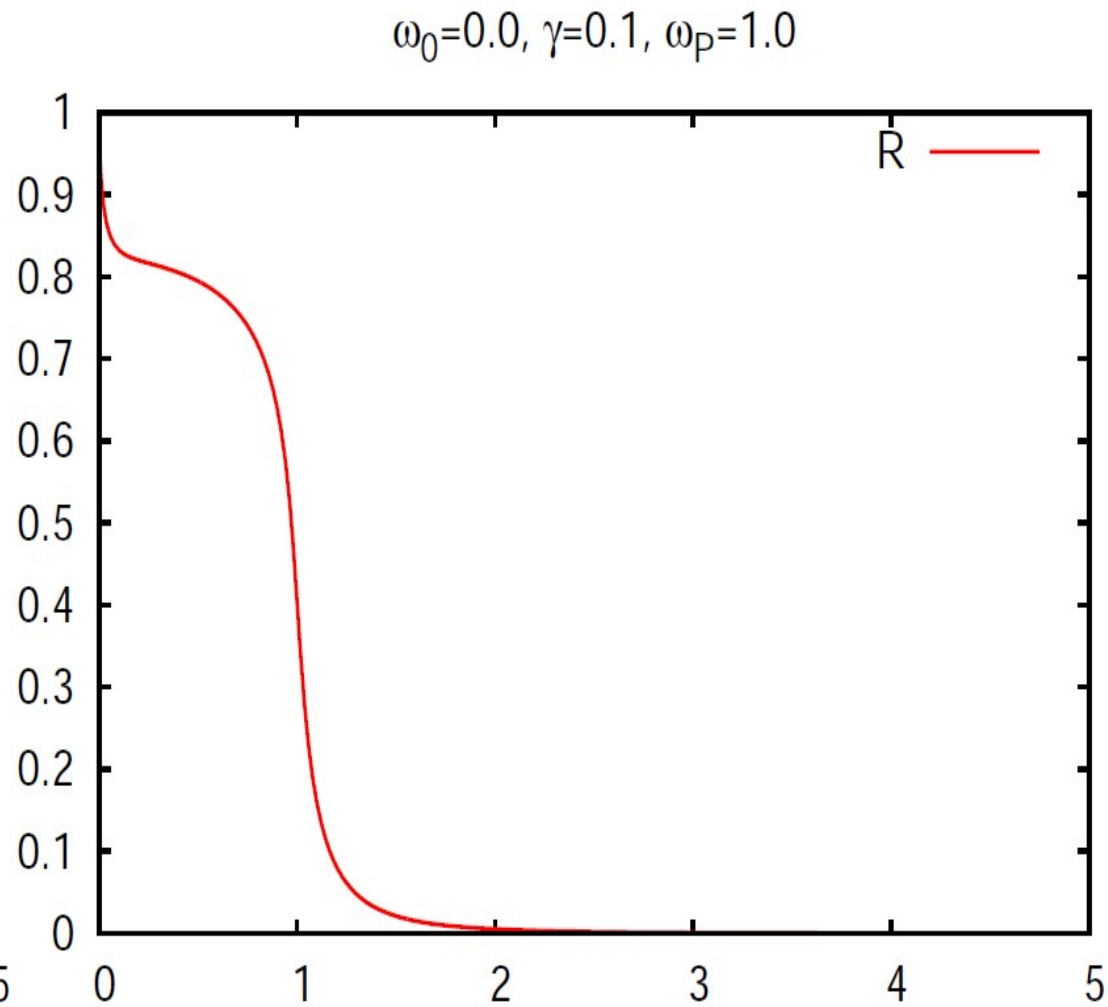

ω_P

Drudeho model

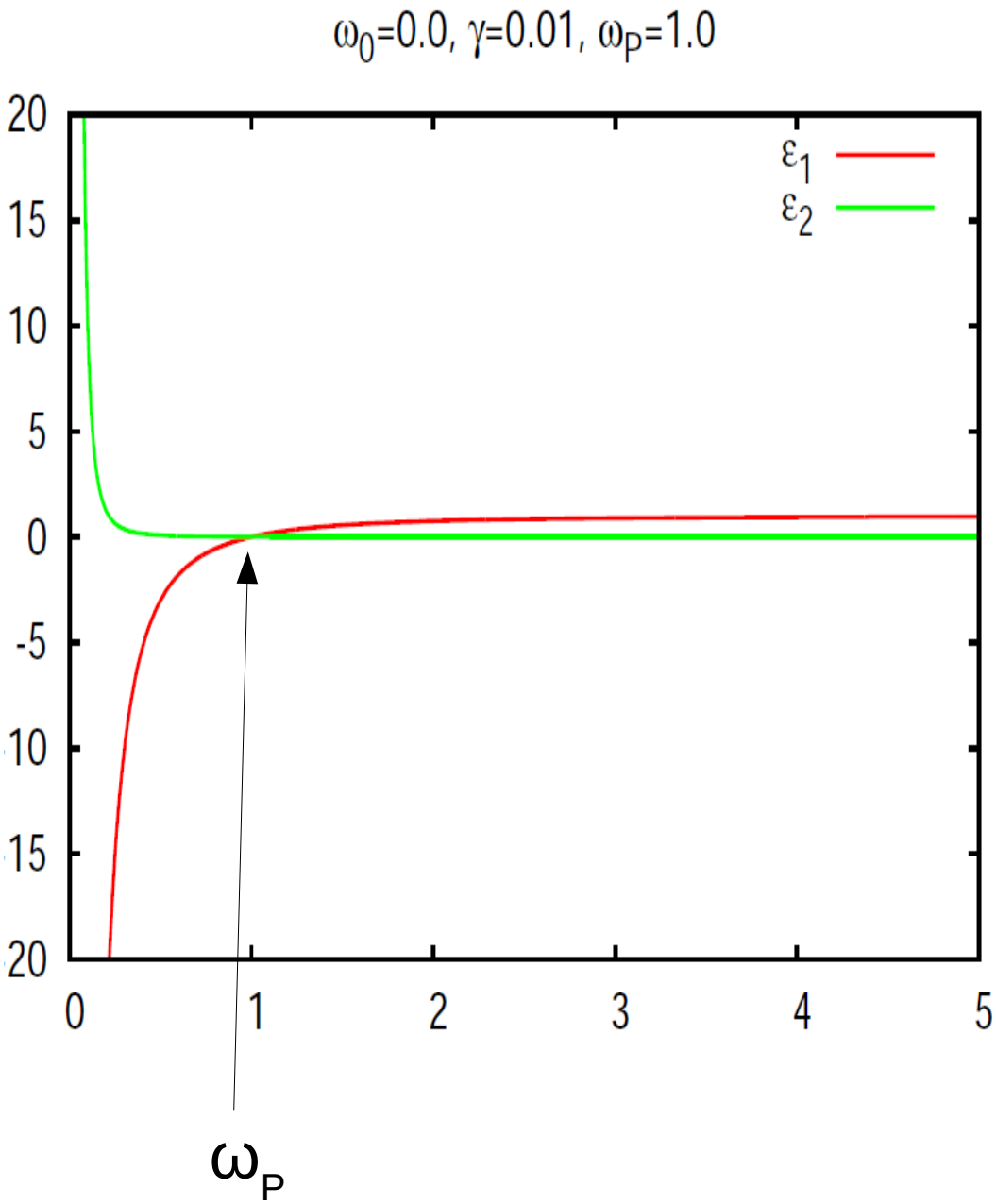

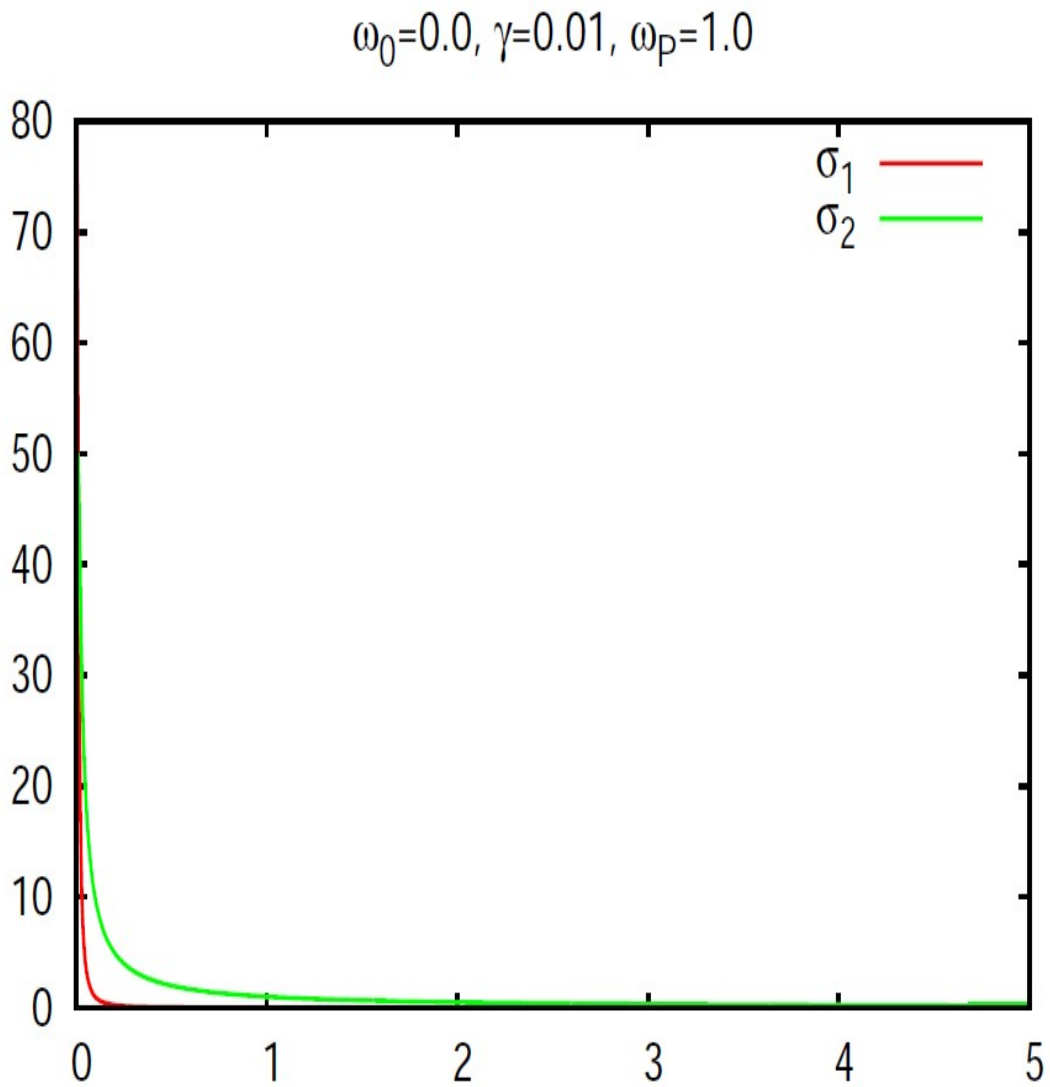

Drudeho model

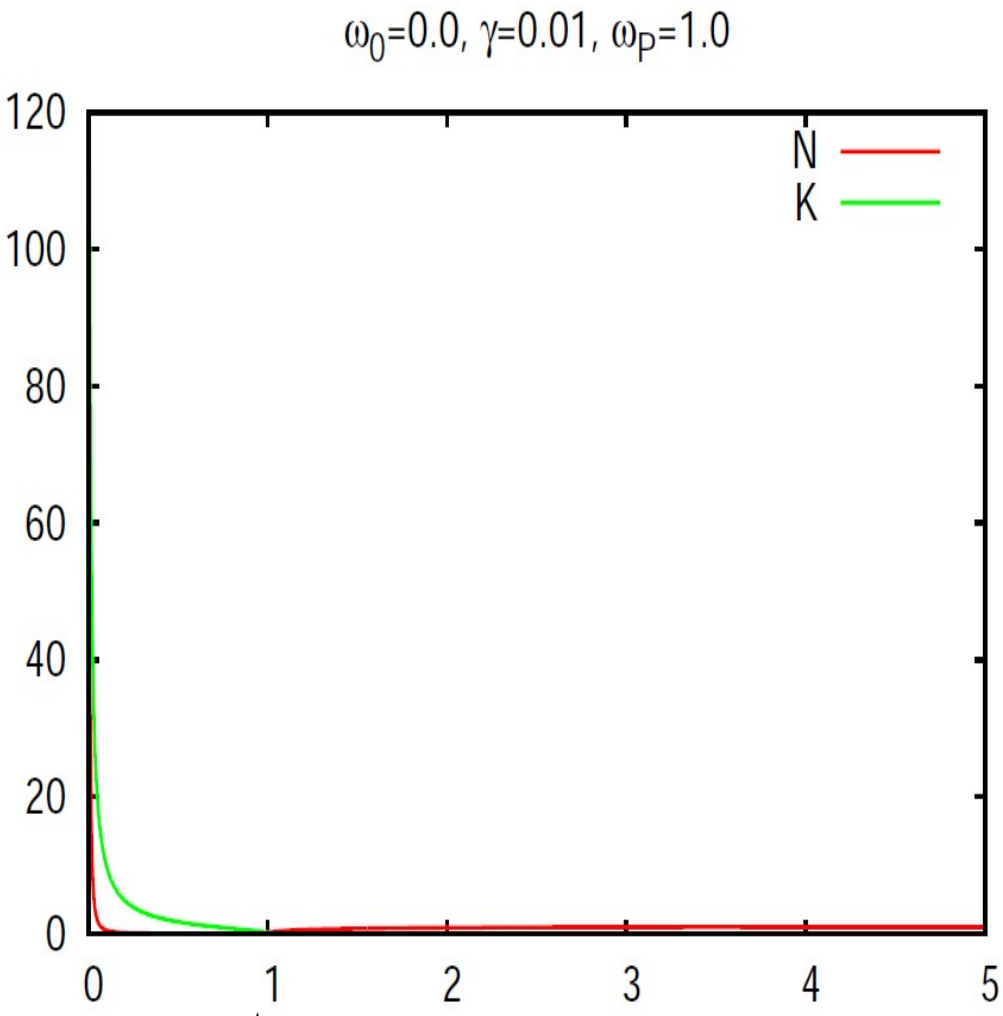

ω_P

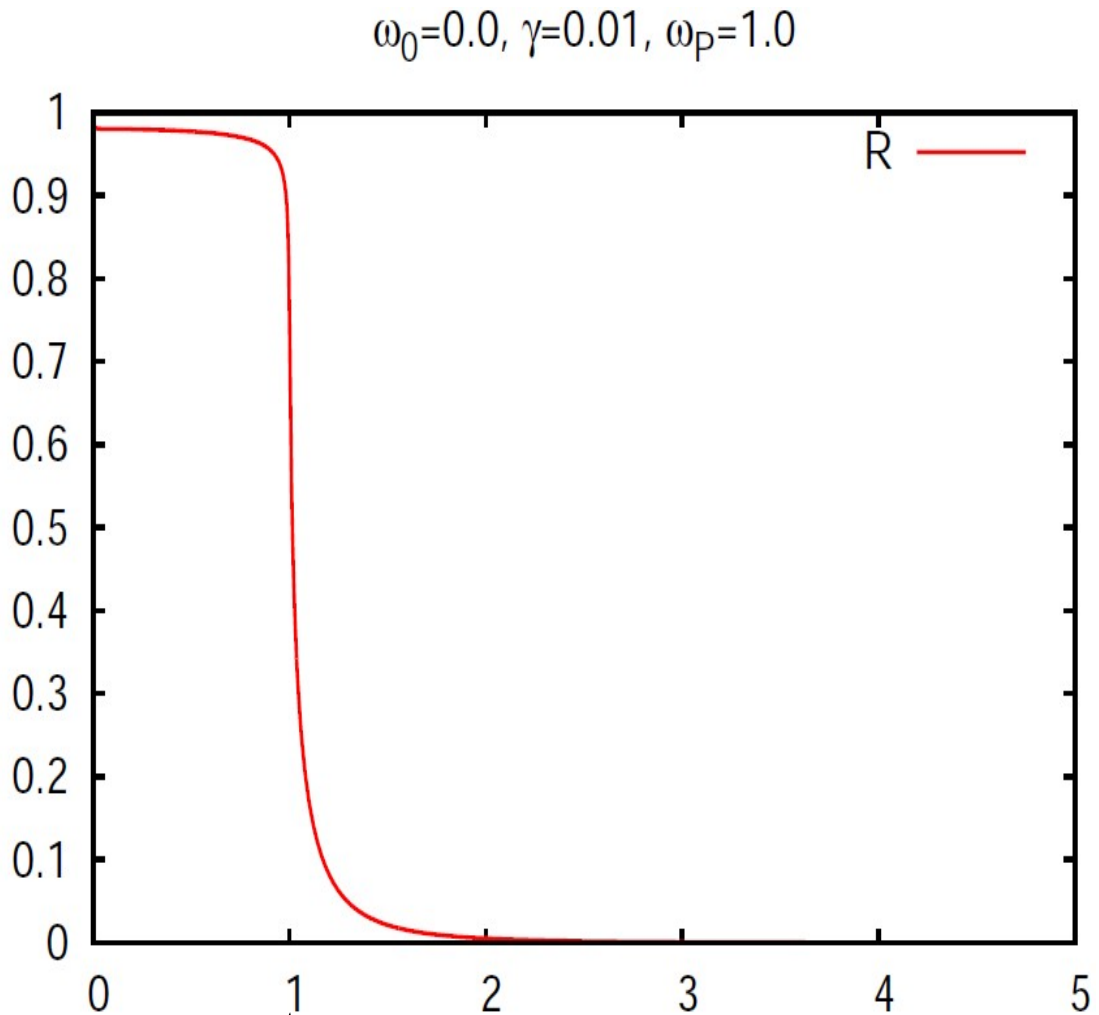

ω_P

Drudeho model

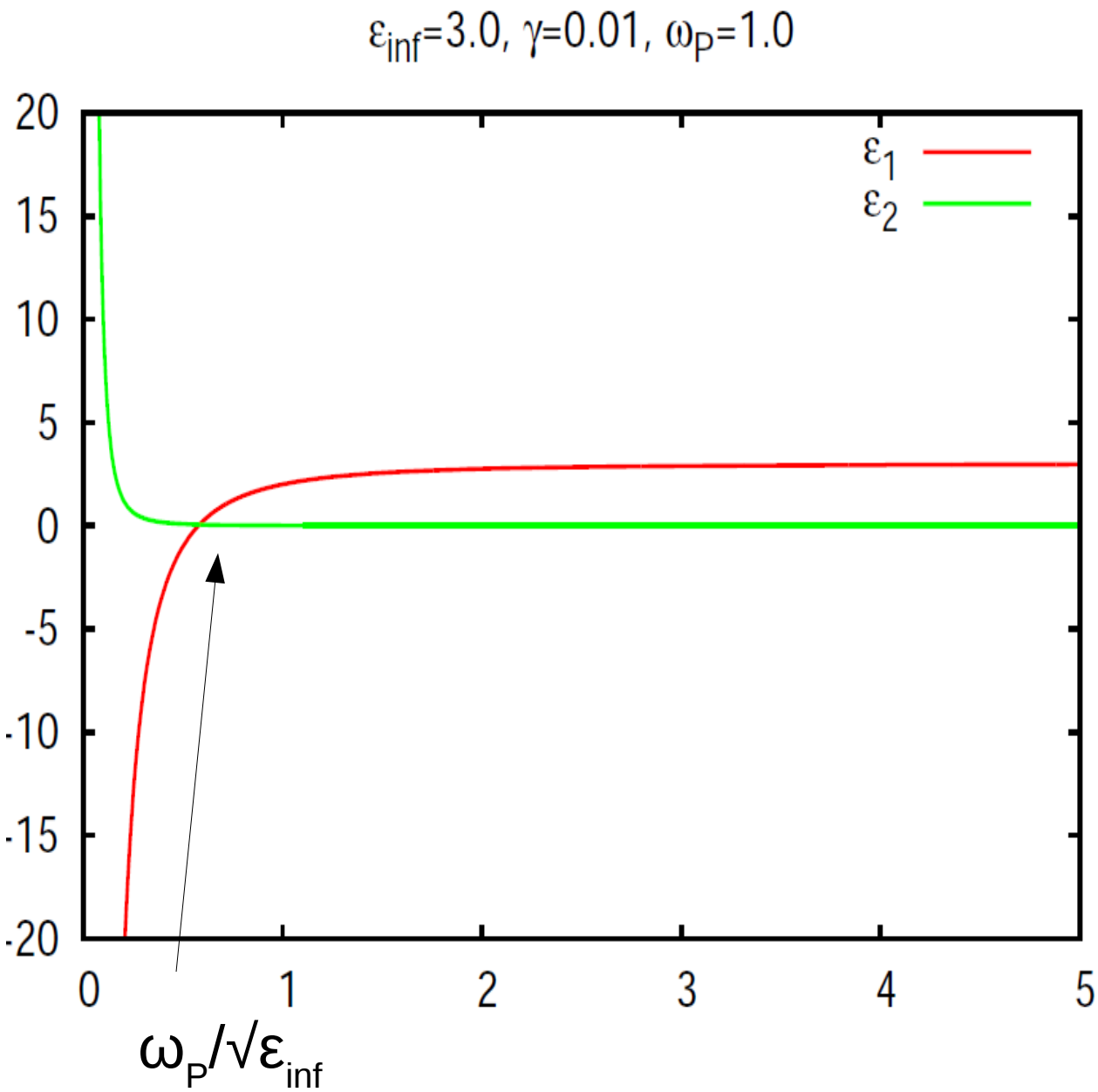

Drudeho model

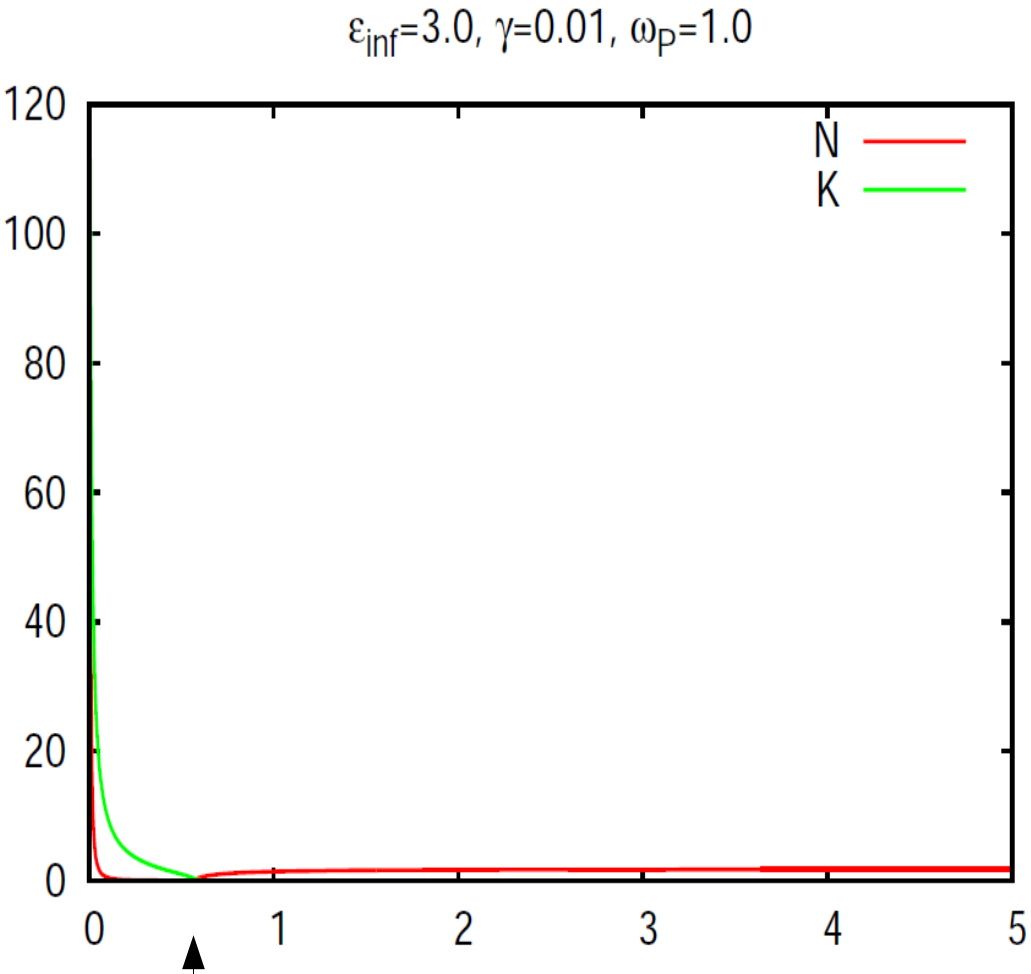

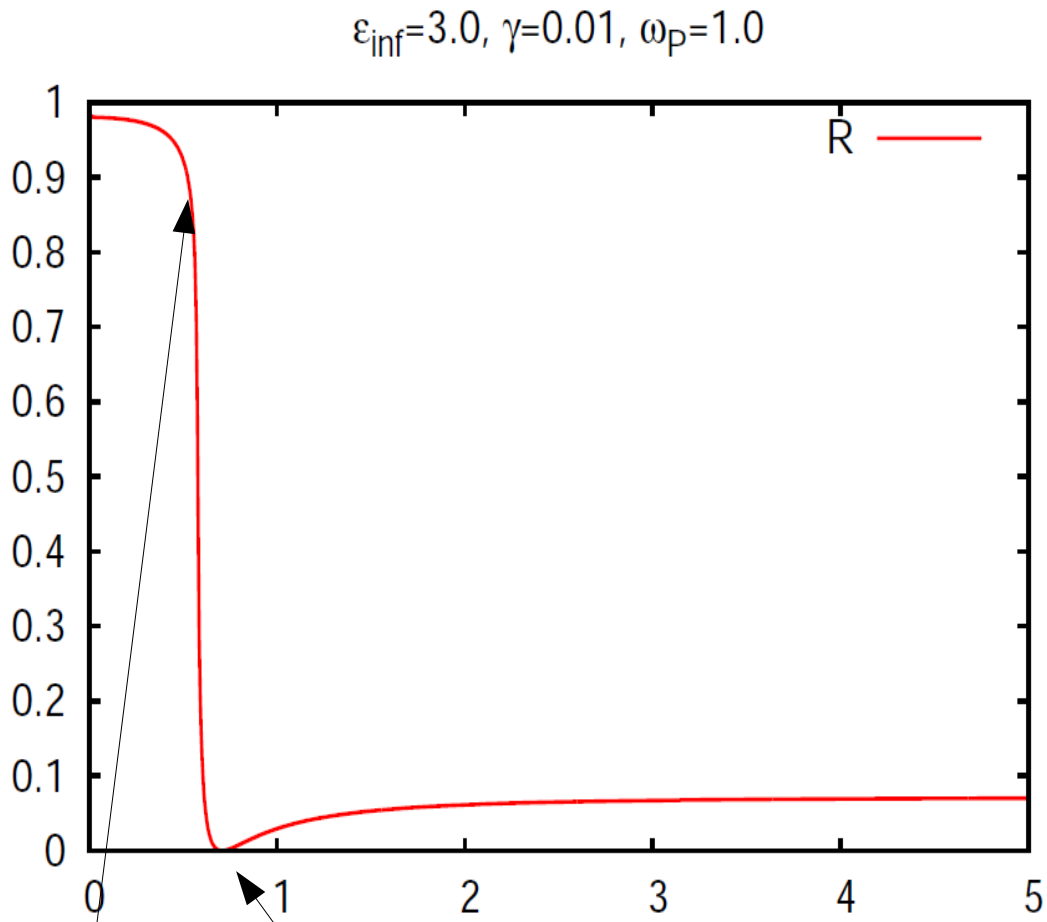

$\omega_P/\sqrt{\varepsilon_{inf}}$

$\omega_P/\sqrt{\varepsilon_{inf}}$
$\varepsilon_1=0$

$\omega_P/\sqrt{\varepsilon_{inf}}-1$
$\varepsilon_1=1$

Drudeho model

- ϵ real and > 0. For ω real, K is real and a transverse electromagnetic wave propagates with the phase velocity $c/\epsilon^{1/2}$.
- ϵ real and < 0. For ω real, K is imaginary and the wave is damped with a characteristic length $1/|K|$.
- ϵ complex. For ω real, $\mathbf{K}$ is complex and the waves are damped in space.
- $\epsilon = \infty$. This means the system has a finite response in the absence of an applied force; thus the poles of $\epsilon(\omega,\mathbf{K})$ define the frequencies of the free oscillations of the medium.
- $\epsilon = 0$. We shall see that longitudinally polarized waves are possible only at the zeros of ϵ.

(CGS) $$\epsilon(\omega)\omega^2 = \epsilon(\infty)(\omega^2 - \tilde{\omega}_p^2)$$

(CGS) $$\omega^2 = \tilde{\omega}_p^2 + c^2K^2/\epsilon(\infty)$$

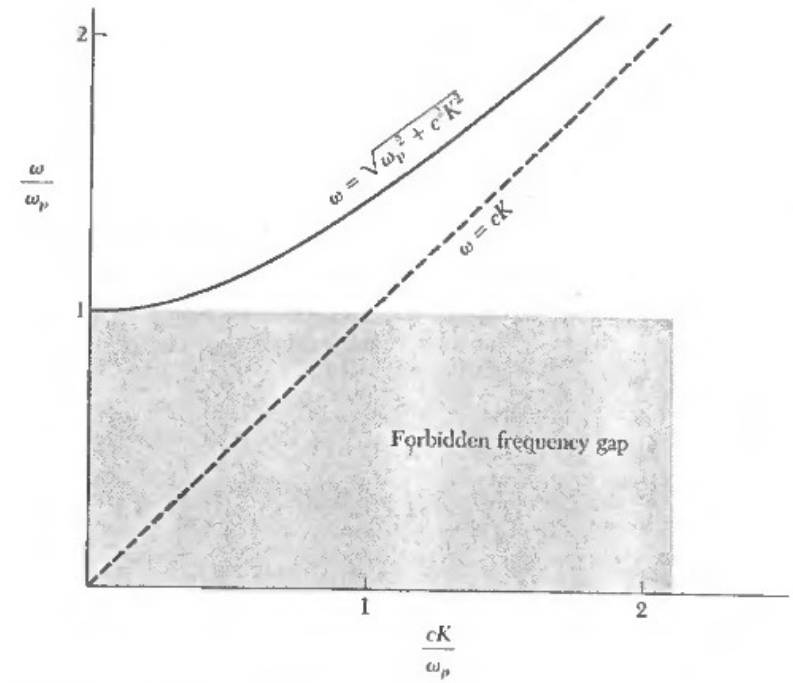

Figure 2 Dispersion relation for transverse electromagnetic waves in a plasma. The group velocity $v_g = d\omega/dK$ is the slope of the dispersion curve. Although the dielectric function is between zero and one, the group velocity is less than the velocity of light in vacuum.

Drudeho model

	$\hbar\omega$ (eV), $\varepsilon_1=0$
Al	11
Au	5.5
Ir	7.8
Mo	1.5
Ni	9.4
Ag	3.8
W	1.3

Drudeho parametry čistých kovů

	$\hbar\omega_P$ (eV)	τ (10^{-14} s)	$\hbar/\tau$ (eV)
Al	7.5 – 13	0.3 – 2.1	1.4 – 0.2
Au	6.9 – 10.5	0.4 – 4.3	1 – 0.1
Ni	3.6 – 4.8	0.2 – 2.2	2.1 – 0.19
Ag	7.8 – 9.8	0.9 – 2.6	0.46 – 0.16

Drudeho parametry čistých kovů

The plasma frequency ω_p is calculated from eqn 7.6, and λ_p is the wavelength co
is frequency.

Metal	Valency	N (10^{28} m^{-3})	$\omega_p/2\pi$ (10^{15} Hz)	λ_p (nm)
Li (77 K)	1	4.70	1.95	154
Na (5 K)	1	2.65	1.46	205
K (5 K)	1	1.40	1.06	282
Rb (5 K)	1	1.15	0.96	312
Cs (5 K)	1	0.91	0.86	350
Cu	1	8.47	2.61	115
Ag	1	5.86	2.17	138
Au	1	5.90	2.18	138
Be	2	24.7	4.46	67
Mg	2	8.61	2.63	114
Ca	2	4.61	1.93	156
Al	3	18.1	3.82	79

M. Fox: Optical properties of solids, Oxford university press, 2001.

Odrazivost stříbra

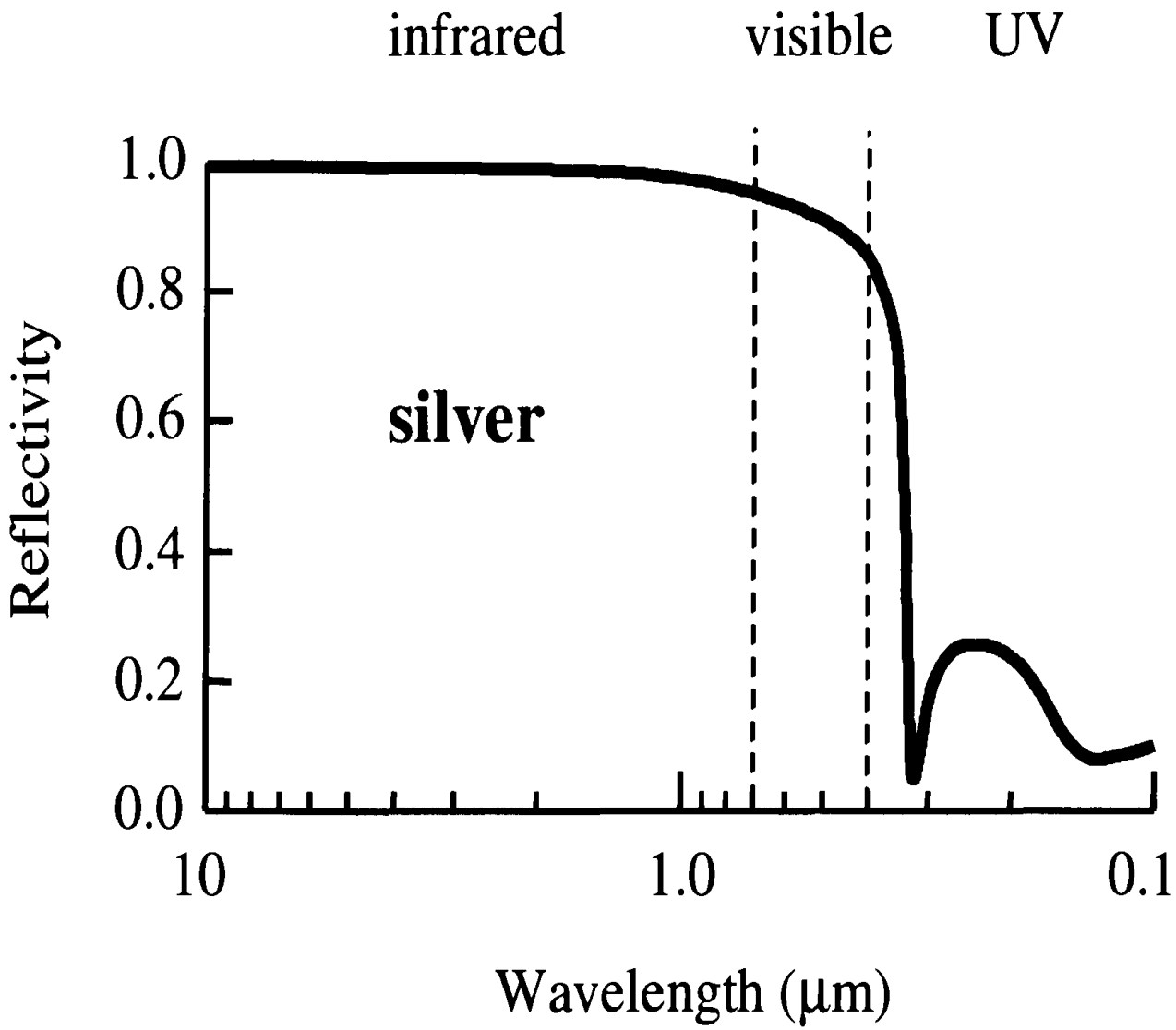

M. Fox: Optical properties of solids, Oxford university press, 2001.

Al

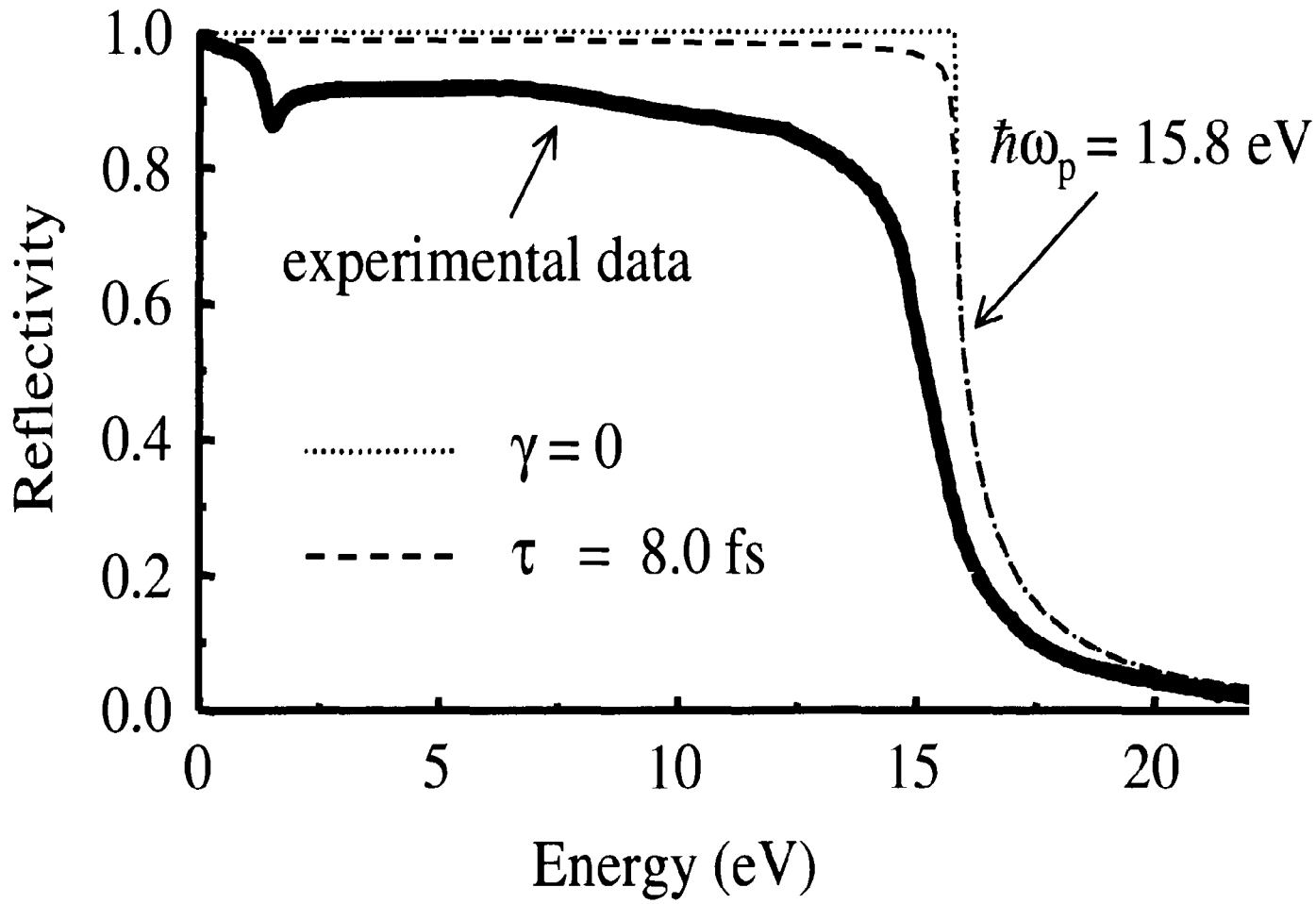

M. Fox: Optical properties of solids, Oxford university press, 2001.

Dopovaný polovodič InSb

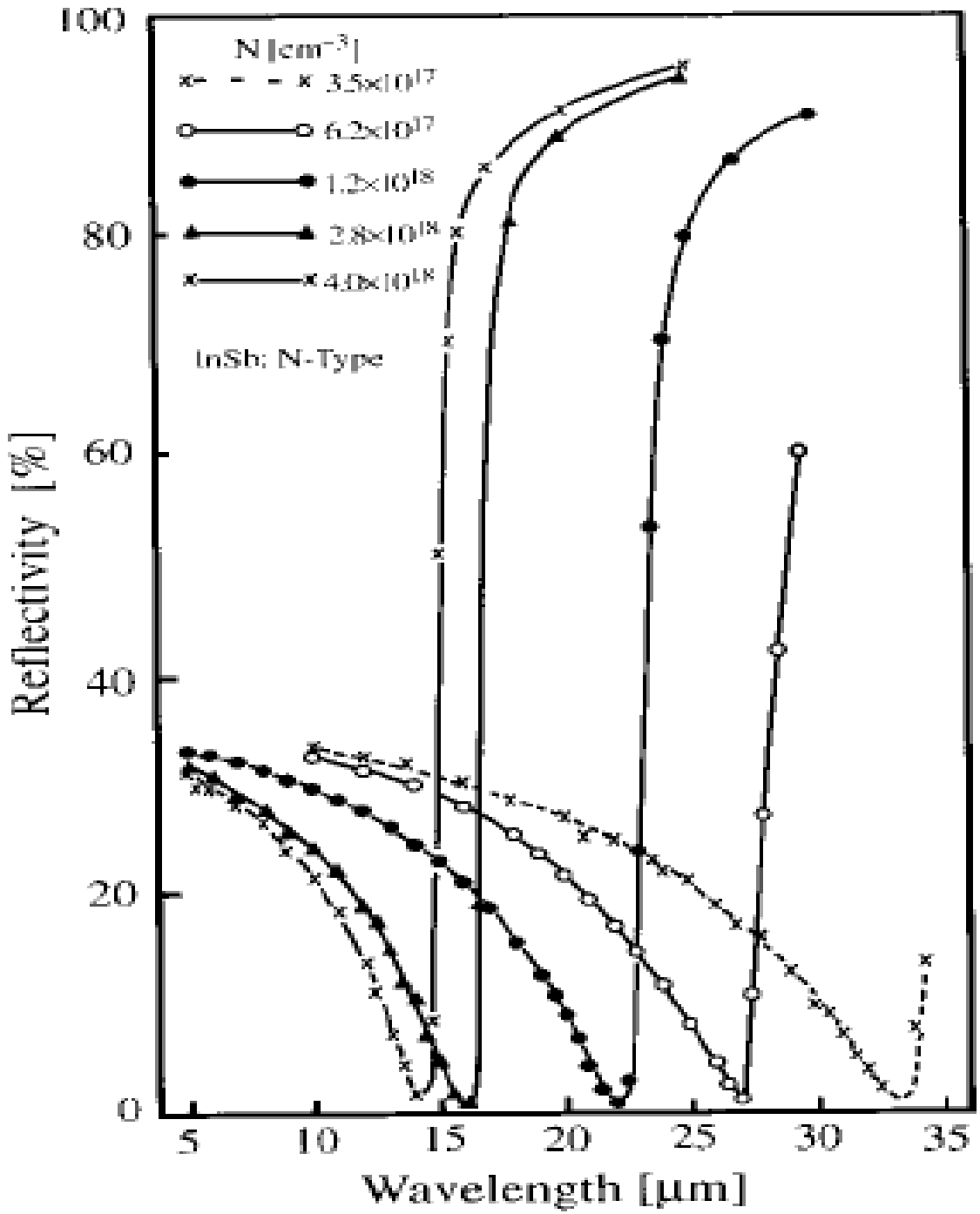

Yu, Cardona, Fundamentals of semiconductors, Springer 1996.

Index lomu a absorpce Al, odrazivost

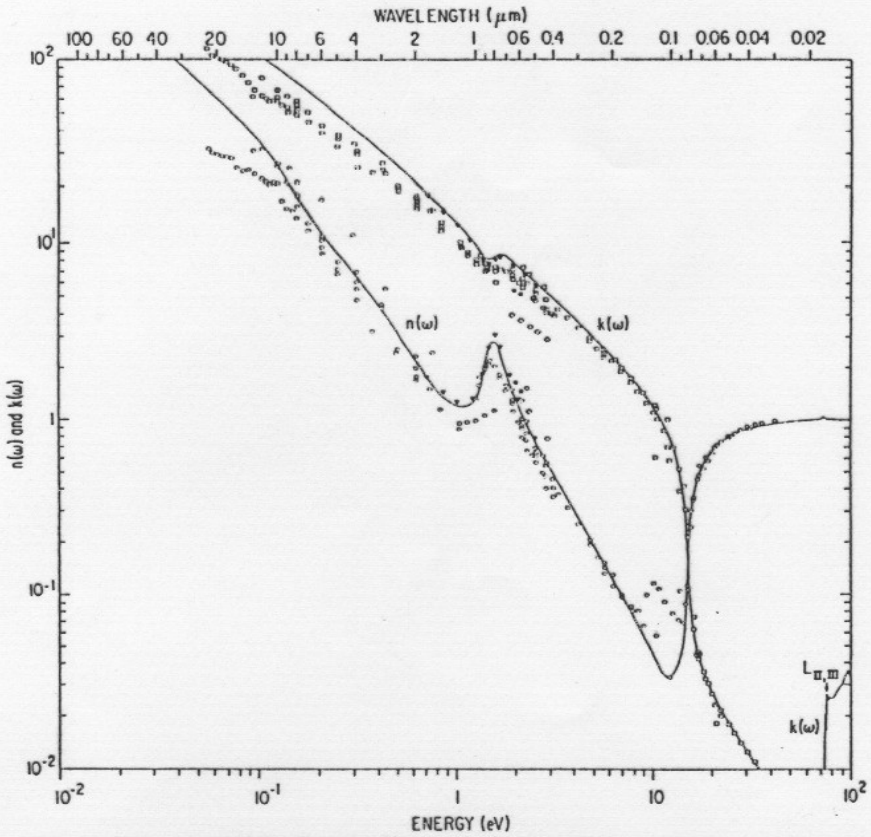

Fig. 14. The complex refractive index $n(\omega) + ik(\omega)$ for aluminum. The curves are taken from Shiles *et al.*'s [7] analysis of uhv reflectance data. A portion of the uhv ellipsometric data of Mathewson and Myers [100] is given for comparison. Quincke's [33] and Drude's [34] results for polished bulk samples are shown for historical interest; considering the materials and techniques available, these early measurements are remarkably good, especially for $n(\omega)$. The remainder of the data points are given to show the range of values of $n(\omega)$ (○) and $k(\omega)$ (□) reported in the literature. Most refer to evaporated films prepared in conventional or high vacuum and measured by using polarimetric, interferometric, and like methods. The sources of these data are given in the references [10, 11, 25, 26, 27, 51, 55 56, 65, 66, 73, 75, 91, and 121–129]. Note that the curves for $n(\omega)$ and $k(\omega)$ curve cross each other at roughly 15 eV, the plasmon energy. This corresponds to the plasmon condition $\varepsilon_1(\omega_p) = n^2(\omega_p) - k^2(\omega_p) \approx 0$. The onset of the L-shell absorption appears in the lower-right-hand corner. The corresponding dispersion

Quincke [33]. ◇; Drude [34], •.)

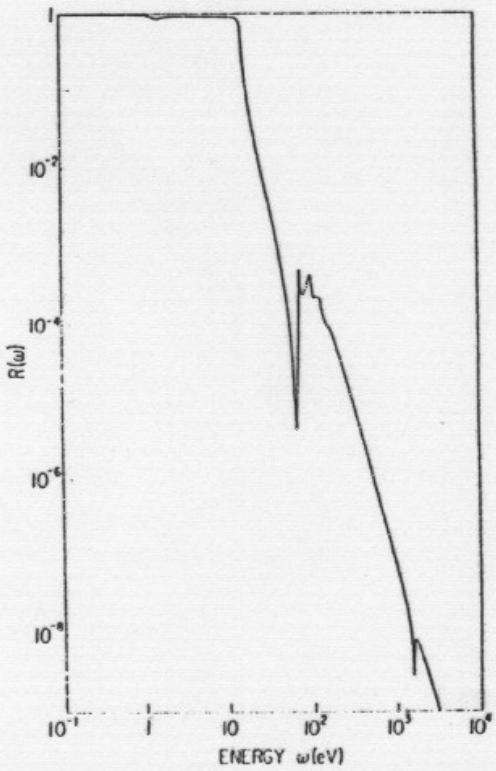

Fig. 15. The reflectance $R(\omega)$ at normal incidence of a smooth oxide-free metal surface in vacuum. (After Shiles *et al.* [7].)

Palik, Handbook of Optical Constants of Solids, Elsevier 1998.

GaAs

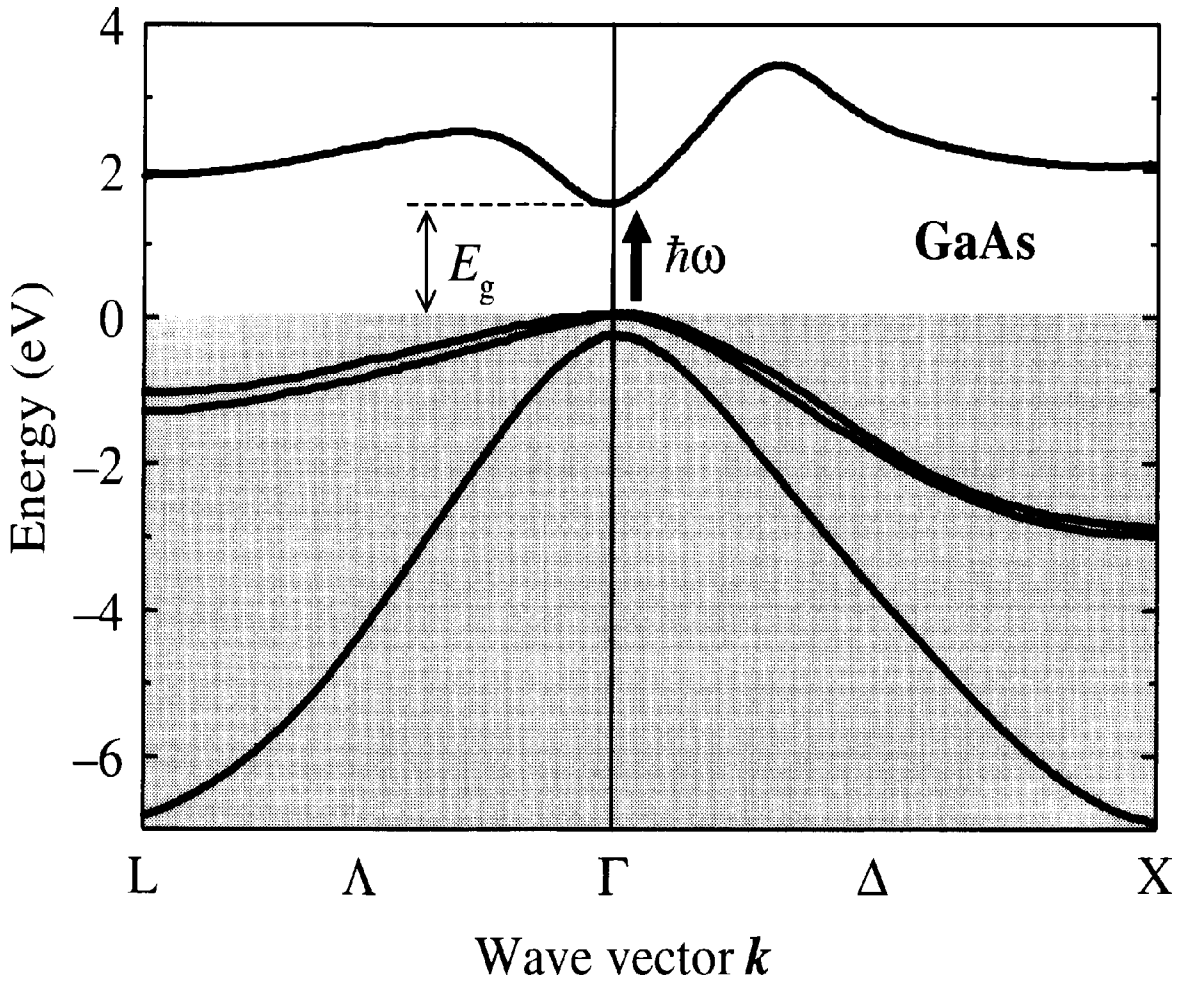

M. Fox: Optical properties of solids, Oxford university press, 2001.

GaAs, pásová struktura

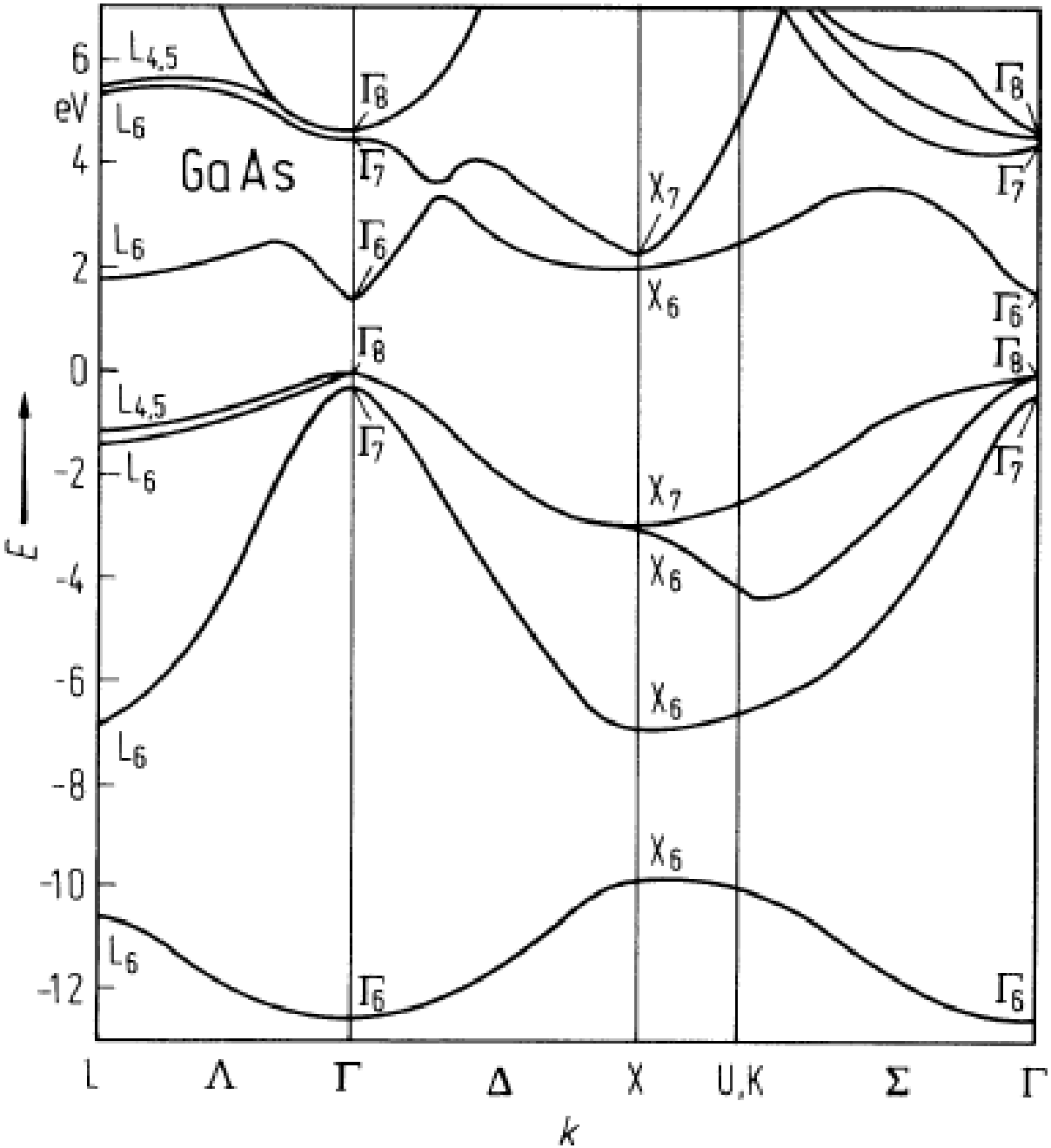

Madelung, Semiconductors data handbook, Springer

GaAs – dielektrická funkce

ε_2

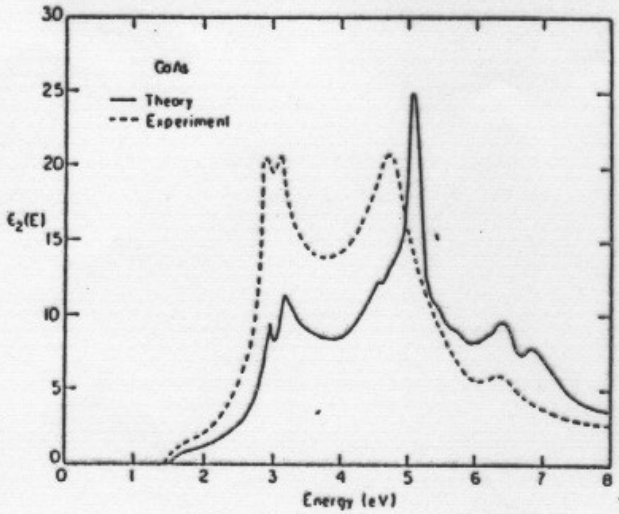

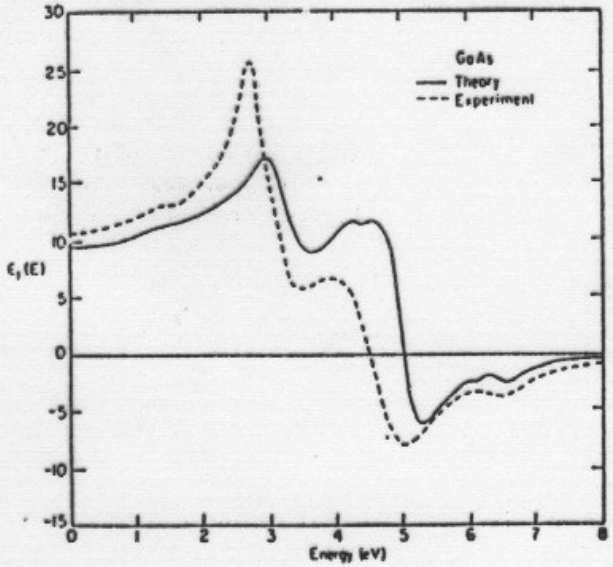

ε_1

R

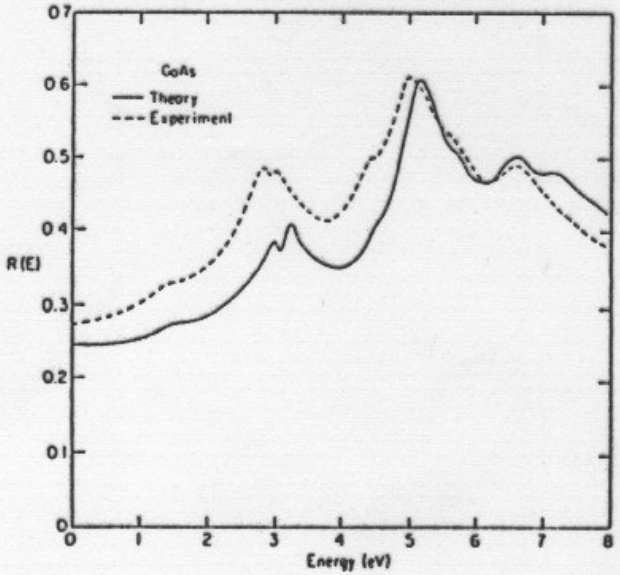

Fig. 8.24. Reflectivity spectrum for gallium arsenide. The experimental data is from [8.7]

105

Chelikovsky, Cohen, Electronic structure and optical properties of semiconductors, Springer, 1989.

InAs

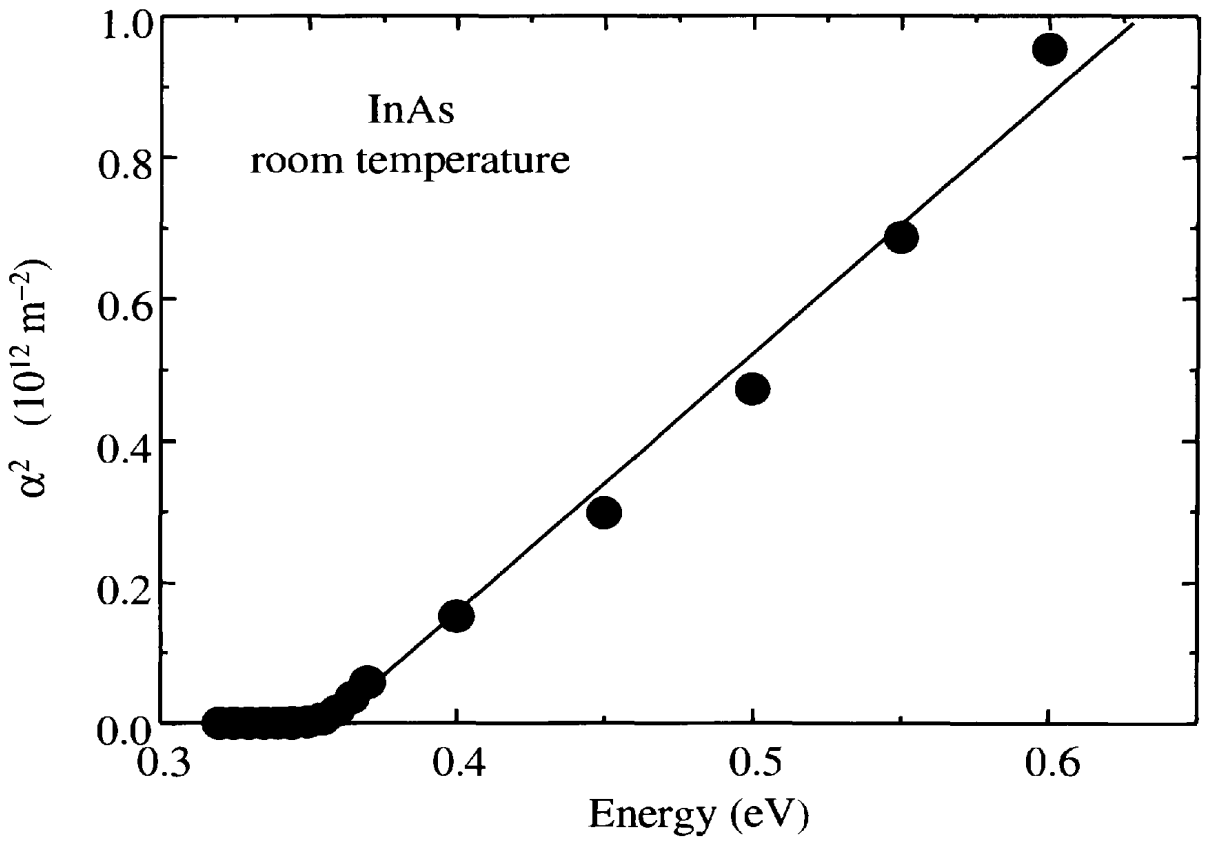

states given by eqn 3.24. We therefore expect the following behaviour
$\hbar\omega$):

$$\text{For } \hbar\omega < E_g, \quad \alpha(\hbar\omega) = 0.$$
$$\text{For } \hbar\omega \geq E_g, \quad \alpha(\hbar\omega) \propto (\hbar\omega - E_g)^{\frac{1}{2}}. \qquad (3$$

M. Fox: Optical properties of solids, Oxford university press, 2001.

InSb

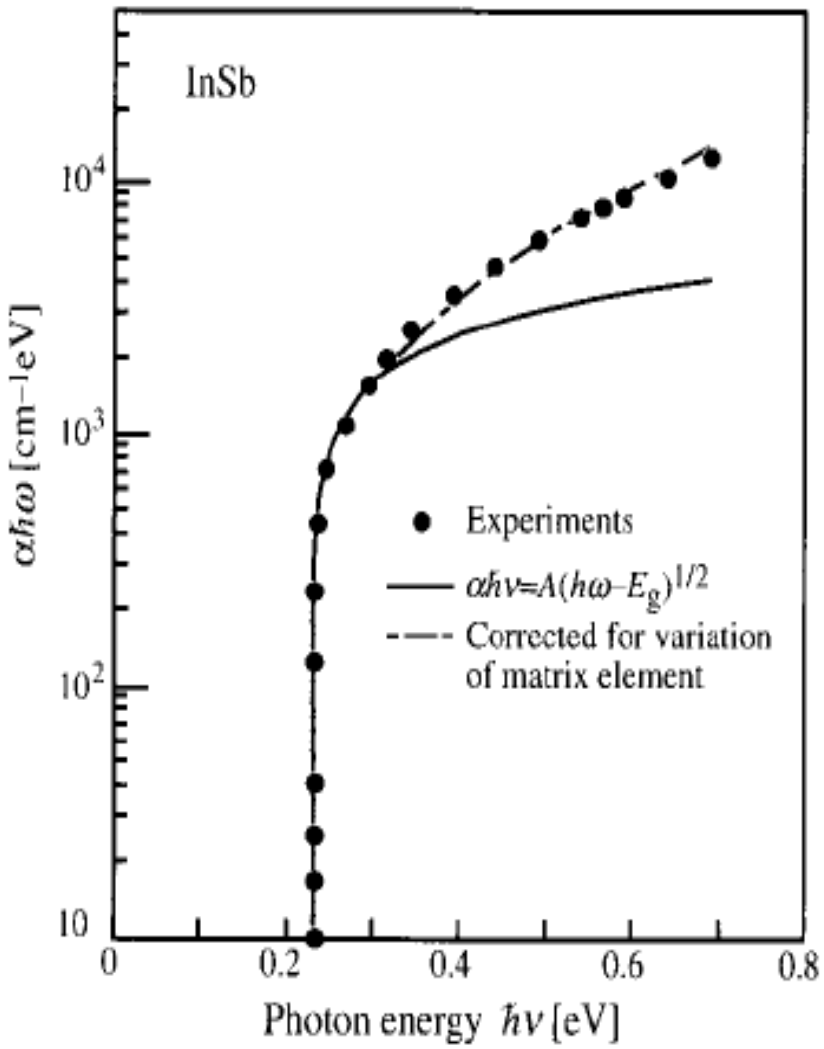

Fig. 6.15. Semilogarithmic plot of the absorption coefficient of InSb at 5 K as a function of photon energy. The *filled circles* represent experimental results from [6.24]. The *curves* have been calculated using various models. The intercept with the x-axis gives the direct bandgap of InSb [6.25]

P. Yu, M. Cardona: Fundamentals of semiconductors, Springer 1996.

GaAs, Ge a Si

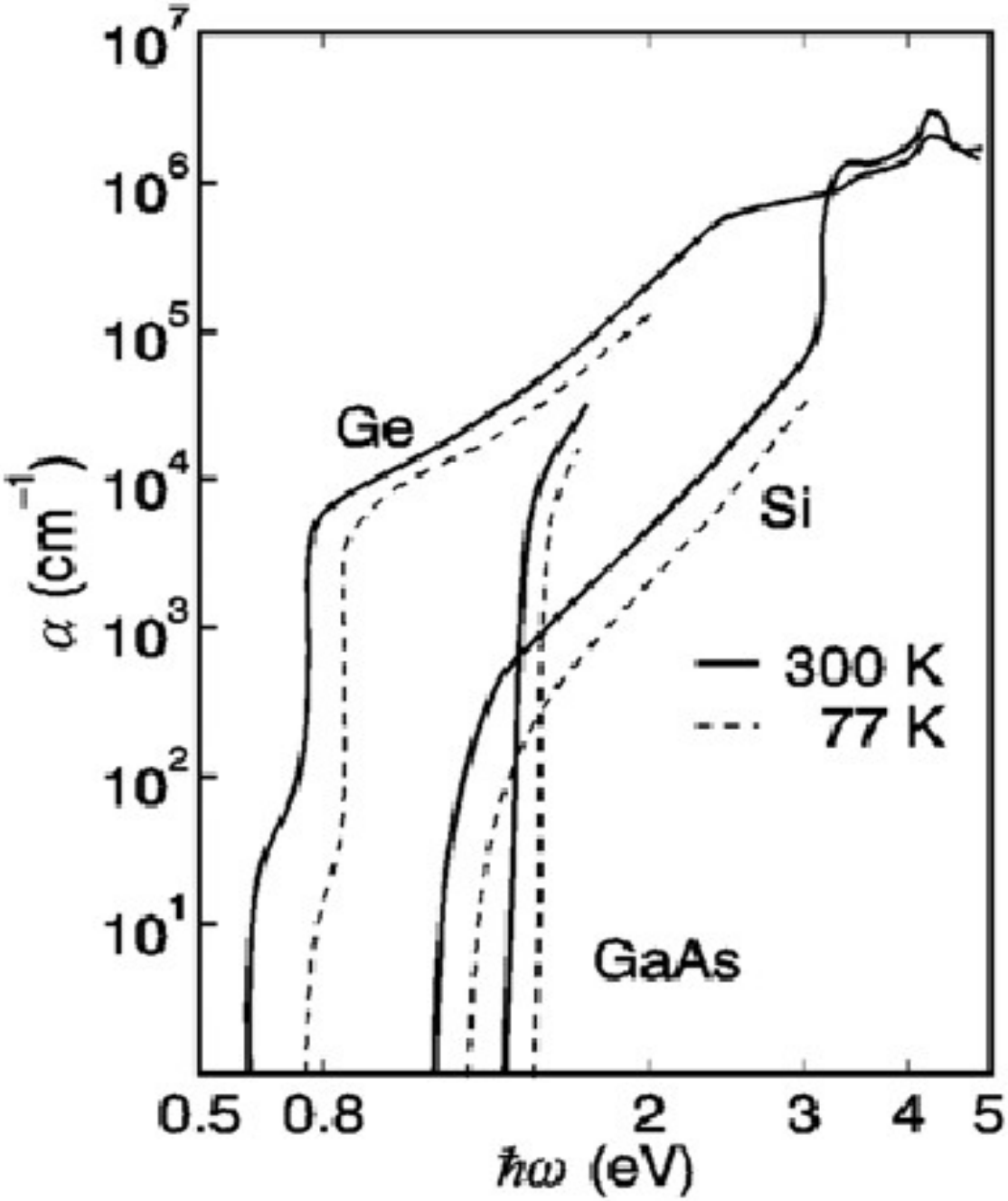

H. Kuzmany: Solid state spectroscopy, Springer 2009.

Si

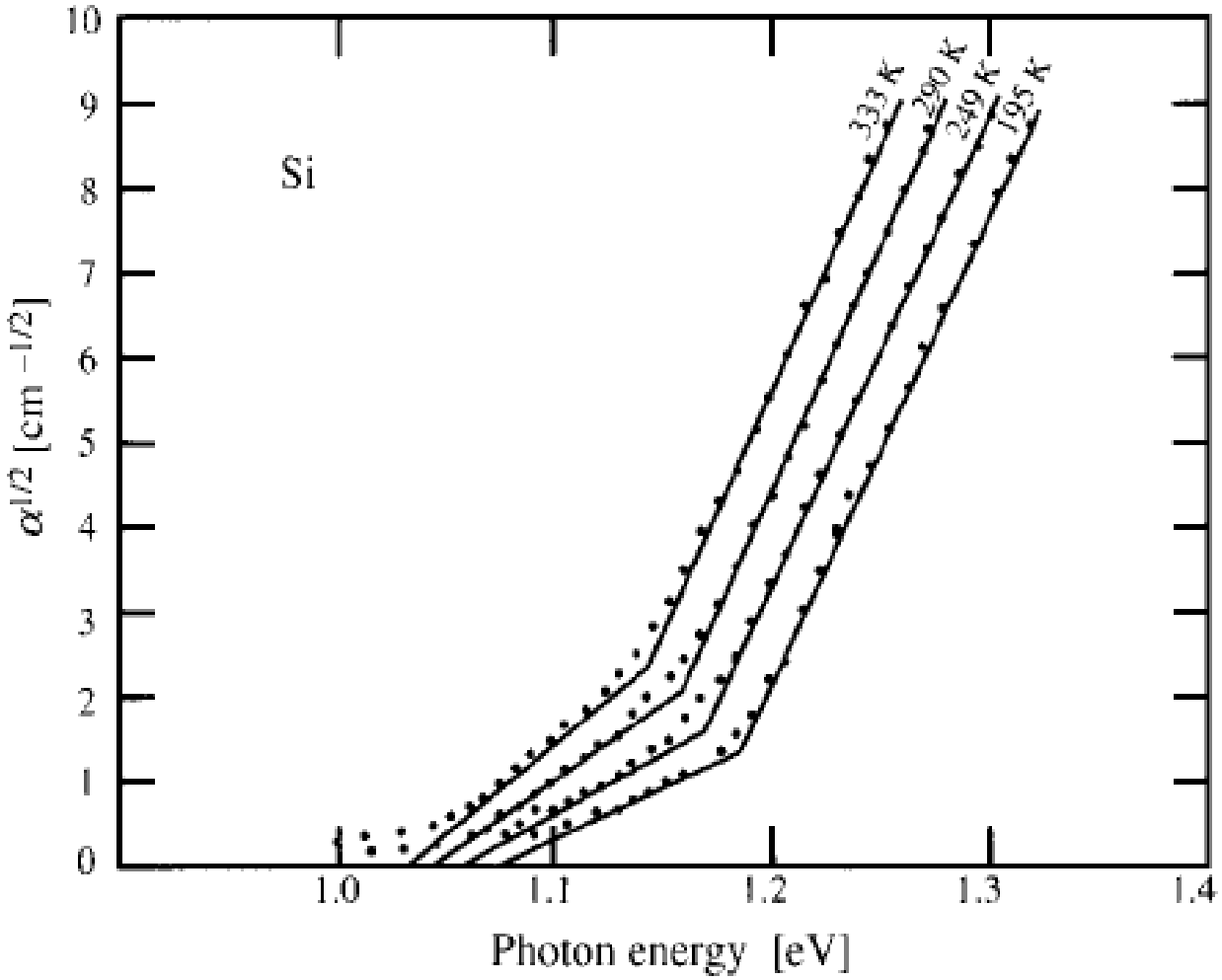

Fig. 6.17. Plots of the square root of the absorption coefficients of Si versus photon energy at several temperatures. The two segments of a straight line drawn through the experimental points represent the two contributions due to phonon absorption and emission [6.26]

P. Yu, M. Cardona: Fundamentals of semiconductors, Springer 1996.

Si

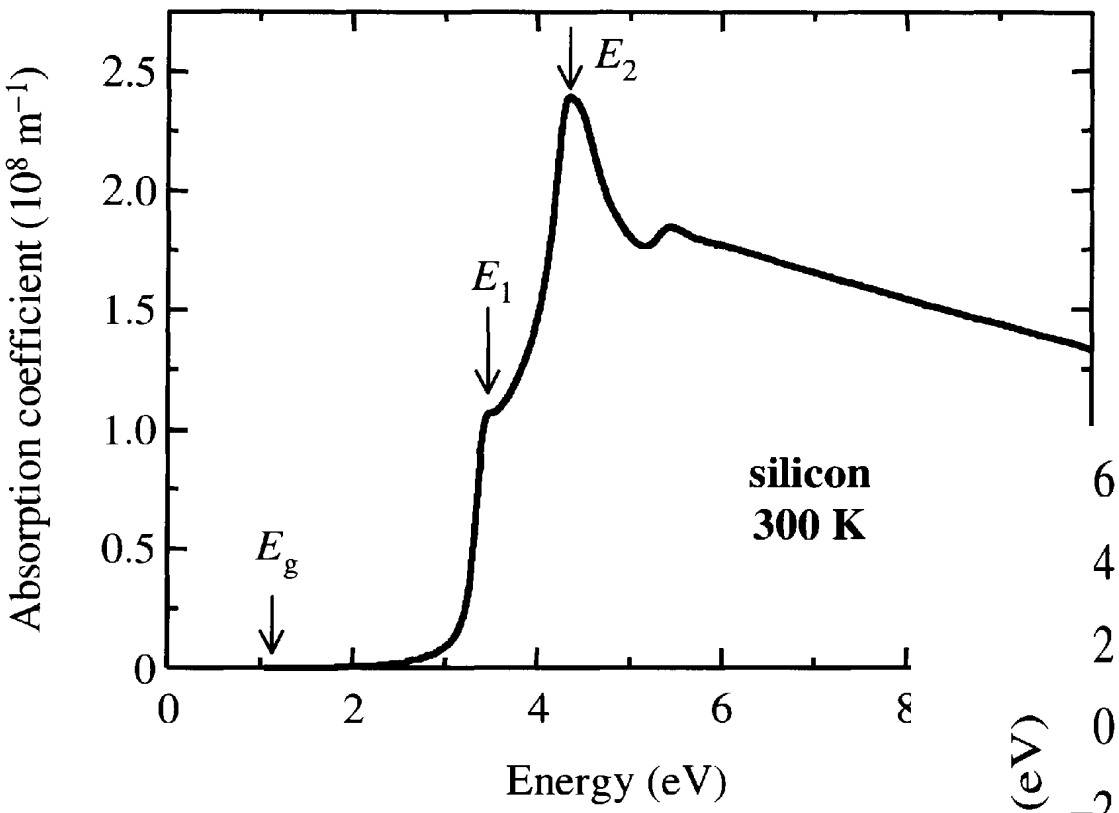

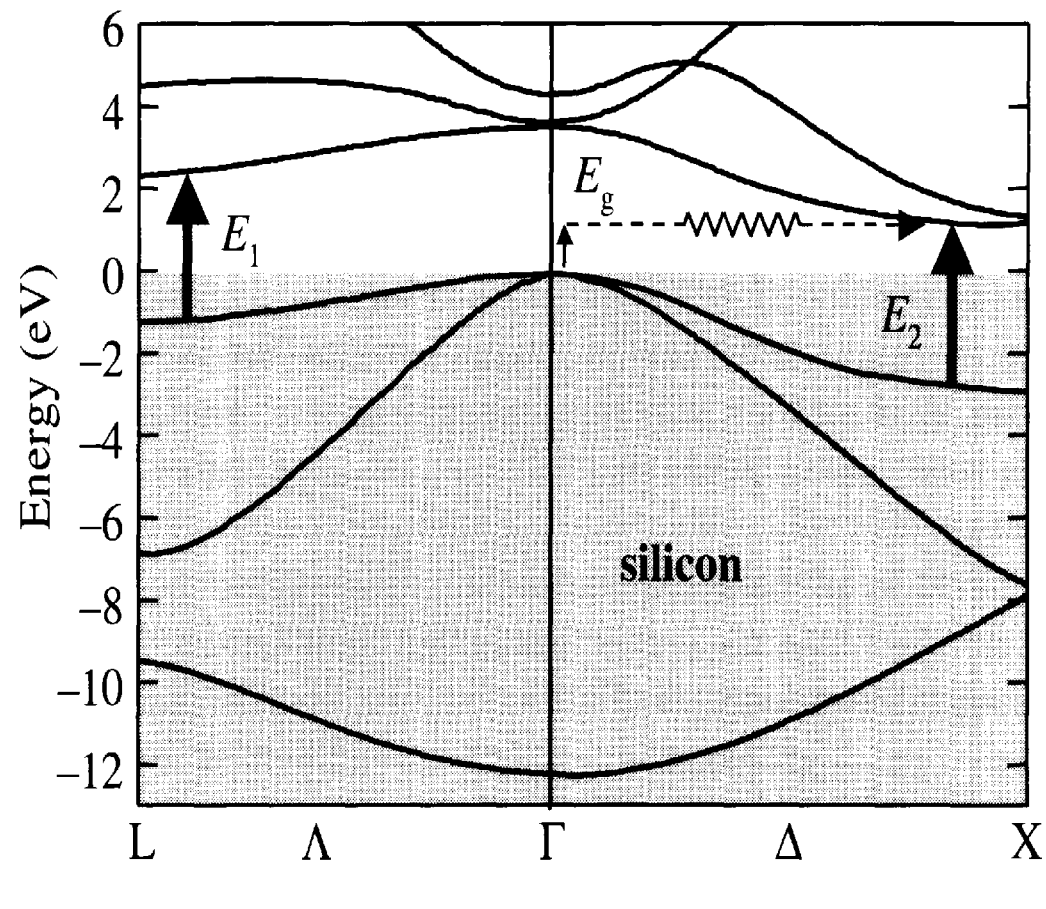

M. Fox: Optical properties of solids, Oxford university press, 2001.

Ge

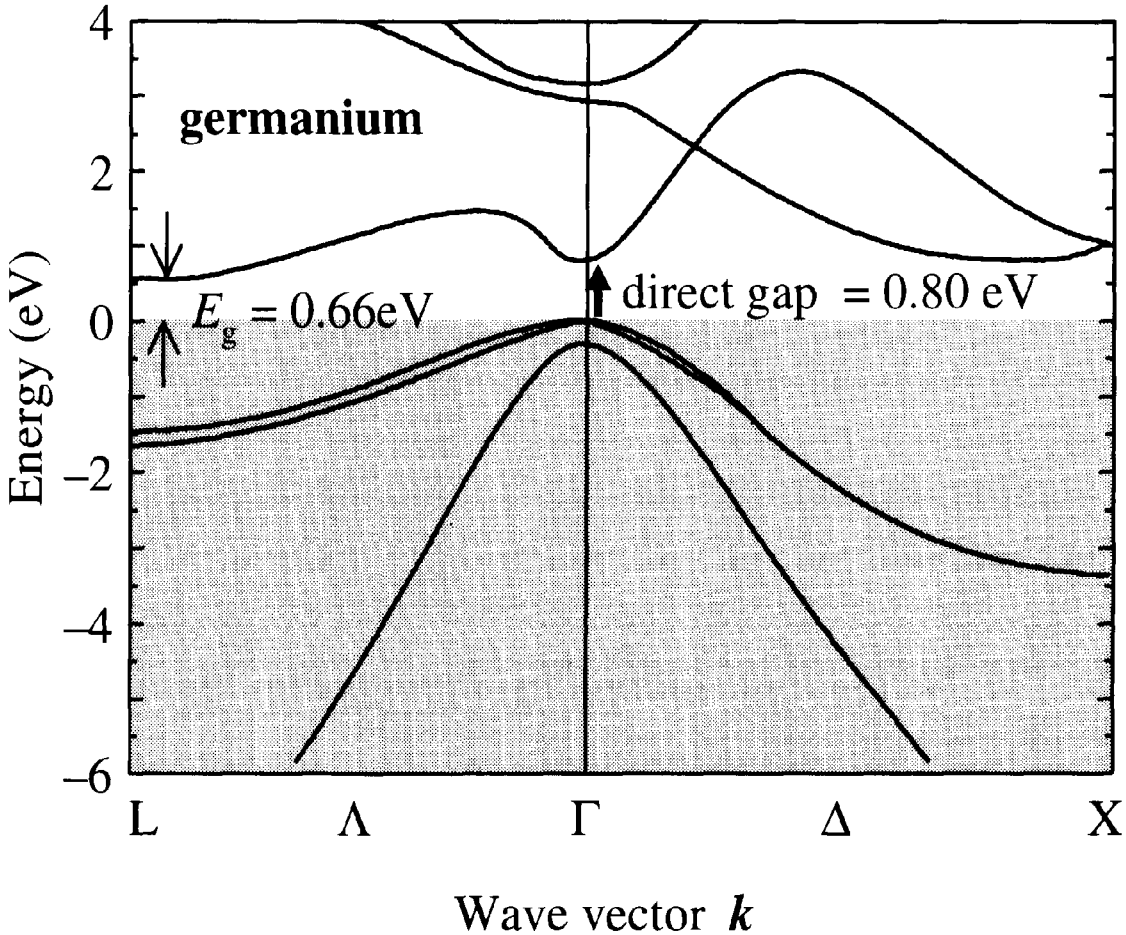

M. Fox: Optical properties of solids, Oxford university press, 2001.

Si_xGe_{1-x}

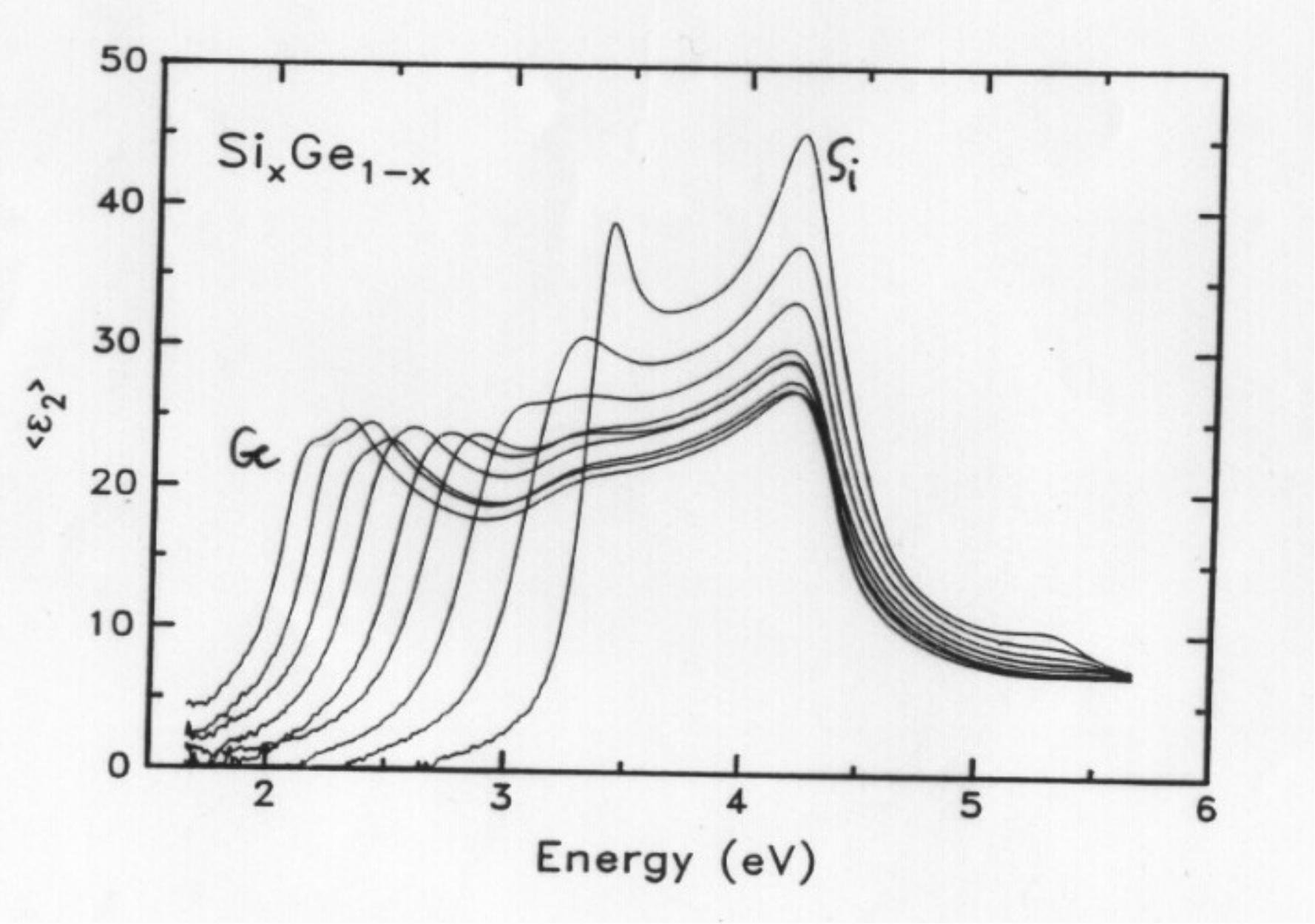

J. Humlíček, M. Garriga, M.I. Alonso, M. Cardona, J. Appl. Phys. **65** , 2827 (1989).

Parametry polovodičů

	a (Å)	E_g (eV)	ε_∞
C (diamant)	3.567	5.50	5.7
Si	5.431	1.2	11.6
Ge	5.657	0.7	16.0
α-Sn	6.491	0	

Parametry polovodičů

Table 1.2 Approximate transparency range band gap wavelength λ_g, and refractive inde n of a number of common semiconductors. is measured at 10 μm. After [1], [2] and [3].

Crystal	Transparency range (μm)	λ_g (μm)	n
Ge	1.8–23	1.8	4.00
Si	1.2–15	1.1	3.42
GaAs	1.0–20	0.87	3.16
CdTe	0.9–14	0.83	2.67
CdSe	0.75–24	0.71	2.50
ZnSe	0.45–20	0.44	2.41
ZnS	0.4–14	0.33	2.20

M. Fox: Optical properties of solids, Oxford university press, 2001.

Amorfní polovodiče

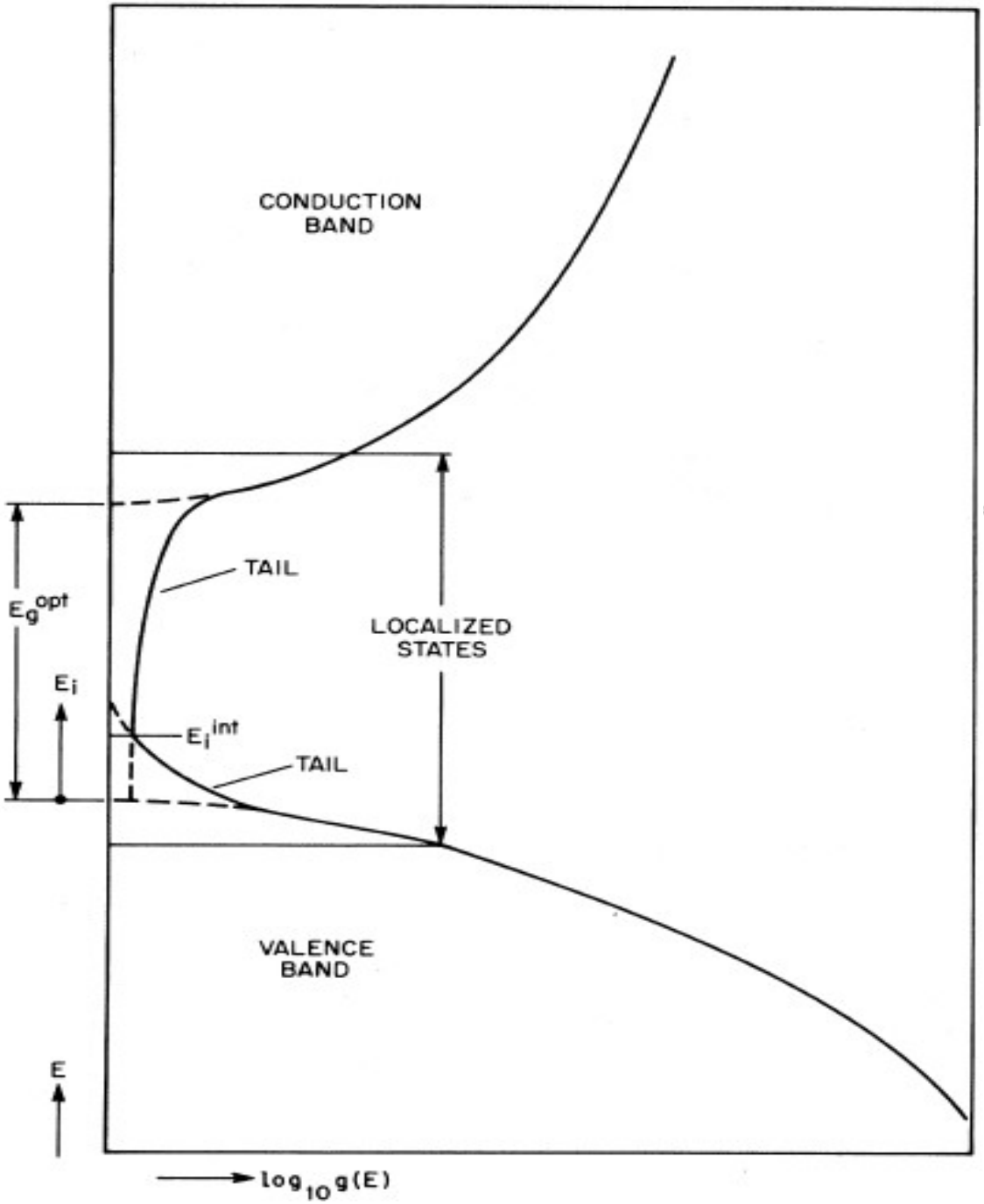

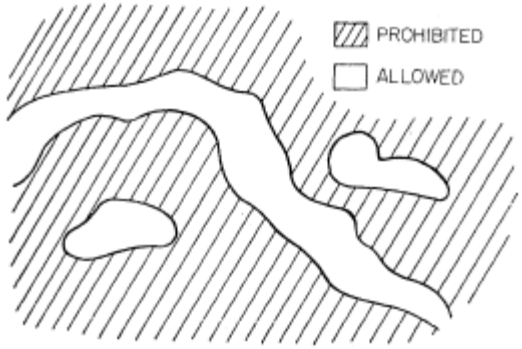

FIG. 5. Regions of allowed and prohibited states in an amorphous semiconductors just above the mobility edge.

Tauc, 1971

Amorfní polovodiče – hustota stavů

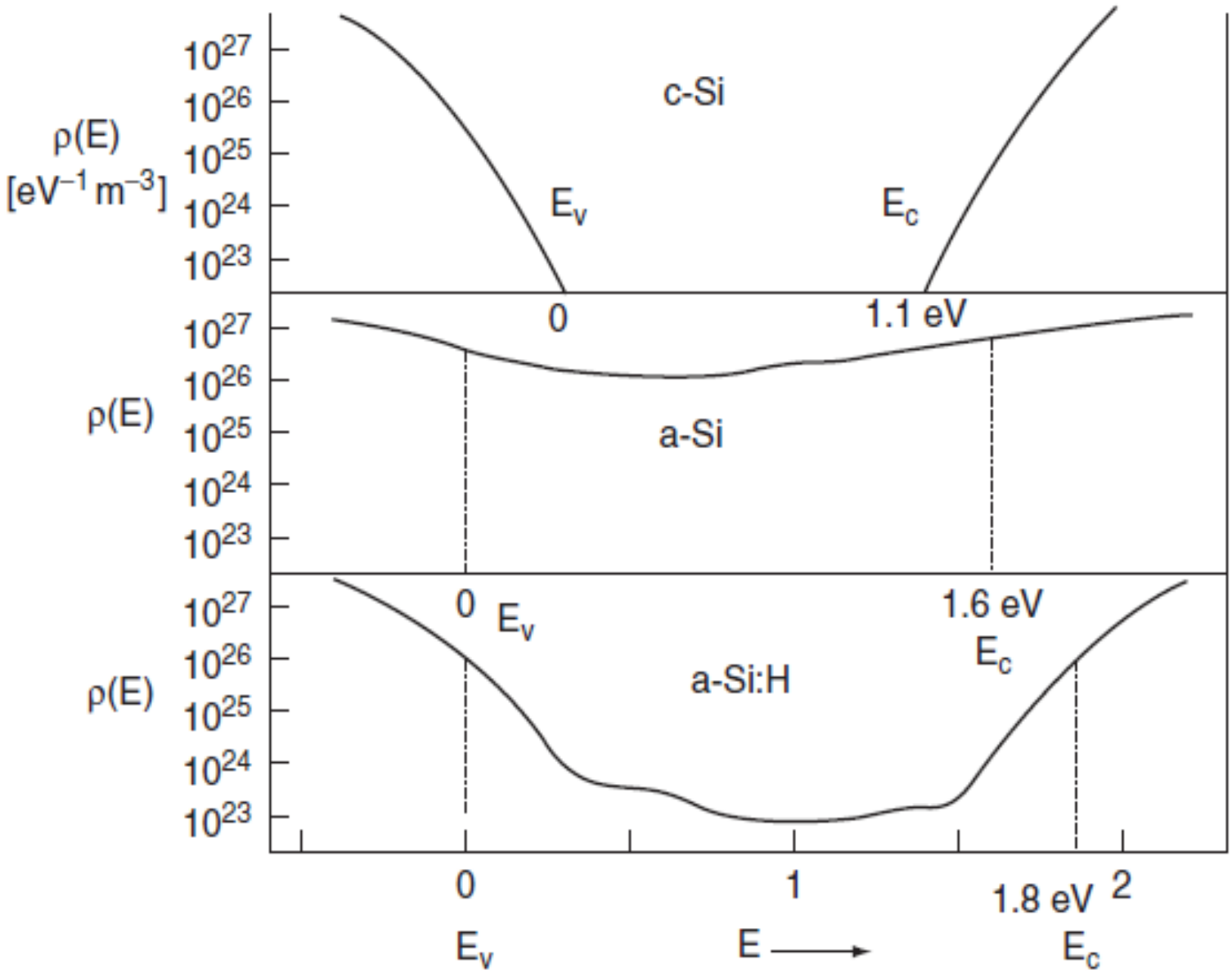

Gersten, Smith, The physics and chemistry of materials, Wiley 2001

Amorfní polovodiče

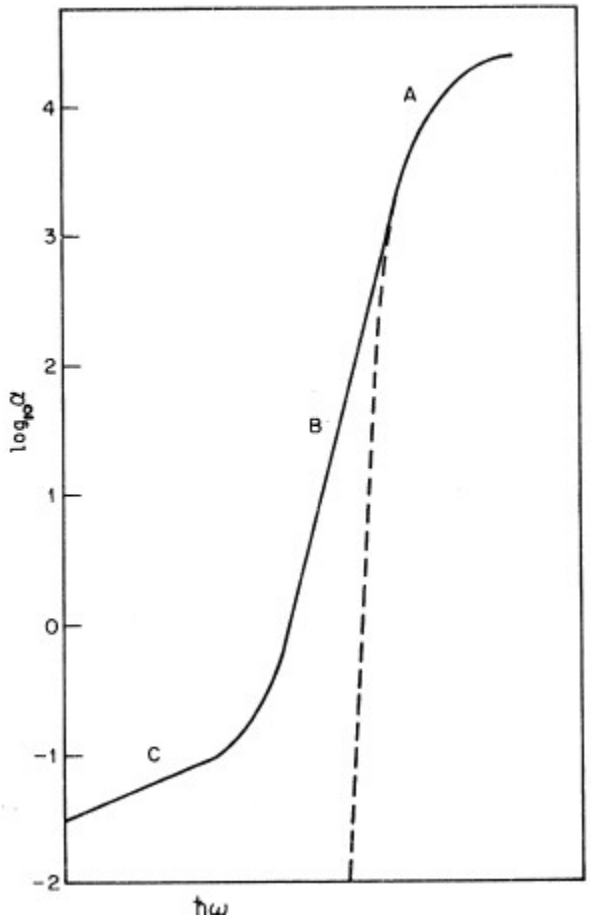

Region A:

$\alpha\hbar\omega = B\,(\hbar\,\omega - E_g)^2$

Taucův gap

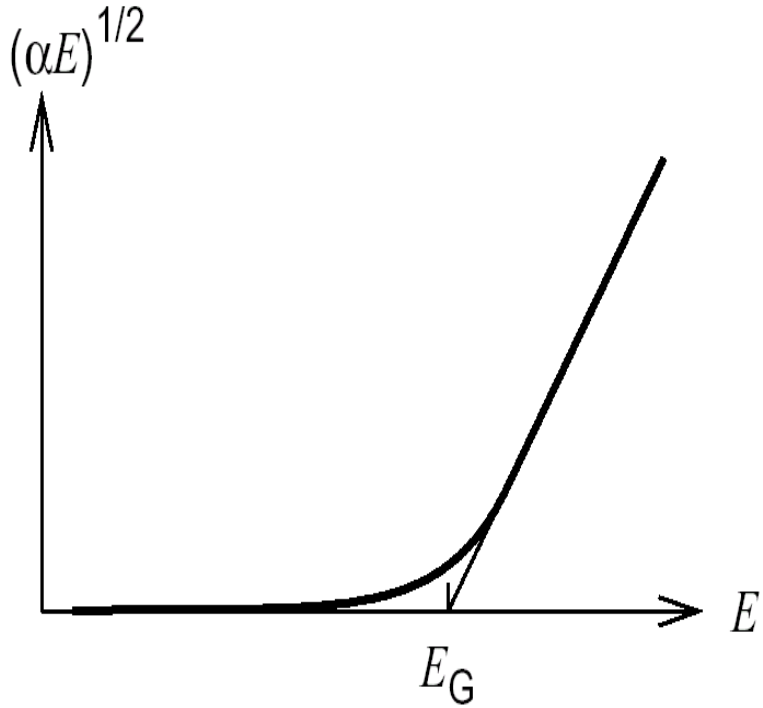

Region B:

$\alpha(\hbar\,\omega) \sim exp\,(\hbar\,\omega/E_u)$

Urbachova energie

Region C:

$\alpha(\hbar\omega) \sim exp\,(\hbar\omega/E_d)$,

defekty

Tauc 1971

Amorfní křemík – dielektrická funkce

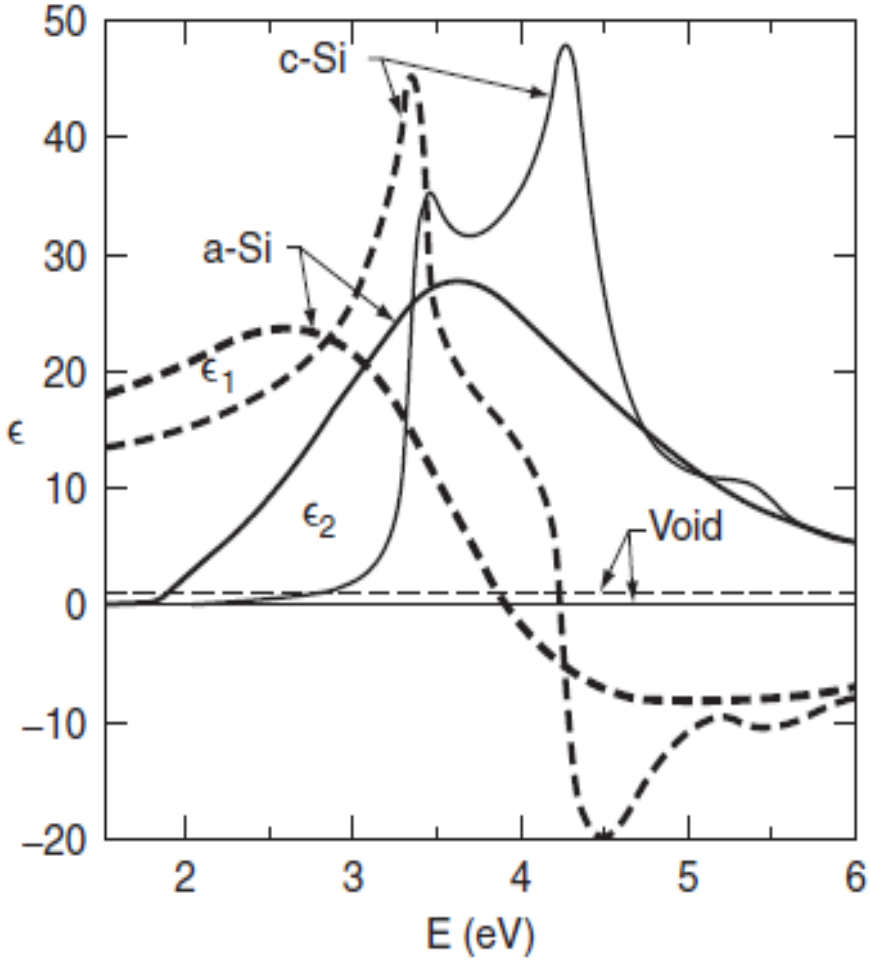

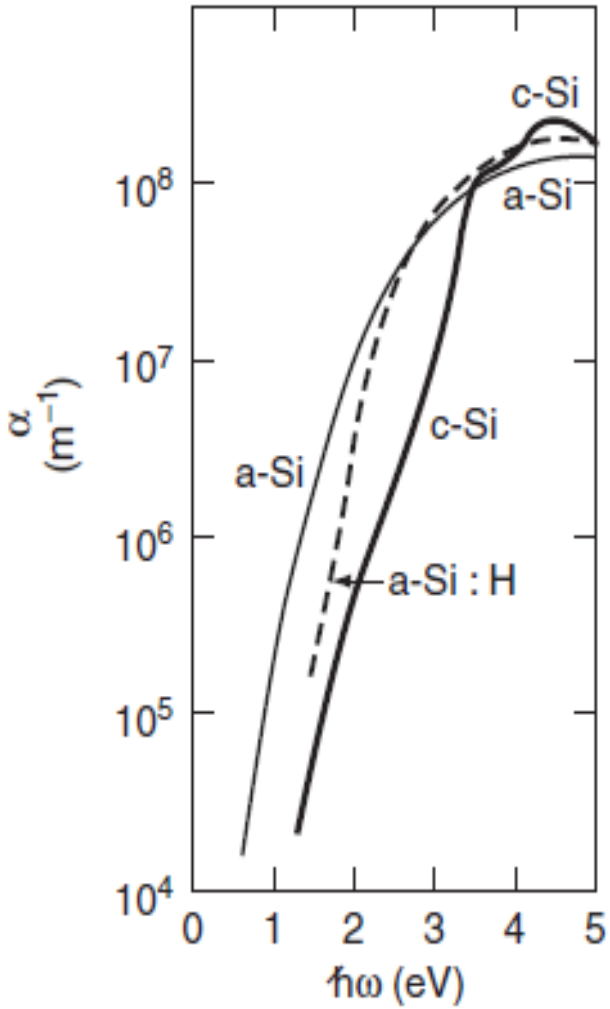

Gersten, Smith, The physics and chemistry of materials, Wiley 2001

Amorfní polovodiče

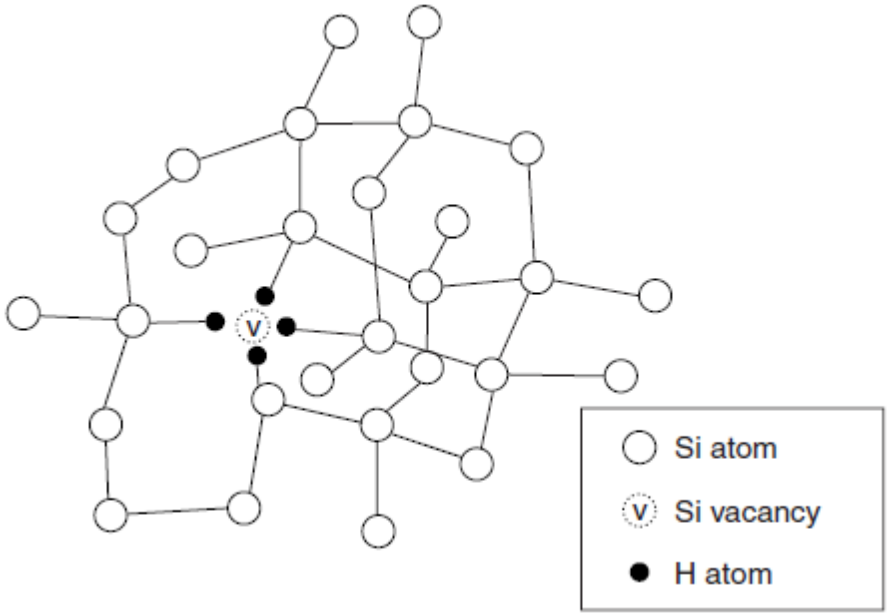

Gersten, Smith, The physics and chemistry of materials, Wiley 2001

Amorfní polovodiče

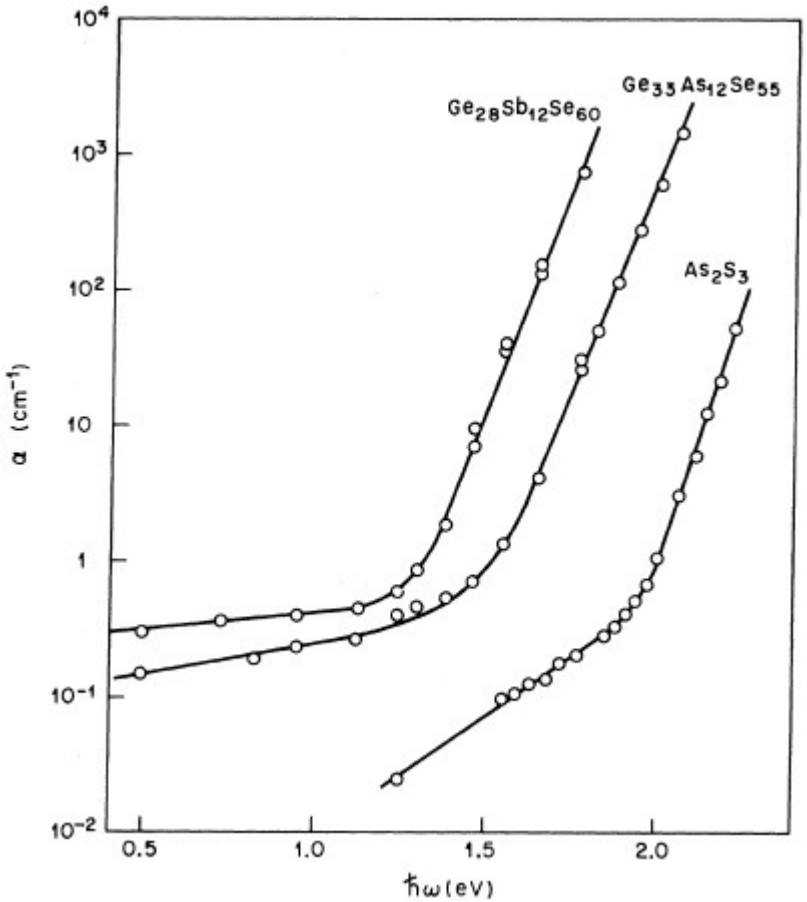

Chalkogenidová skla
Tauc 1972

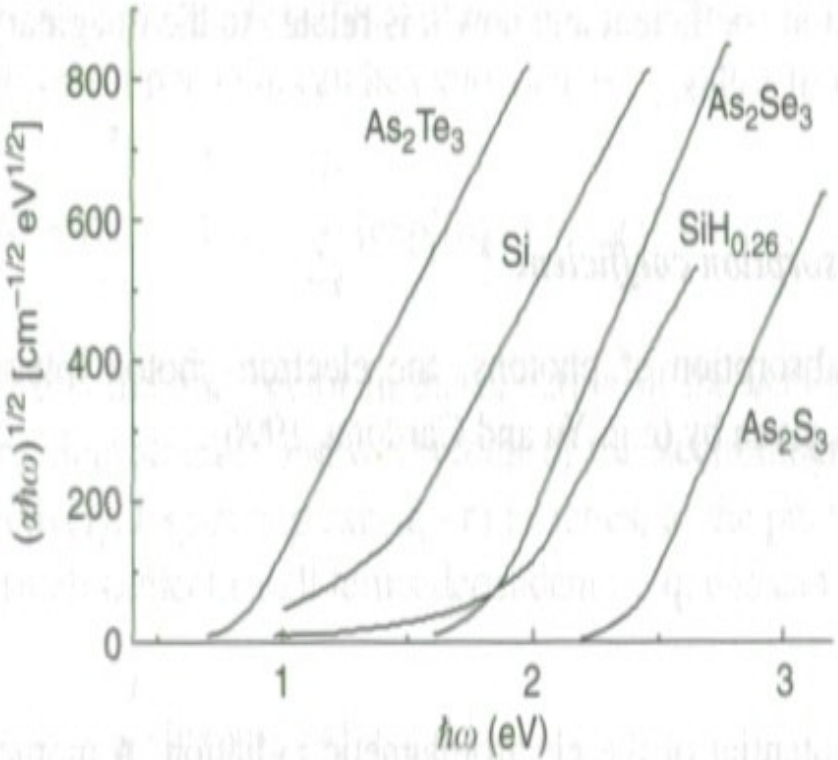

Figure 4.5 Tauc plots for different a-semiconductors (Morigaki, 1999).

SiO_2

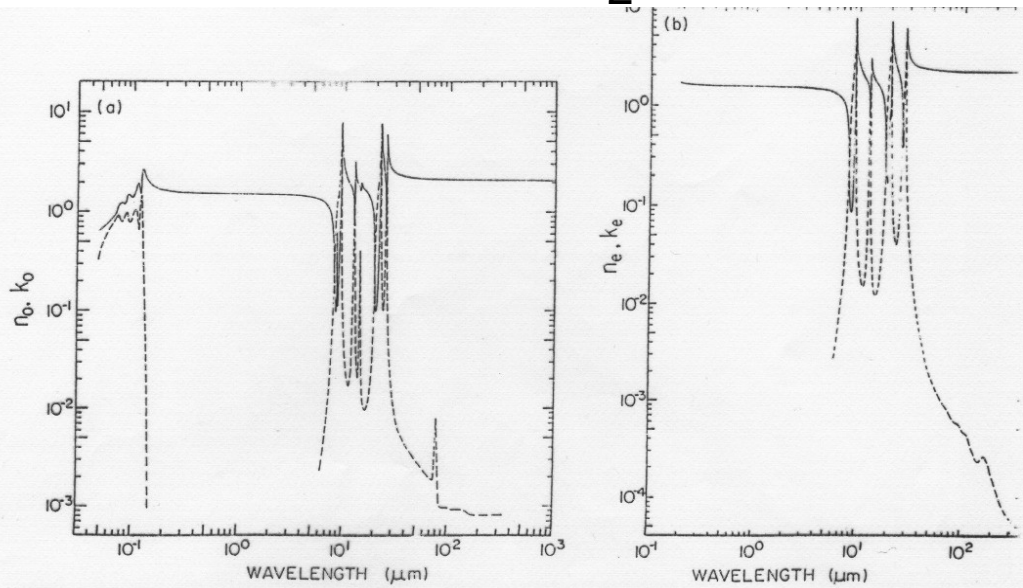

Fig. 9. (a) Log–log plot of n_o (——) and (– – – –) k_o versus wavelength in micrometers for silicon dioxide (type α, crystalline). (b) Log–log plot of n_e (——) and (– – – –) k_e versus wavelength in micrometers for silicon dioxide (type α, crystalline).

krystalický

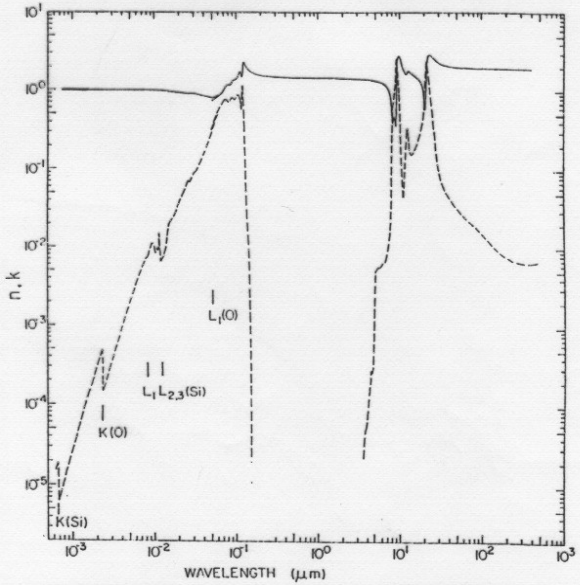

Fig. 10. Log–log plot of n (——) and k (– – – –) versus wavelength in micrometers for silicon dioxide (glass).

amorfní

Palik, Handbook of Optical Constants of Solids, Elsevier 1998.

SiO_2, GeO_2

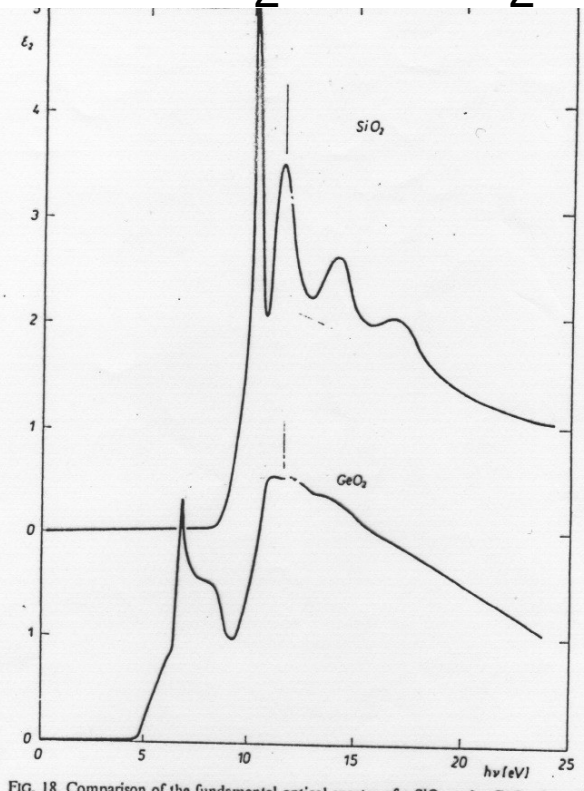

FIG. 18. Comparison of the fundamental optical spectra of g-SiO_2 and g-GeO_2 (from Ref. 51).

SiO_2

GeO_2

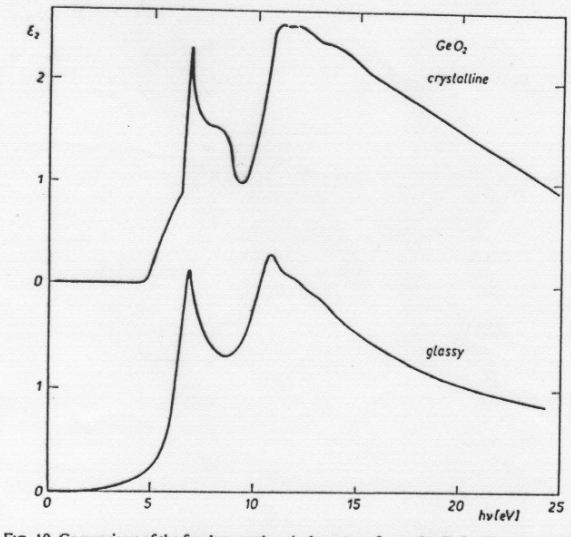

FIG. 19. Comparison of the fundamental optical spectra of c- and g-GeO_2. Note that c-GeO_2 is not only polycrystalline but also probably microcrystalline and contains "a few percent H_2O"; that is, the microcrystalline diameters are probably ≲100 Å (i.e., the same scale as observed by Zarzycki[40]) (from Ref. 51).

Krystalický
a amorfní GeO_2

Palik, Handbook of Optical Constants of Solids, Elsevier 1998.

Mezipásové přechody v kovech – hliník

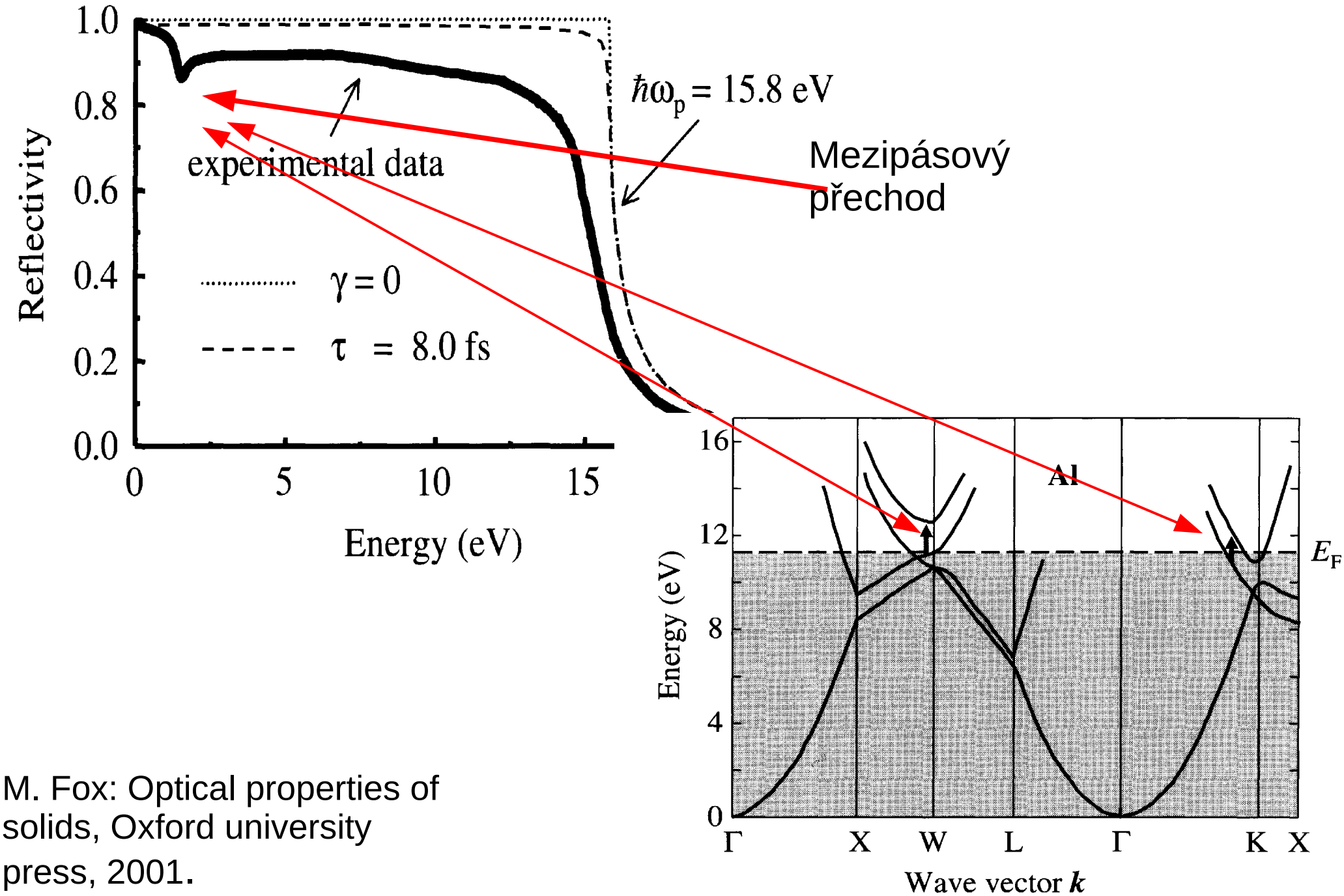

M. Fox: Optical properties of solids, Oxford university press, 2001.

Mezipásové přechody v kovech – měď

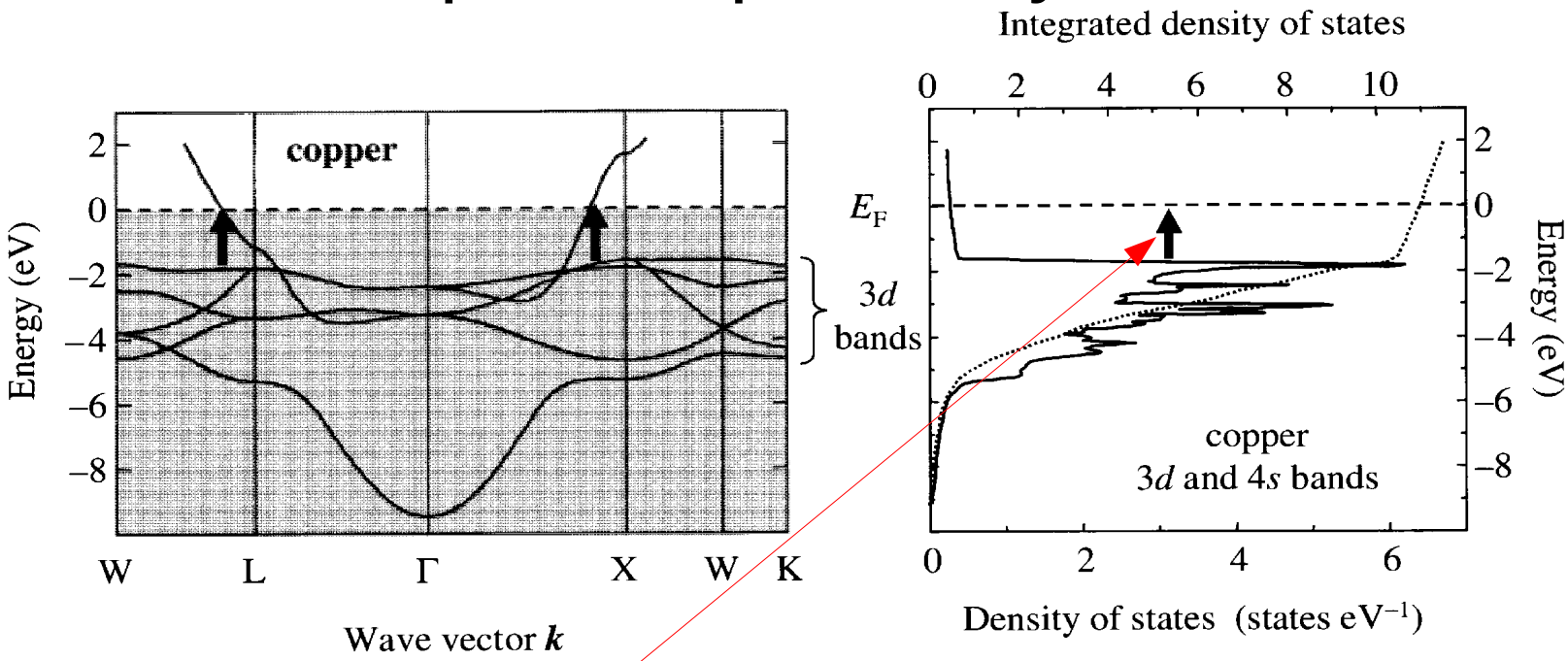

Fig. 7.5 Calculated band structure of copper. The transitions from the 3*d* bands responsible for the interband transitions around 2 eV are identified. The right hand side of the figure shows the density of states calculated from the band structure. The strongly peaked features between about −2 eV and −5 eV are due to the 3*d* bands. The dotted line is the integrated density of states. The Fermi level corresponds to the energy where the integrated density of states is equal to 11. After [5].

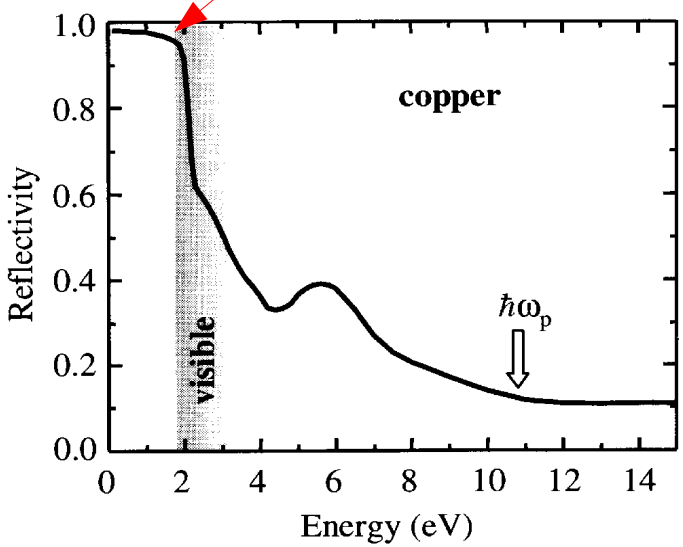

Fig. 7.6 Reflectivity of copper from the infrared to the ultraviolet spectral region. The reflectivity drops sharply above 2 eV due to interband transitions. After [6].

M. Fox: Optical properties of solids, Oxford university press, 2001.

Mezipásové přechody v kovech – zlato

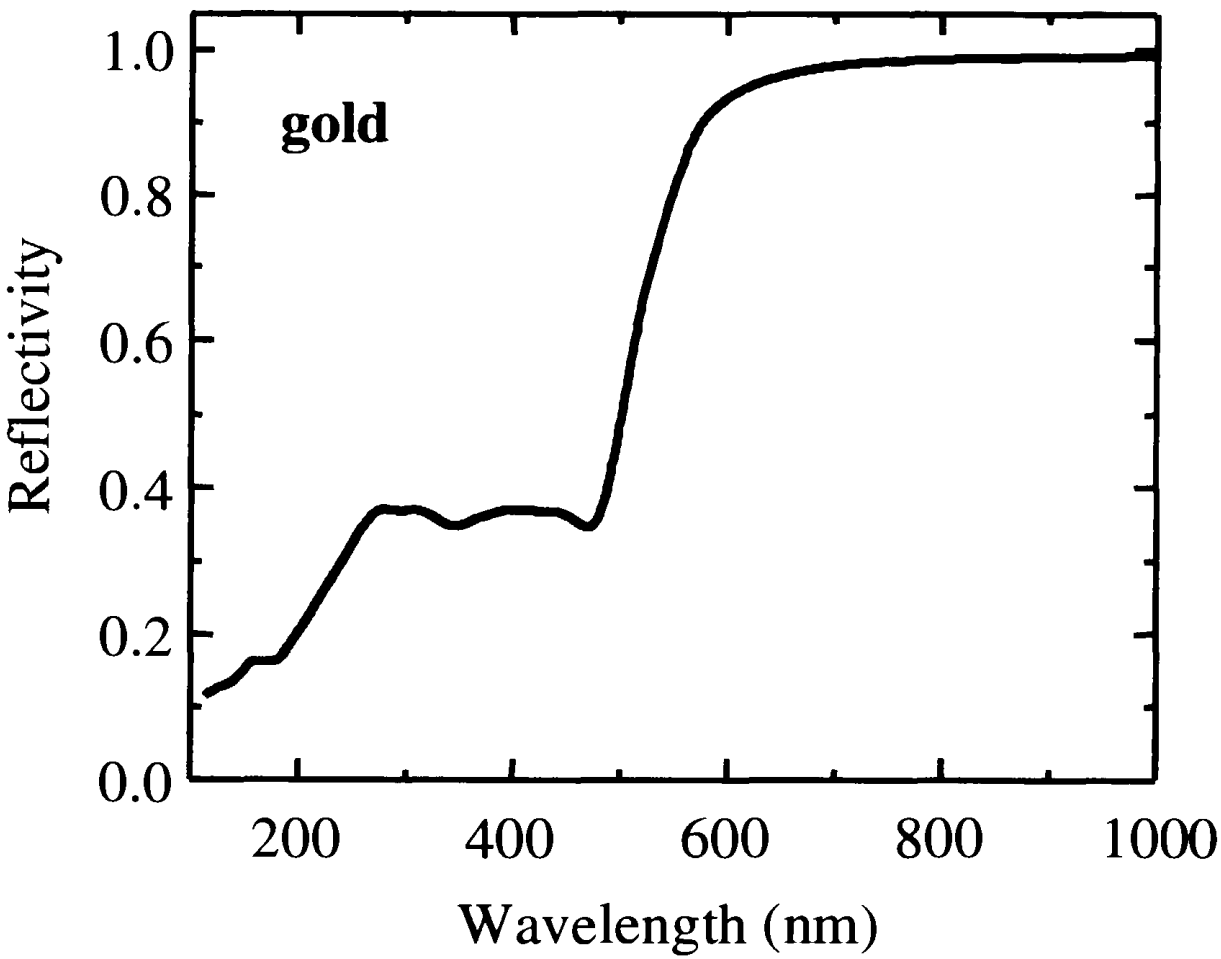

(7.13)

M. Fox: Optical properties of solids, Oxford university press, 2001.

Mezipásové přechody v kovech – Cu, Au, Ag

Cu

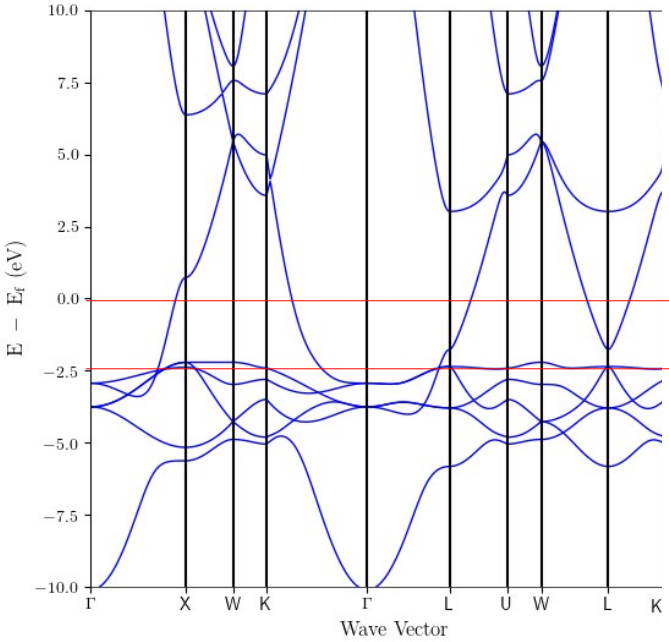

Ag

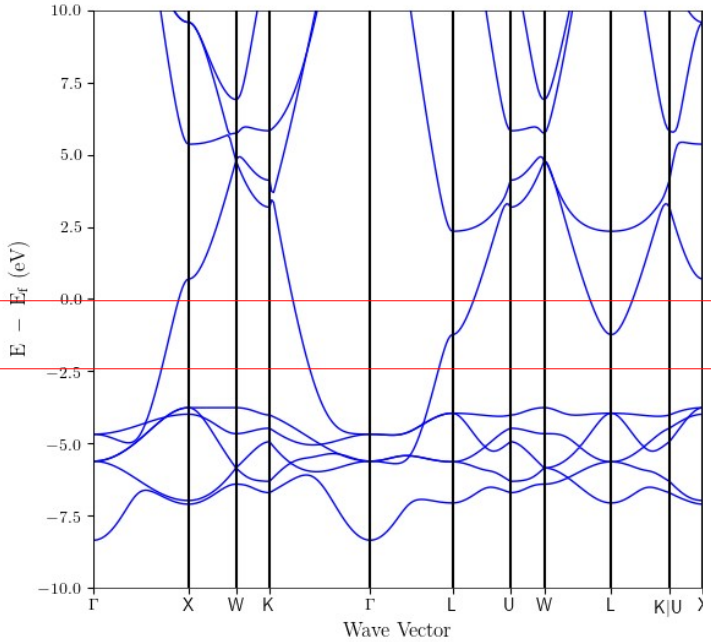

Au

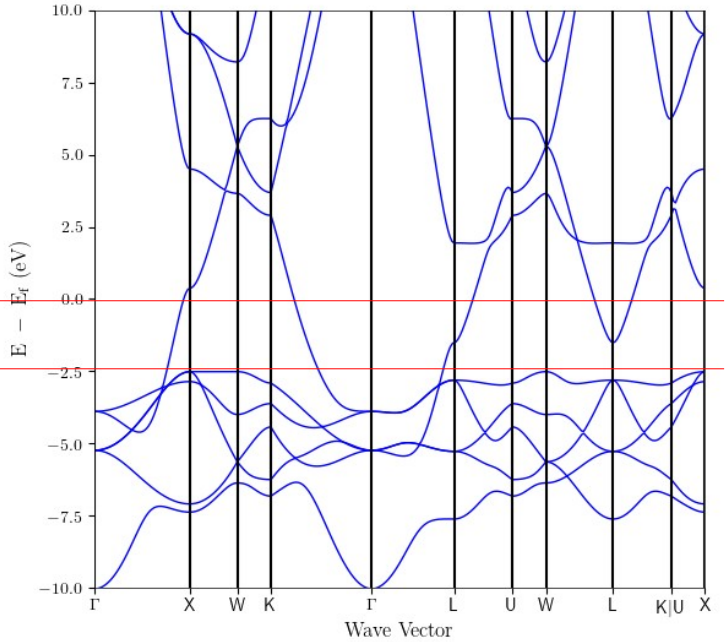

Materials database project

Polovodičové nanostruktury

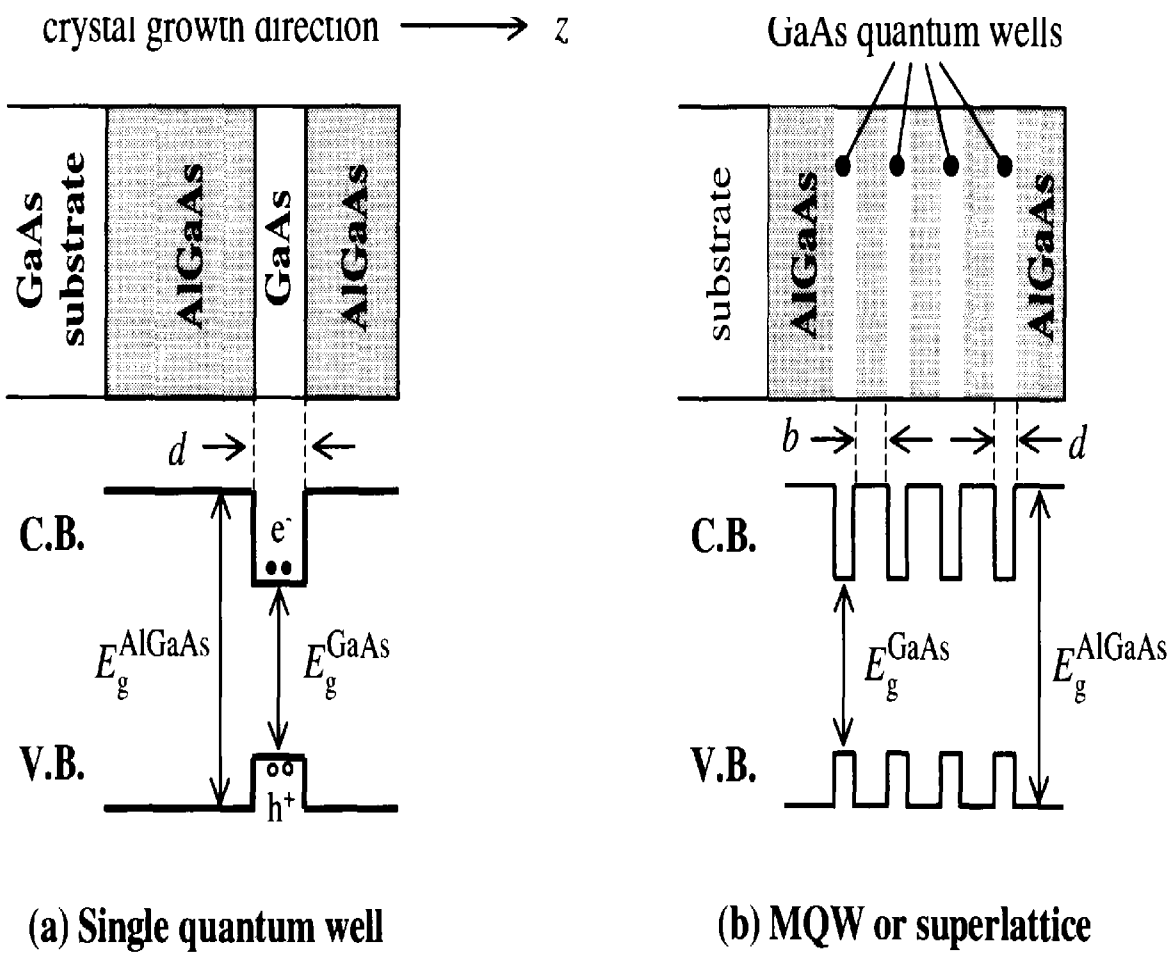

Fig. 6.1 (a) Schematic diagram of a single GaAs/AlGaAs quantum well. The quantum well is formed in the thin GaAs layer sandwiched between AlGaAs layers which have a larger band gap. The lower half of the figure shows the spatial variation of the conduction band (C.B.) and the valence band (V.B.). (b) Schematic diagram of a GaAs/AlGaAs multiple quantum well (MQW) or superlattice structure. The distinction between an MQW and a superlattice depends on the thickness b of the barrier separating the quantum wells.

M. Fox: Optical properties of solids, Oxford university press, 2001.

Polovodičové nanostruktury

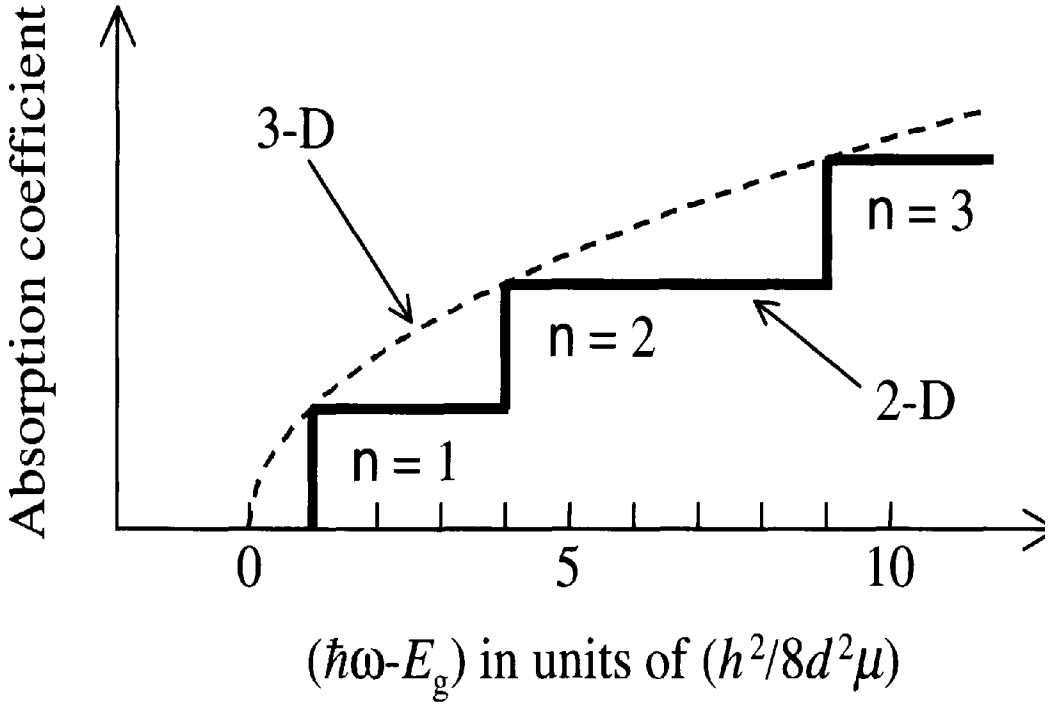

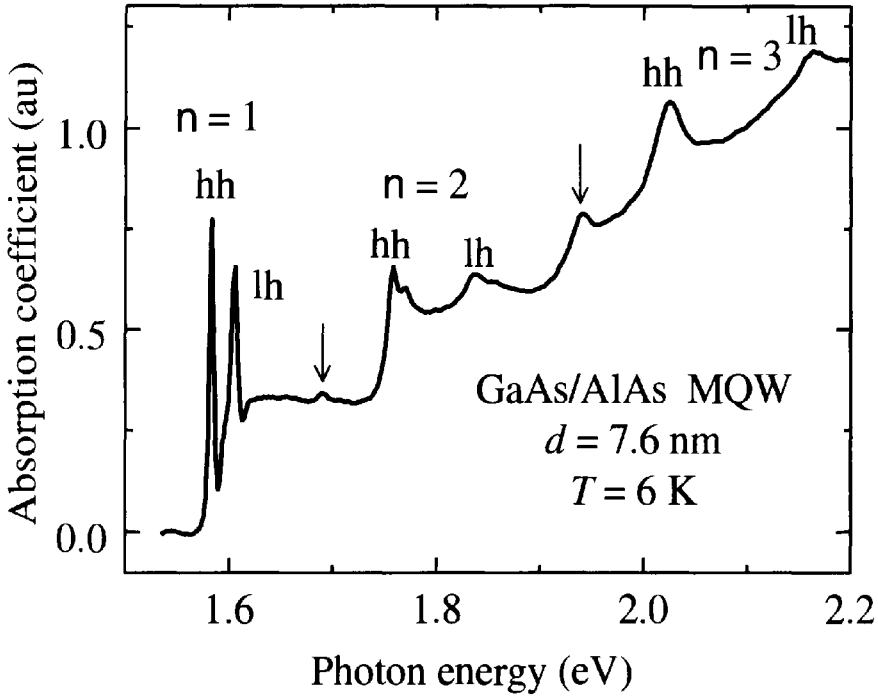

Fig. 6.9 Absorption coefficient of a 40 period GaAs/AlAs MQW structure with 7.6 nm quantum wells at 6 K. After [1], copyright 1996 Taylor & Francis Ltd., reprinted with permission.

M. Fox: Optical properties of solids, Oxford university press, 2001.

Polovodičové nanostruktury

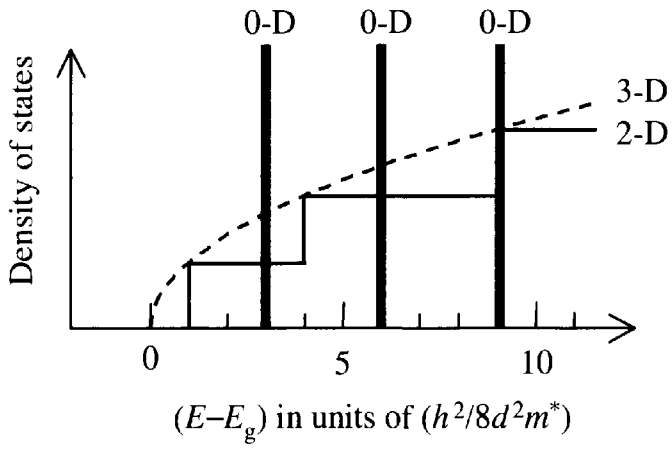

Fig. 6.15 Variation of the electron density of states with dimensionality. The dashed line is for a bulk semiconductor with a band gap of E_g. The thin solid line is for a quantum well of width d with infinite barriers. The thick solid lines are for a cubic quantum dot of dimension d with infinite barriers.

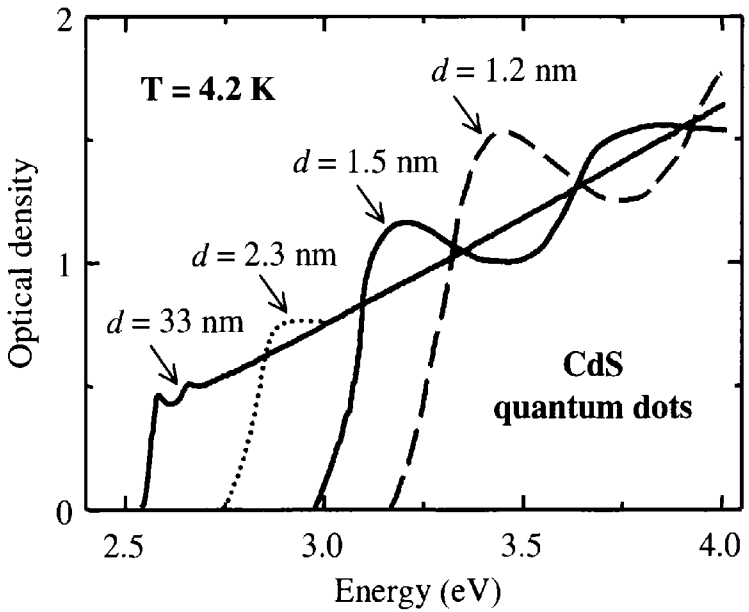

Fig. 6.16 Absorption spectra of glasses with CdS microcrystals of varying sizes at 4.2 K. The sample with $d = 33$ nm effectively represents the properties of bulk CdS. After [3], reprinted with permission.

M. Fox: Optical properties of solids, Oxford university press, 2001.

Excitony v GaAs

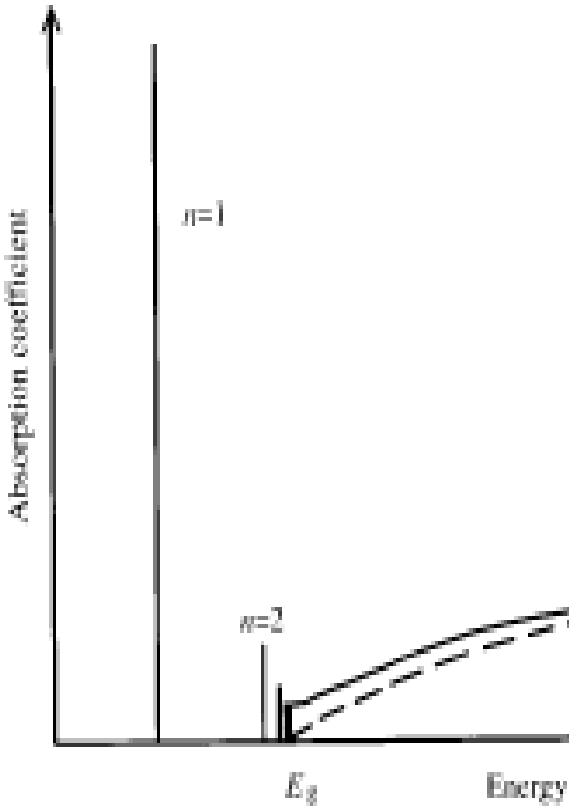

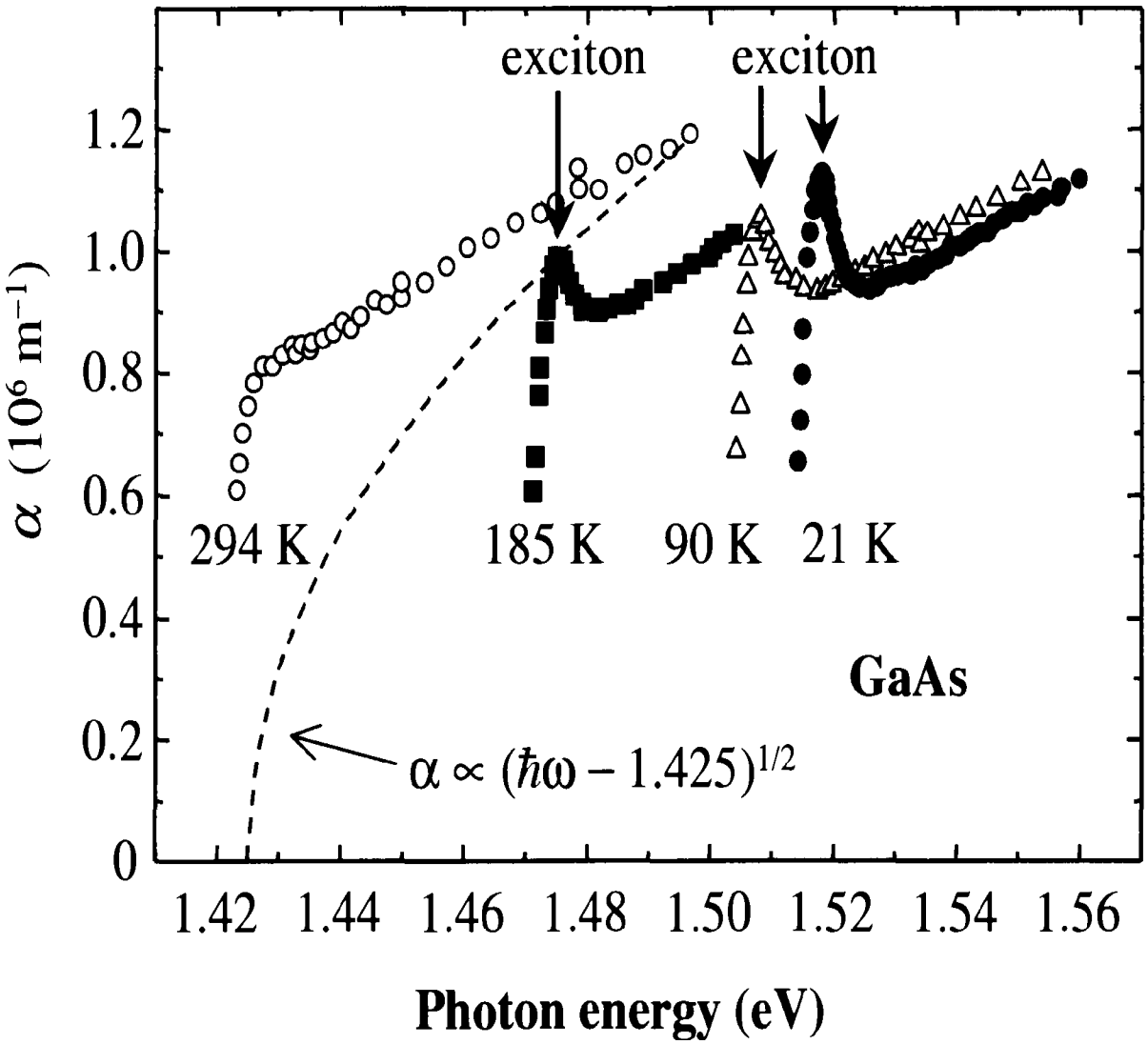

P. Yu, M. Cardona: Fundamentals of semiconductors, Springer 1996.

Optická skla

	Corning	Schott	n_d (587.56nm)	ν_d
517 642 korunové	B1764	BK7	1.517	64.2
805 254 flintové	E0525	SF6	1.805	25.4
křemenné			1.458	67.8

	SiO_2	B_2O_3	Al_2O_3	Na_2O K_2O	BaO	CaO	PbO
517 642 korunové	68	11	1	16	1	2	-
805 254 flintové	27	-	-	2	-	-	71

Abbeho číslo

Vd = (nd-1)/(nF-nC)

D: 587.56 nm (Yellow helium line)

F: 486.13 nm (Blue hydrogen line)

C: 656.27 nm (Red hydrogen line)

Ve = (ne-1)/(nF'-nC')

E: 546.07 nm (Green mercury line)

F': 479.99 nm (Blue cadmium line)

C': 643.85 nm (Red cadmium line)

http://refractiveindex.info/

Tavený křemen

Table 1.3 Refractive index of synthetic fused silica versus wavelength. After [2].

Wavelength (nm)	Refractive index
213.9	1.53430
239.9	1.51336
275.3	1.49591
334.2	1.47977
404.7	1.46962
467.8	1.46429
508.6	1.46186
546.1	1.46008
632.8	1.45702
706.5	1.45515
780.0	1.45367
1060	1.44968
1395	1.44583
1530	1.44427
1970	1.43853
2325	1.43293

M. Fox: Optical properties of solids, Oxford university press, 2001.

Optická skla

Table 1.4 Composition, refractive index and ultraviolet transmission of common glasses. The letters after the names give the abbreviations used identify the glass type. The composition figures are the percentage by mass. The refractive index is measured at 546.1 nm, and the transmission for a 1 cm plate at 310 nm. After [1], [4].

Name	SiO_2	B_2O_3	Al_2O_3	Na_2O	K_2O	CaO	BaO	PbO	P_2O_5	n	T
Fused silica	100									1.460	0.91
Crown (K)	74			9	11	6				1.513	0.4
Borosilicate crown (BK)	70	10		8	8	1	3			1.519	0.35
Phosphate crown (PK)		3	10		12	5			70	1.527	0.46
Light flint (LF)	53			5	8			34		1.585	0.008
Flint (F)	47			2	7			44		1.607	–
Dense flint (SF)	33				5			62		1.746	–

M. Fox: Optical properties of solids, Oxford university press, 2001.

Optická skla – vliv 1% at. příměsi na index lomu

OX	Δn (10^{-4})	$\Delta\nu$
B_2O_3	0	0
Al_2O_3	+4	-0.25
Na_2O	+15	-0.2
K_2O	+10	-0.2
BaO	+30	-0.3
CaO	+24	-0.4
PbO	+30	-0.65
La_2O_3	+42	-0.3
TiO_2	+54	-1.45

Optická skla, index lomu vs. Abbeho číslo

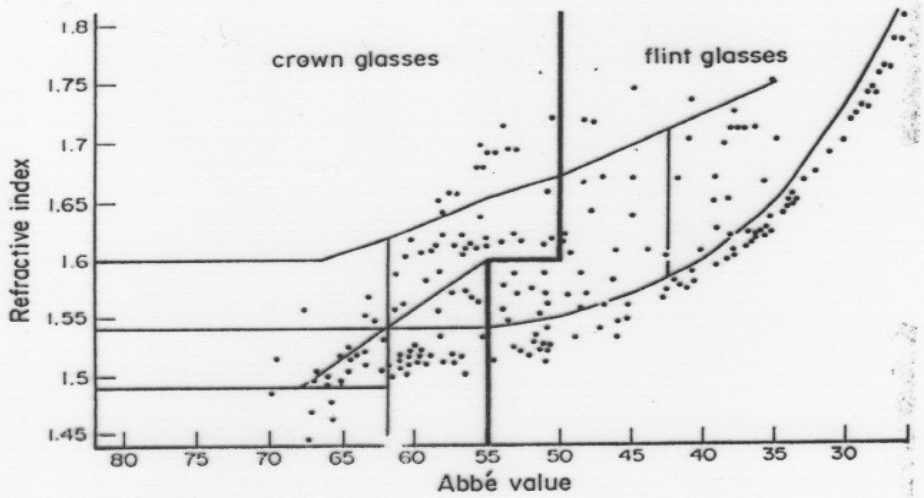

Figure 1
Refractive index against Abbé value diagram

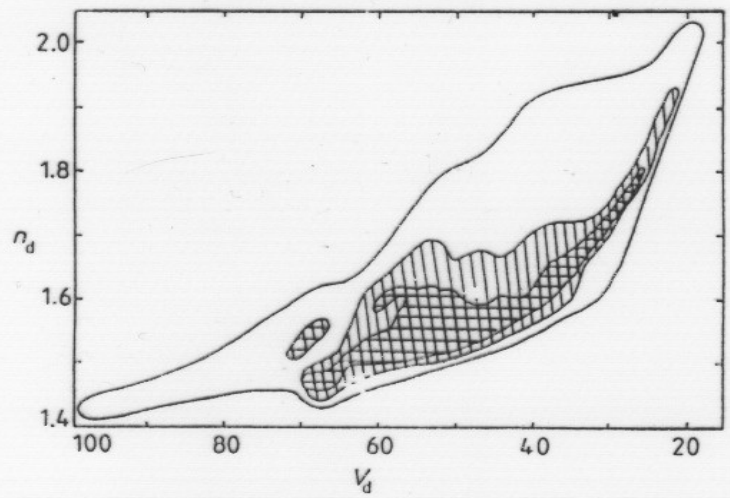

Figure 3.2 Reciprocal dispersive power $(n_d - 1)/(n_f - n_c)$ plotted against n_d for commercial optical glasses (Gliemeroth 1982). 1881 ▦, 1939 ▥, 1981 □.

Optická skla, index lomu vs. Abbeho číslo

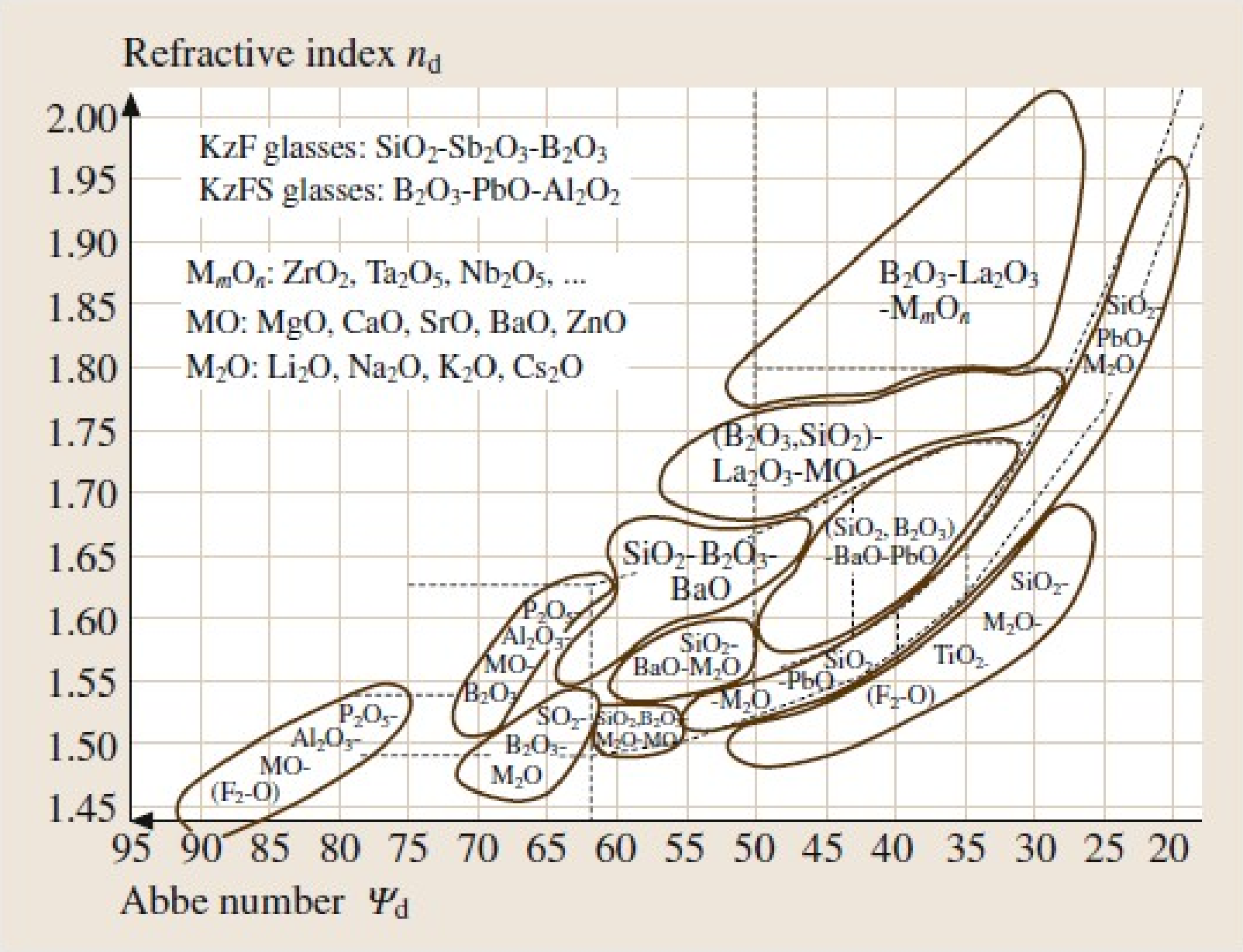

Martienssen, Warlimont, Springer Handbook of condensed matter materials data, Springer, 2004.

Optická skla – propustnost 10mm

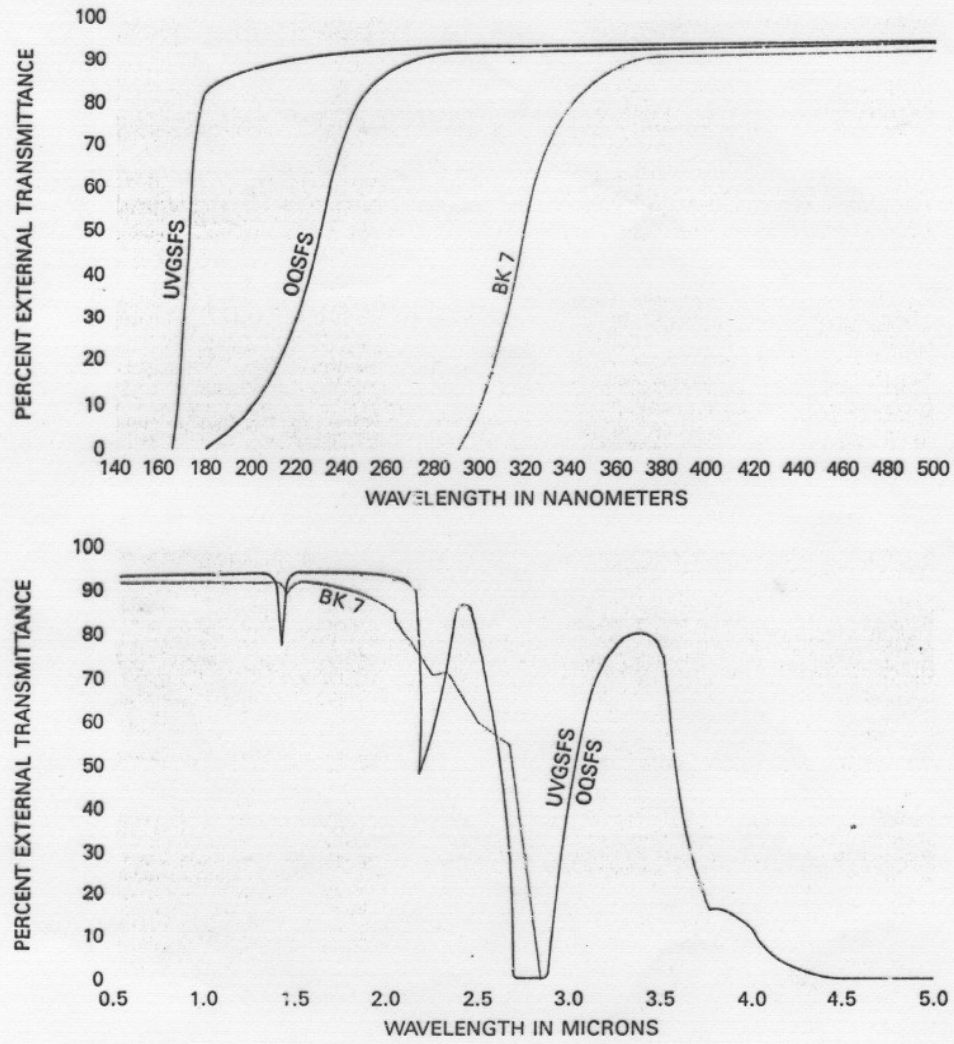

COMPARISON OF UNCOATED EXTERNAL TRANSMITTANCES for ultraviolet grade synthetic fused silica (UVGSFS), optical quality synthetic fused silica (OQSFS) and a common optical glass (BK 7), all of 10mm thickness.

Optická skla

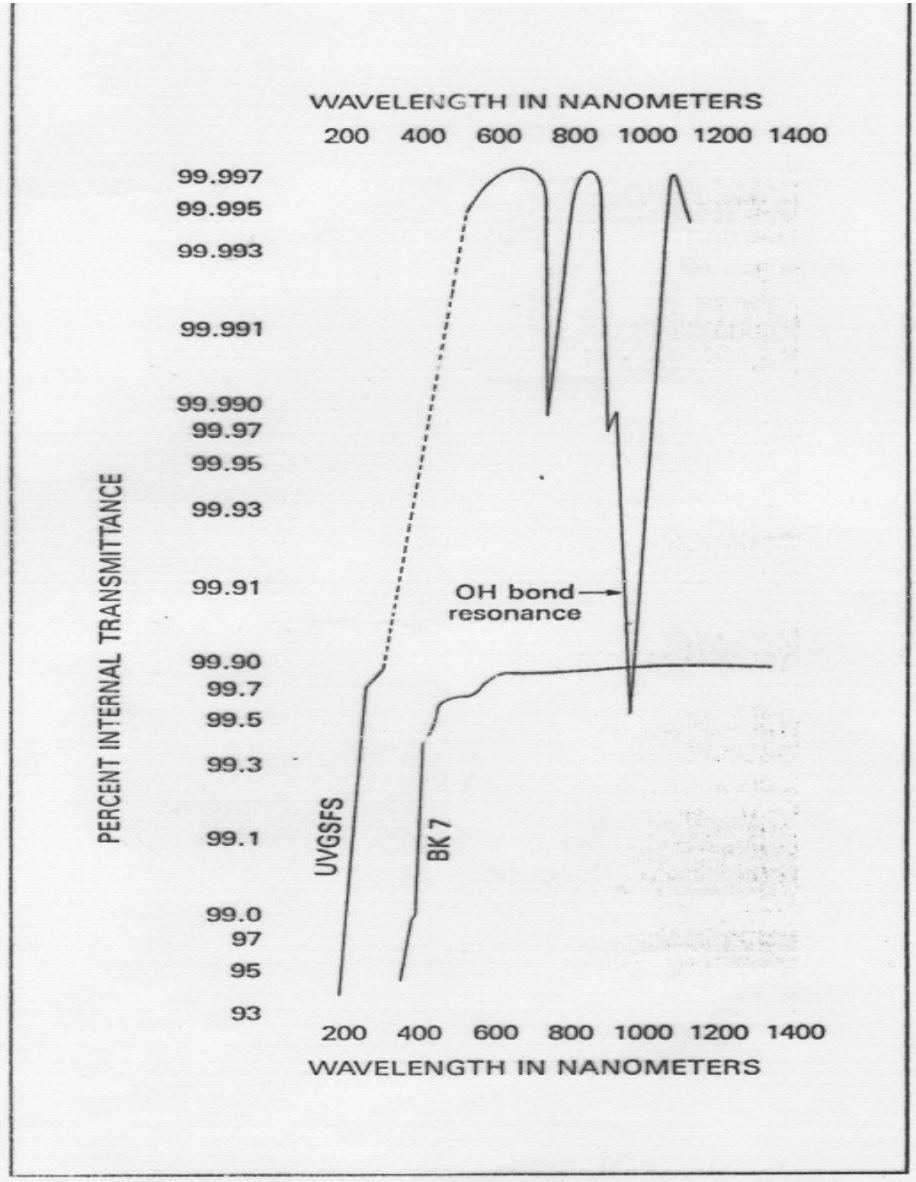

SEMILOGARITHMIC COMPARISON OF INTERNAL TRANSMITTANCES of UV grade synthetic fused silica and BK 7.

Korunové sklo

OPTICAL CROWN GLASS

Optical crown glass is a low index, commercial quality glass in which index of refraction, transmittance and homogeneity are not controlled as carefully as in optical quality glasses such as BK 7. Optical crown is a suitable material in applications where component tolerances are fairly loose or as a substrate material for mirrors. Transmittance characteristics for optical crown are shown in the graph; relevant properties of optical crown are tabulated below.

Refractive Index of Optical Crown Glass

Wavelength (nm)	Refractive Index, n	Fraunhofer Designation	Source	Spectral Region
435.8	1.53394	g	mercury arc	blue
480.0	1.52960	F′	cadmium arc	blue
486.1	1.52908	F	hydrogen arc	blue
546.1	1.52501	e	mercury arc	green
587.6	1.52288	d	helium arc	yellow
589.0	1.52280	D_2	sodium arc	yellow
643.8	1.52059	C′	cadmium arc	red
656.3	1.52015	C	hydrogen arc	red

OPTICAL CROWN GLASS CONSTANTS

Abbe Factor:

$$v_e = \frac{n_e - 1}{n_{F'} - n_{C'}} = 58.3 \quad v_d = \frac{n_d - 1}{n_F - n_C} = 58.8$$

Dispersion: $(n_F - n_c) = 0.0089$

Glass type designation: B270

Density: 2.55 g cm^{-3} at 23 °C

Transformation temperature: 521 °C

Softening temperature: 708 °C

Coefficient of linear expansion:
(20 to 300 °C) = 93.3 x 10^{-7} $°C^{-1}$

Specific heat: C_p (20 to 100 °C) = 0.184 cal. g^{-1} $°C^{-1}$

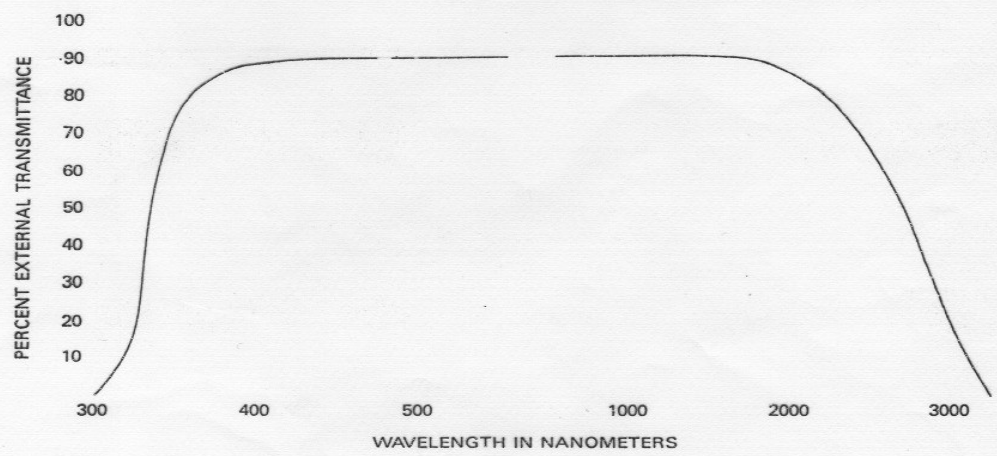

EXTERNAL TRANSMITTANCE FOR OPTICAL CROWN GLASS of 10mm thickness.

Diamant

Propustná oblast 0.3 – 100 μm (typ Ia)

λ (μm)	n
3	2.3818
4	2.3812
5	2.3809
8	2.3806
10	2.3805
12	2.3805

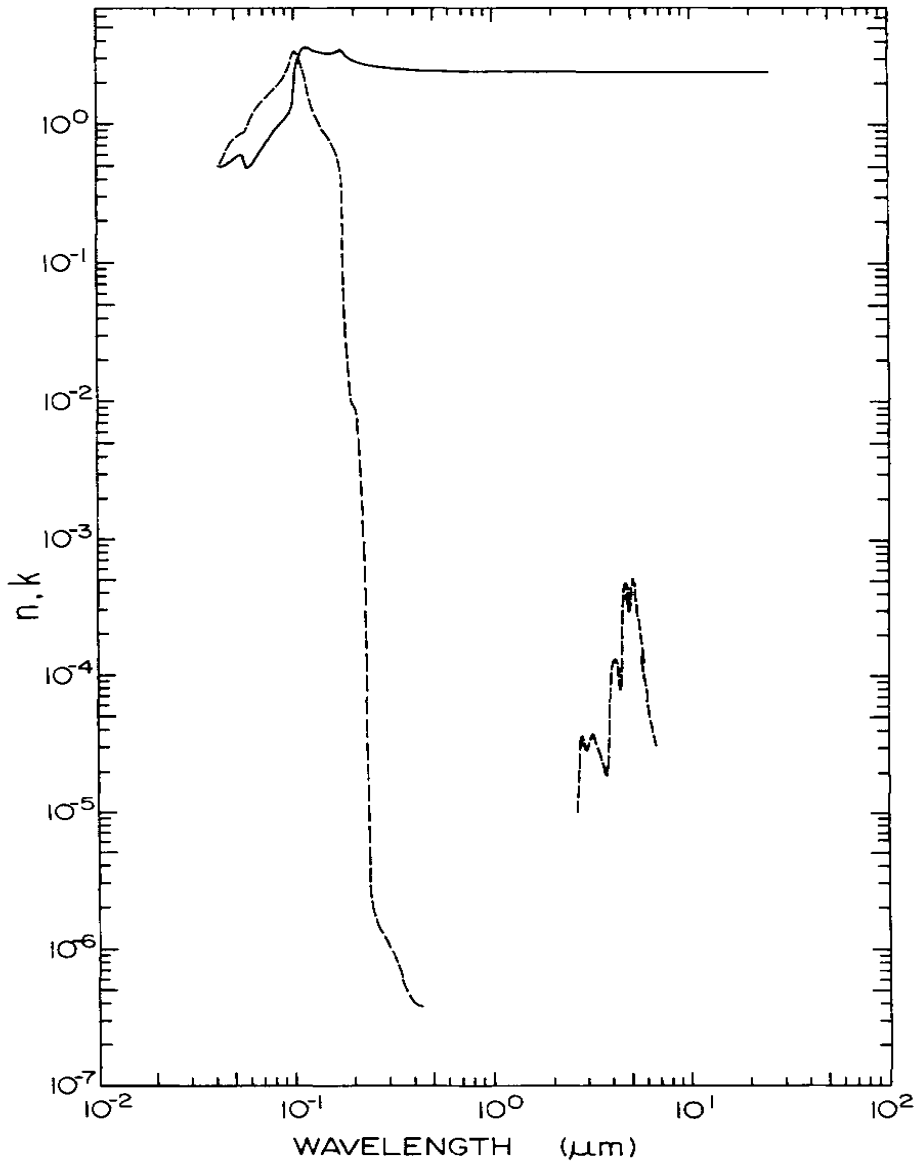

Fig. 5. Log–log plot of n(——) and k(– – –) versus wavelength in micrometers for cut carbon.

Palik, Handbook of Optical Constants of Solids, Elsevier 1998.

Diamant

Propustnost v IR oboru, cca 1mm

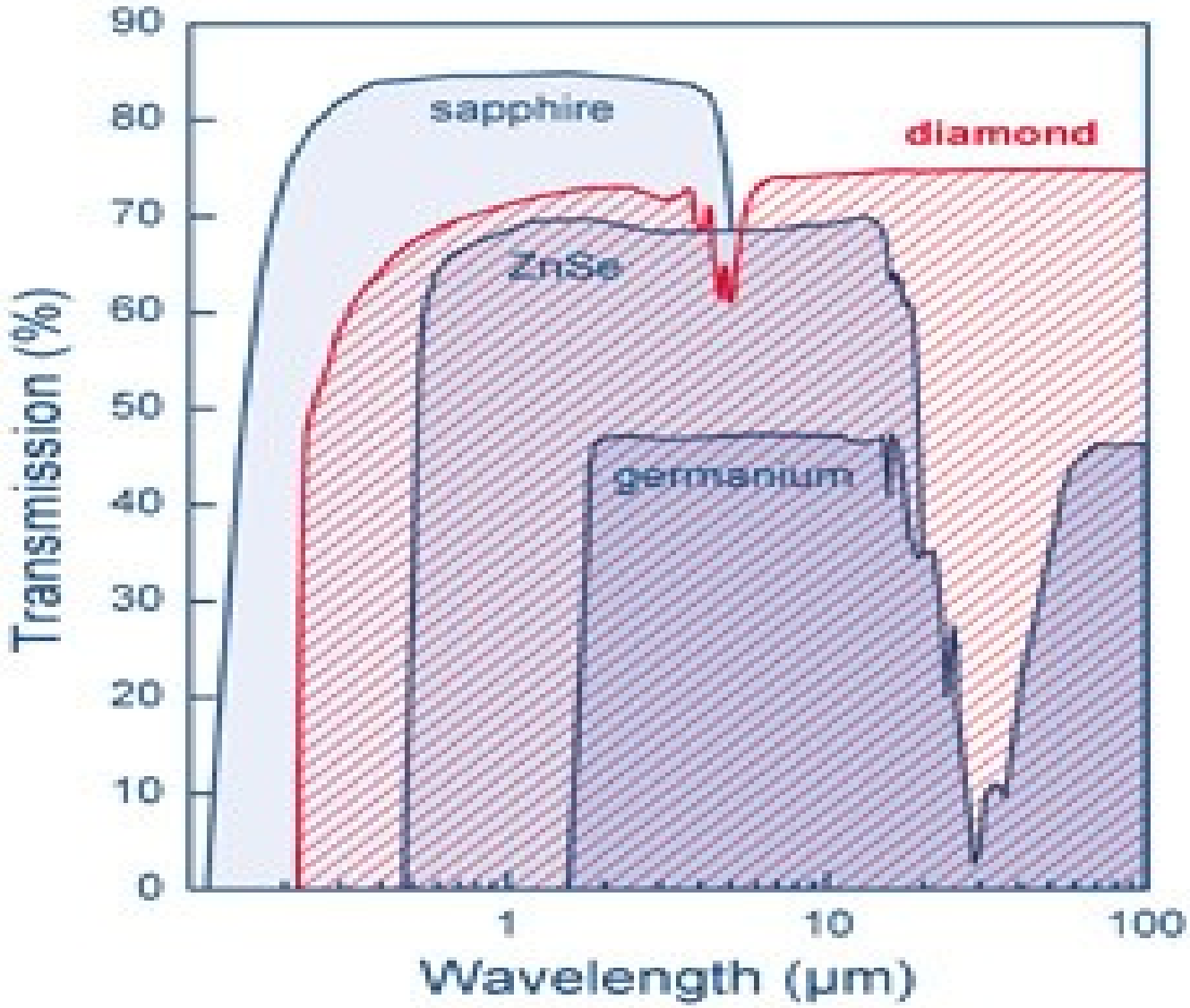

http://www.diamond-

Safír – Al_2O_3

SAPPHIRE* CONSTANTS

Density: 3.98 g cm^{-3} at 25 °C
Young's Modulus: *3.7 x 10^{10} dynes/mm^2
Poisson's Ratio: *–0.02
Moh hardness: 9 (by definition)
Softening Point: 1800 °C
Specific Heat at 25 °C: 0.18 cal/g °C
Coefficient of linear expansion:
(0 °C to 500 °C) ° 7.7 x 10^{-6} °C

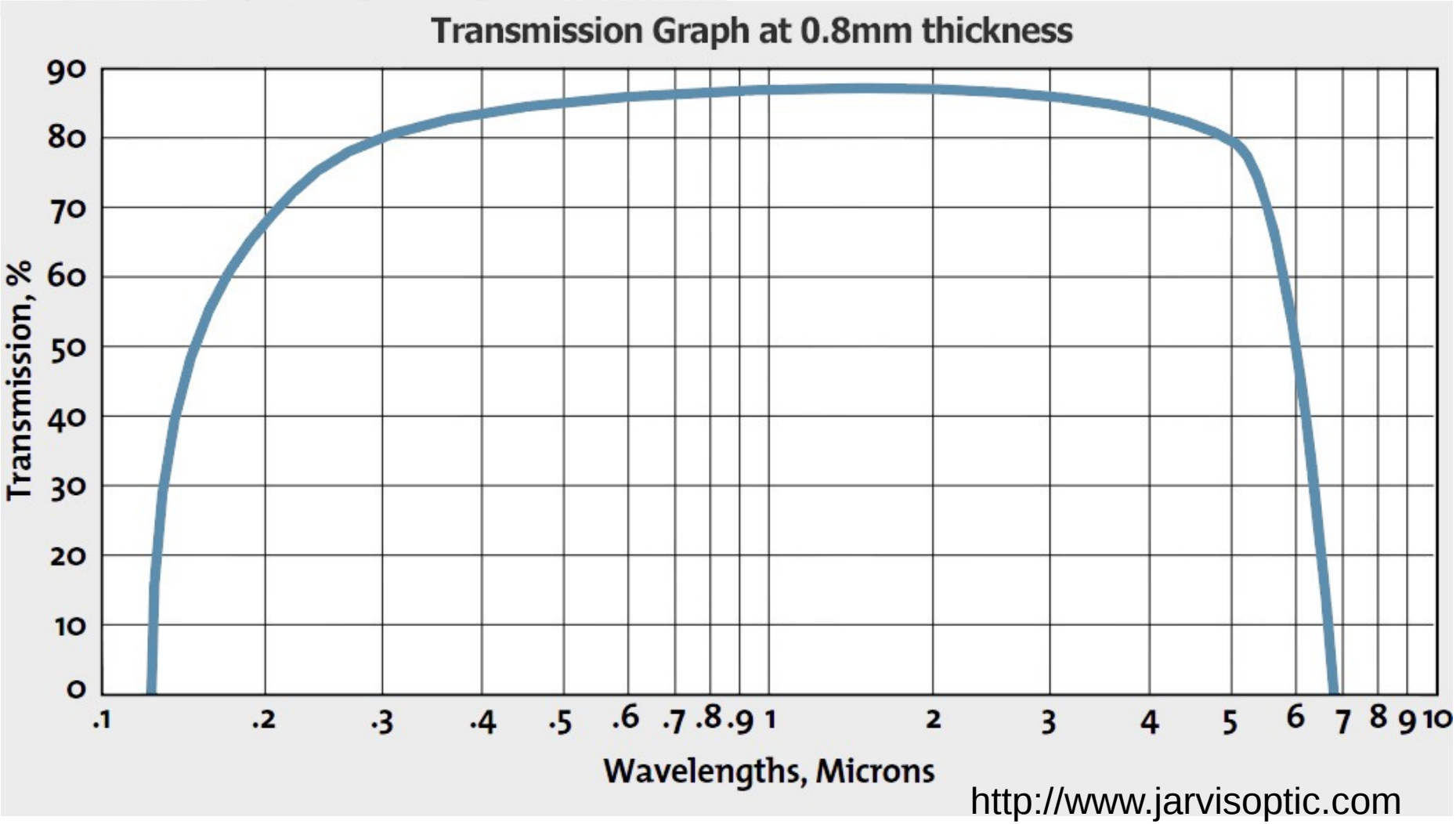

http://www.jarvisoptic.com

Safír – Al_2O_3, Rubín – Al_2O_3+Cr

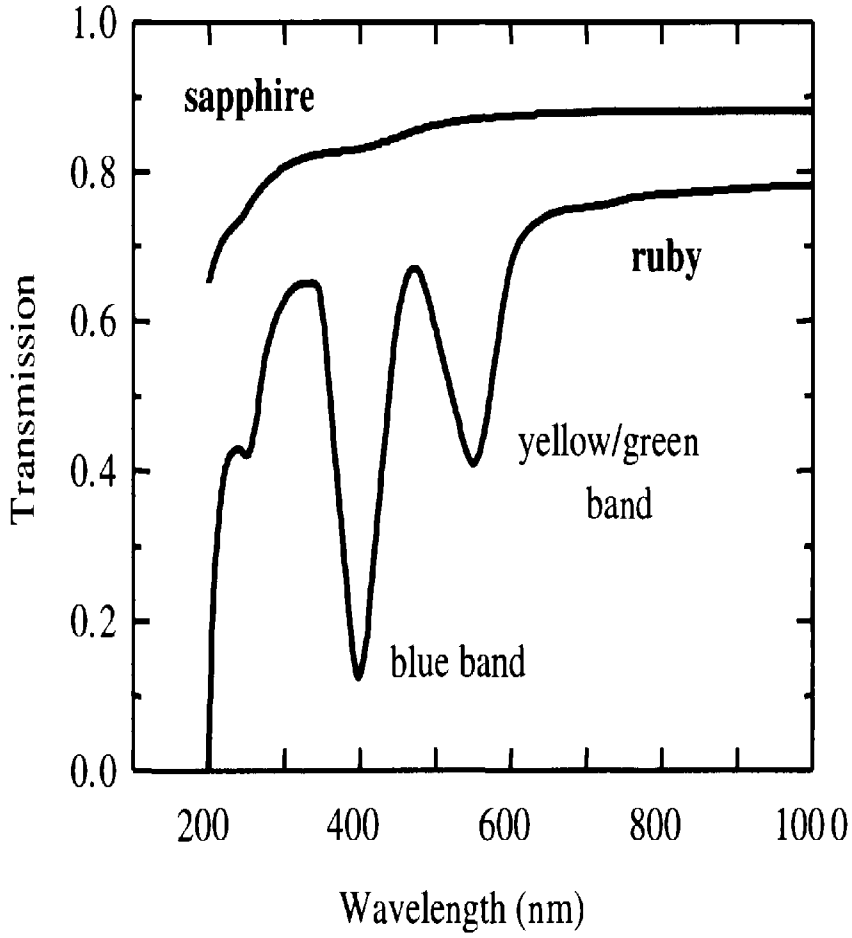

Fig. 1.7 Transmission spectrum of ruby (Al_2O_3 with 0.05 % Cr^{3+}) compared to sapphire (pure Al_2O_3). The thicknesses of the two crystals were 6.1 mm and 3.0 mm respectively. After [6], reprinted with permission.

M. Fox: Optical properties of solids, Oxford university press, 2001.

Safír, CdSe

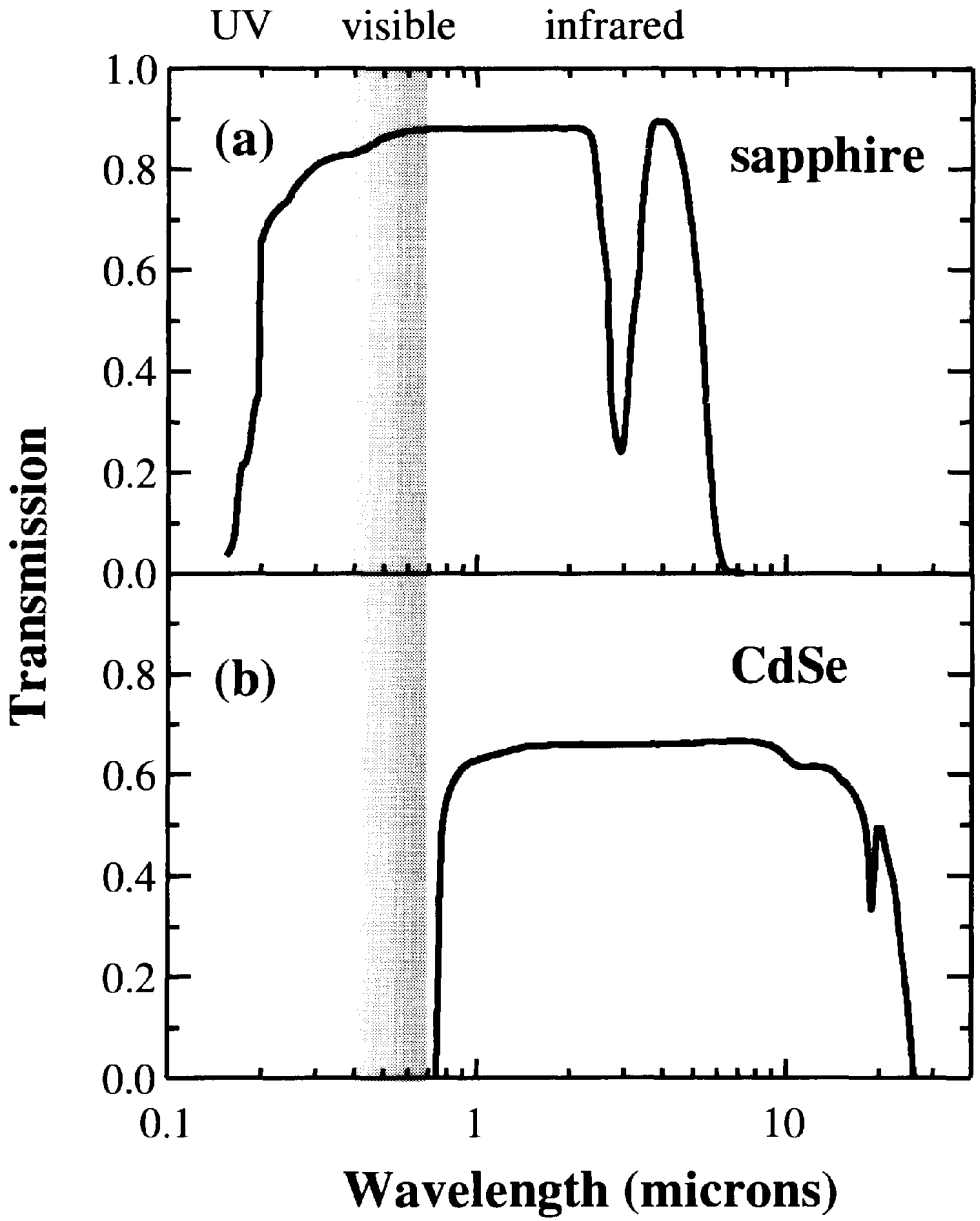

Fig. 1.4 (a) Transmission spectrum of a sapphire (Al_2O_3) crystal of thickness 3 mm. (b) Transmission spectrum of a CdSe crystal of thickness 1.67 mm. After [1].

M. Fox: Optical properties of solids, Oxford university press, 2001.

Propustné materiály

Table 1.1 Approximate transparency rang
and refractive index n of a number of crys
talline insulators. n is measured at 546 nm
Values of n are given both for the o-ray an
e-ray of birefringent materials. After [1] an
[2].

Crystal	Transparency range (μm)	n
Al_2O_3 (sapphire)	0.2–6	1.771 (o) 1.763 (e)
BaF_2	0.2–12	1.476
Diamond	0.25–> 80	2.424
KBr	0.3–30	1.564
KCl	0.21–25	1.493
KI	0.3–40	1.673
MgF_2	0.12–8	1.379 (o) 1.390 (e)
NaCl	0.21–20	1.55
NaF	0.19–15	1.326
SiO_2 (quartz)	0.2–3	1.546 (o) 1.555 (e)
TiO_2 (rutile)	0.45–5	2.652 (o) 2.958 (e)

M. Fox: Optical properties of solids, Oxford university press, 2001.

ZnS

Propustná oblast 0.4 – 12 μm

λ (μm)	n
0.4	2.5452
1	2.2917
5	2.2466
12	2.1710

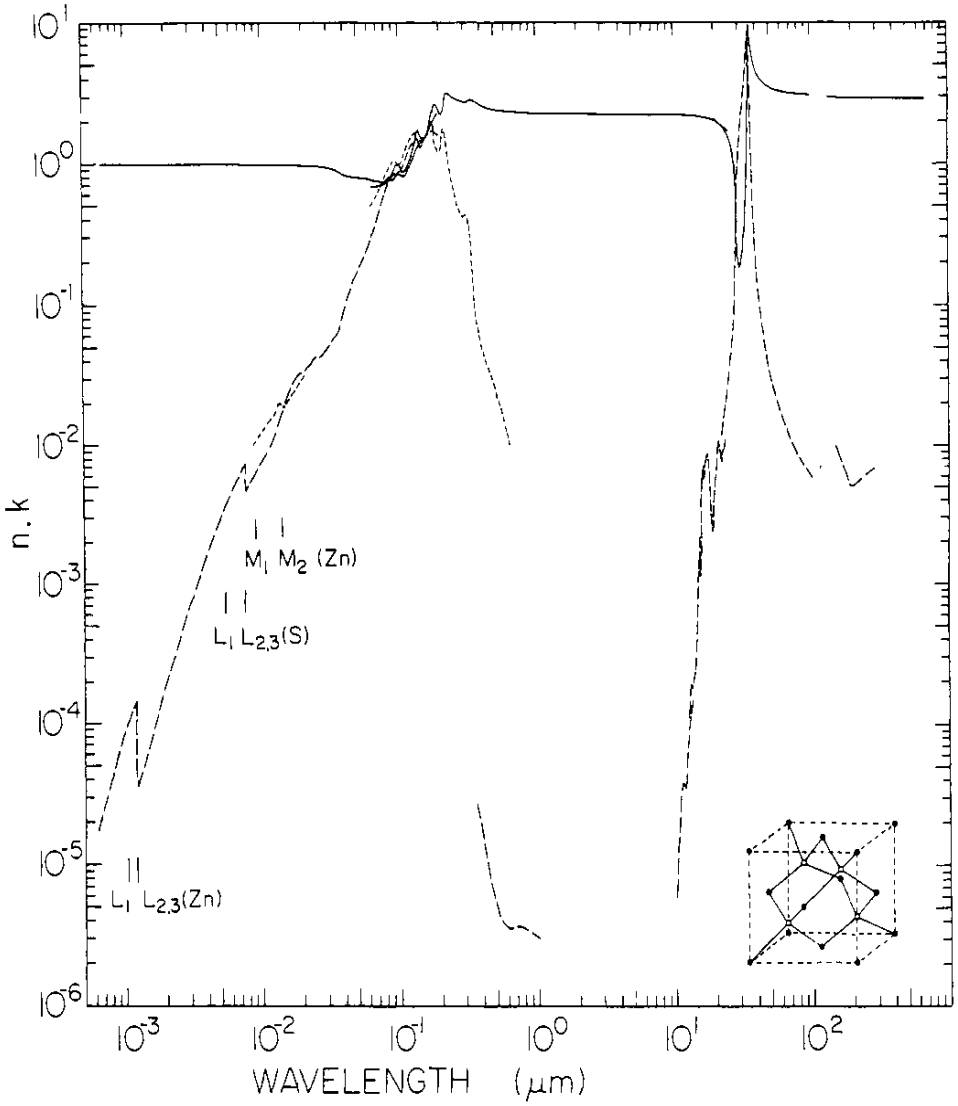

Palik, Handbook of Optical Constants of Solids, Elsevier 1998.

ZnSe

Propustná oblast 0.5 – 17 μm

λ (μm)	n
0.7	2.5568
1	2.4892
5	2.4295
12	2.3930

Halogenidy

	E_g (eV)	n	při λ (μm)
NaCl	8.97	1.3822	20
KCl	8.50	1.3947	20
KBr	7.6	1.2978	40
AgCl	3.0	1.9069	20
CsBr	7.5	1.5587	40
CsI	5.1	1.5797	60
KRS5 54% TlI_3 + 46% $TlBr_3$	2.4	2.2105	40

Halogenidy

NaCl

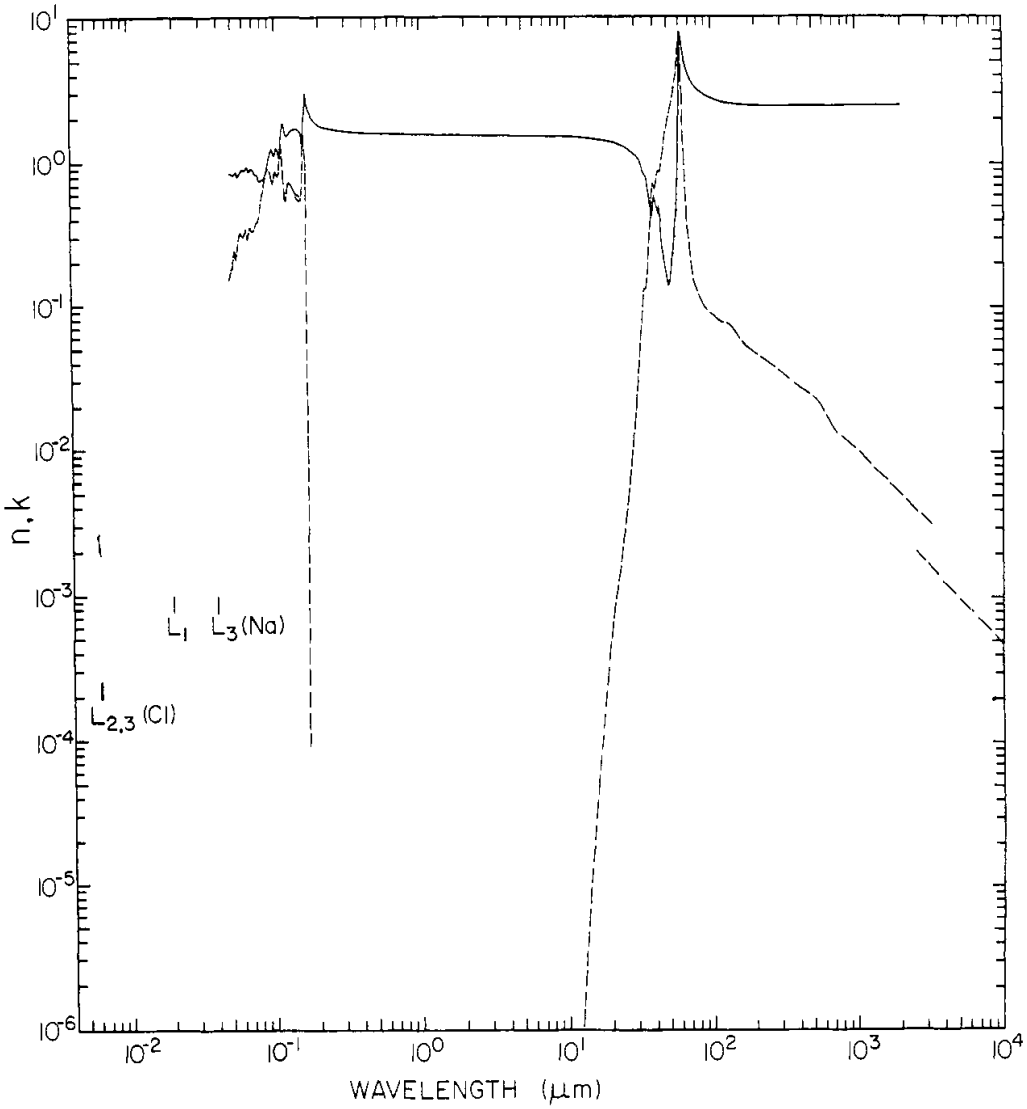

Fig. 13. Log–log plot of n (——) and k (----) versus wavelength in micrometers f sodium chloride.

LiF

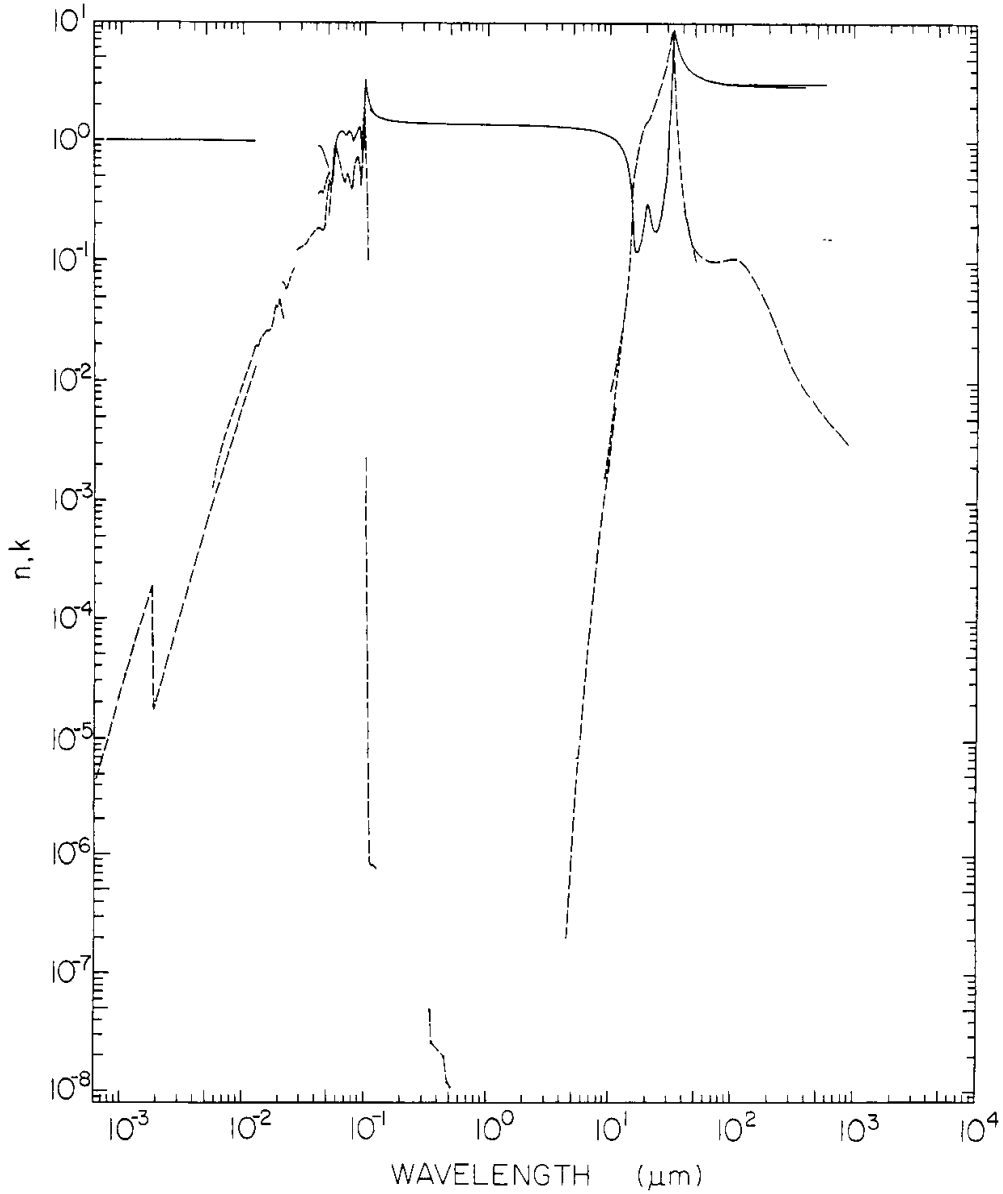

Fig. 6. Log–log plot of n (——) and k (----) versus wavelength in micrometers for lithiu fluoride. Note the incredibly small values of k in the transparent region centered near 1 μ

Palik, Handbook of Optical Constants of Solids, Elsevier 1998.

Halogenidy

	$3\nu_{LO}$ (cm^{-1})
NaCl	795
KCl	615
KBr	489
AgCl	597
CsBr	342
CsI	270

Laserové poškození

Pulsy 1.06 μm (NdYAG)

	Pt (J/cm^2)
BK7	cca 50
SF6	cca 7

10.6 μm (CO_2)

	P (MW/cm^2)
Ge	600
GaAs	100
ZnSe	800
KCl	100 – 1000

Fluoridová skla

ZBLA:
56% ZrF_4
34% BaF_2
6% LaF_3
4% AlF_3

BIZYbT:
30% Ba
30% In
20% Zn
10% Yb
10% Th

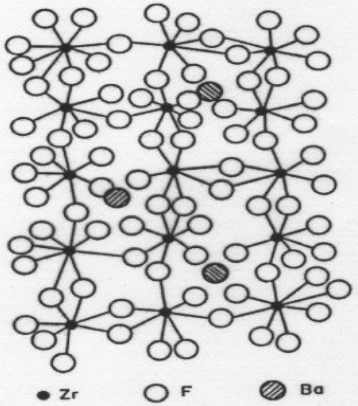

Figure 4
A structural model for fluorozirconate glass

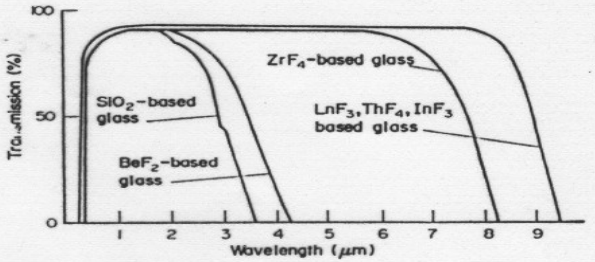

Figure 5
Optical transmission range for fluoride glasses and SiO_2 (sample thickness 4 mm)

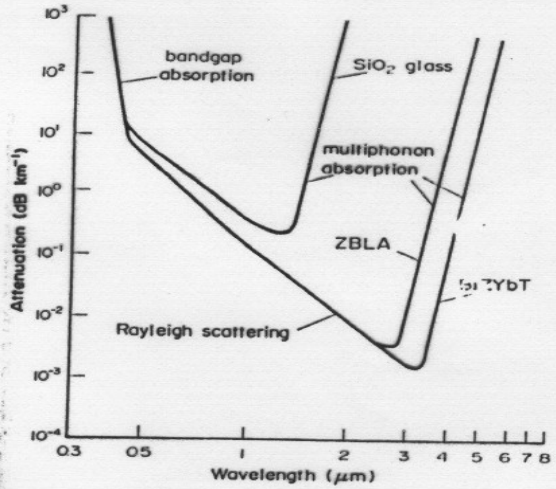

Figure 6
Ultratransparency region (very low absorption) for fluoride and SiO_2 glasses

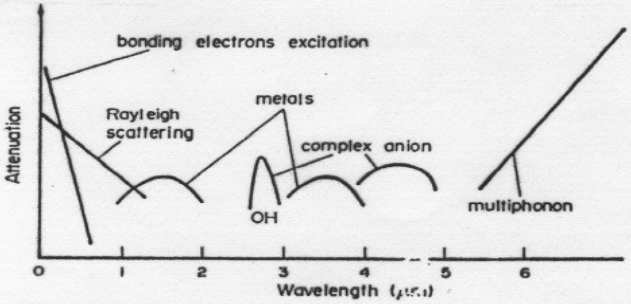

Figure 7
Extrinsic absorption mechanisms in fluoride glasses: electronic excitation of 3d electrons in Fe^{2+}, Co^{2+}, Ni^{2+},

Fluoridová skla

ZBLAN útlum na 1km

ZrF_4-BaF_2-LaF_3-AlF_3-NaF

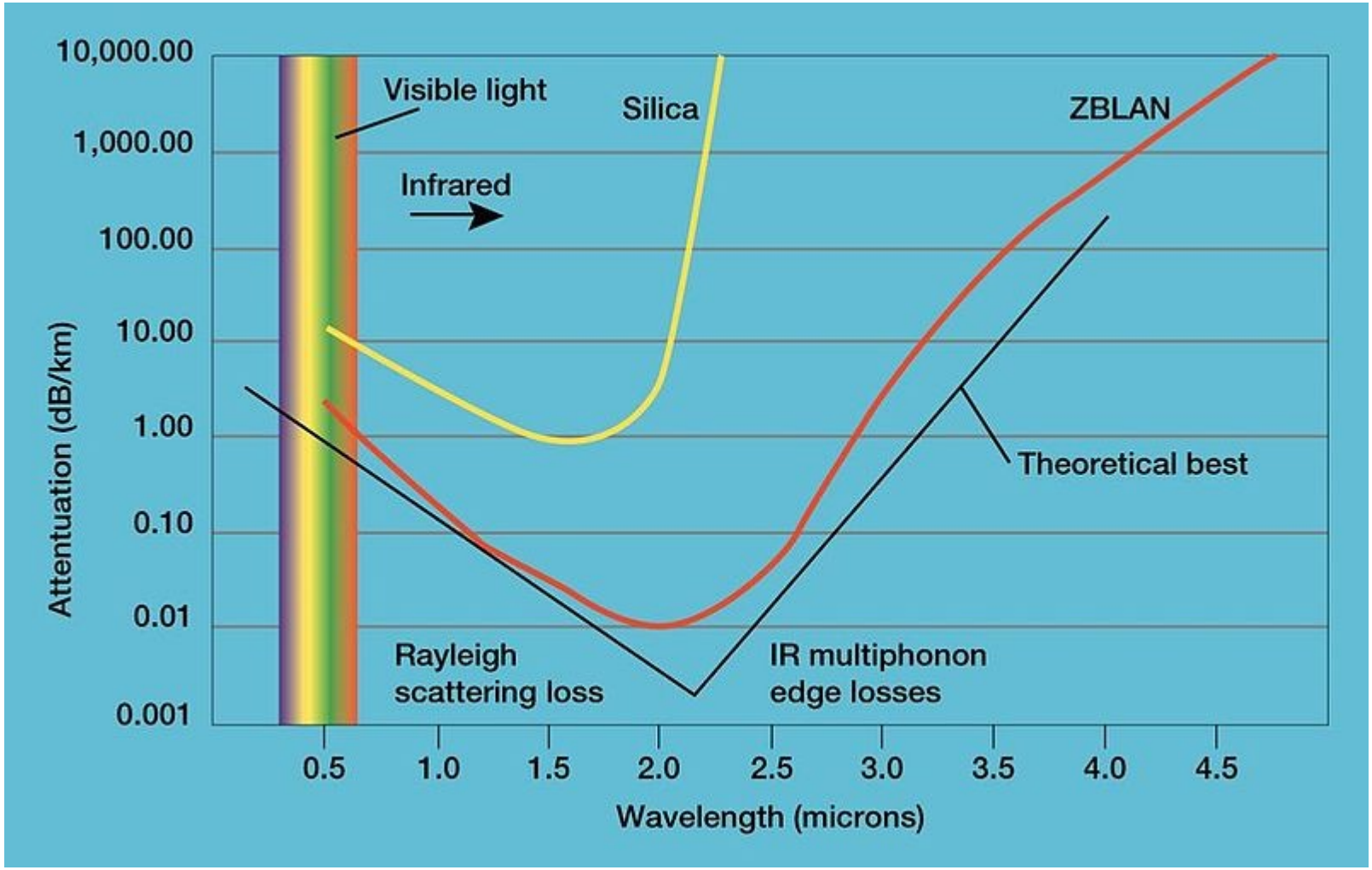

www.science.nasa.gov

Vodivé průhledné materiály

ITO – indium tin oxide

Typicky cca In_2O_3 90%, SnO_2 10%, hmotnostně

Gap cca 4eV

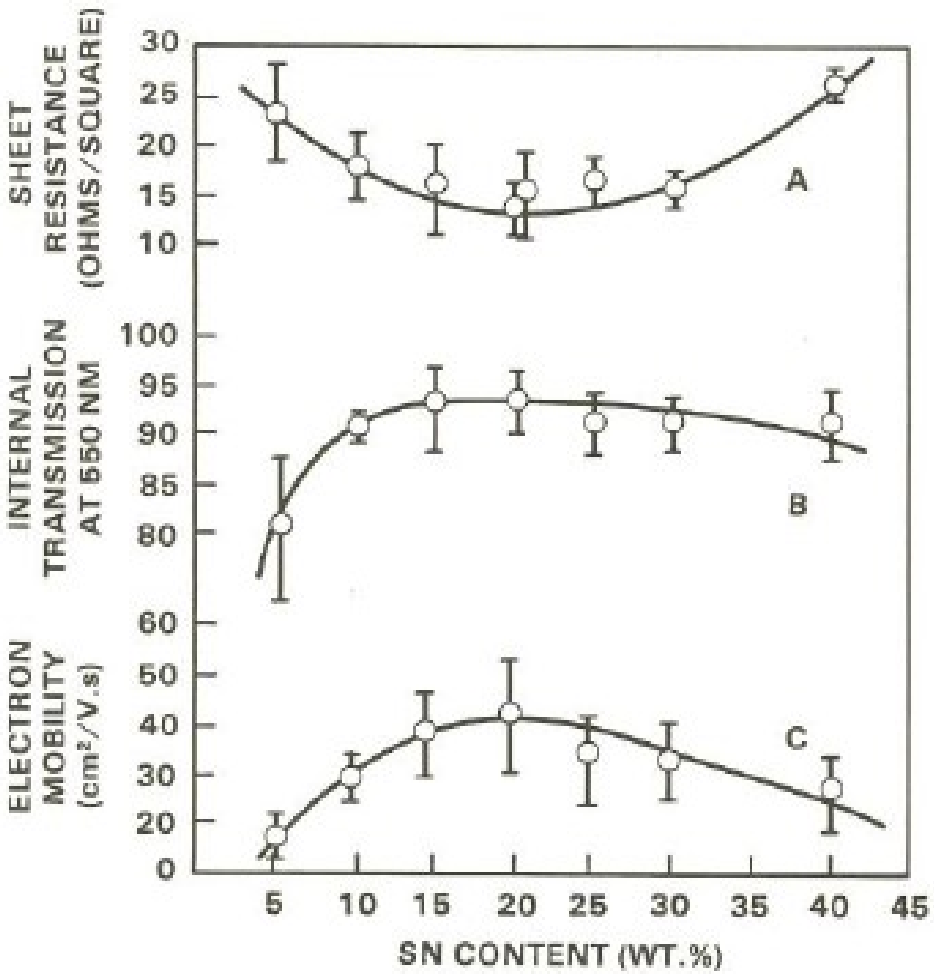

Vrstva cca 140nm
Materion.com

Další materiály:

AZO – aluminium zinc oxide
Nevýhoda nižší životnost a odolnost proti vlhkosti
ITO také může být leptáno na jemnější strukturu.

GZO (Ga), IZO (In)
Vodivé polymery

Grafen, uhlíkové nanotrubky

Použití:
Displeje, solární panely, etc.

materiál	minimální odpor μΩ.cm
ITO	114
In2O3	100
SnO2	400
ZnO	120
ZnO:Al	1300
CdSnO2	130

Propustnost vzduchu a záření černého tělesa

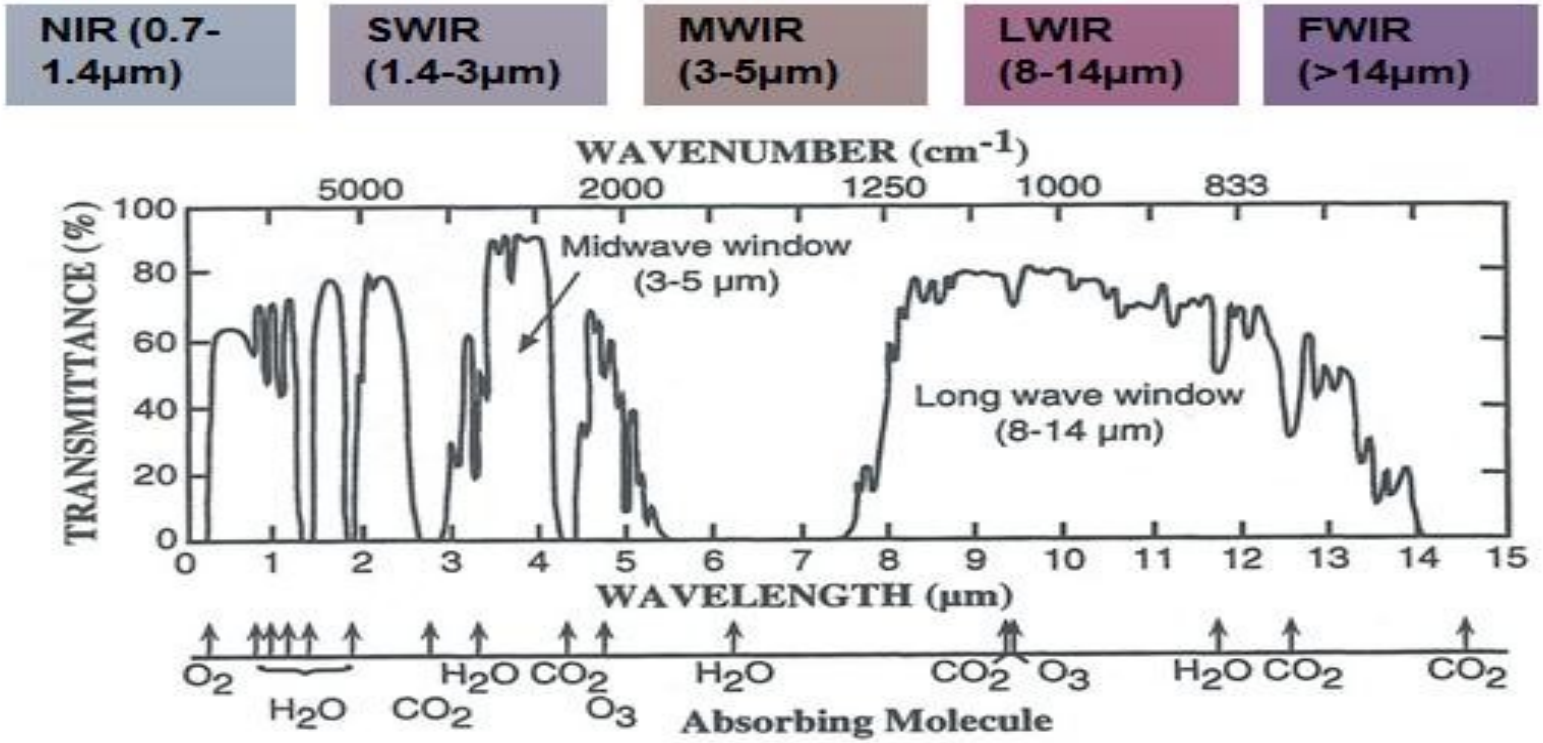

Dráha 1 km

www.schott.com

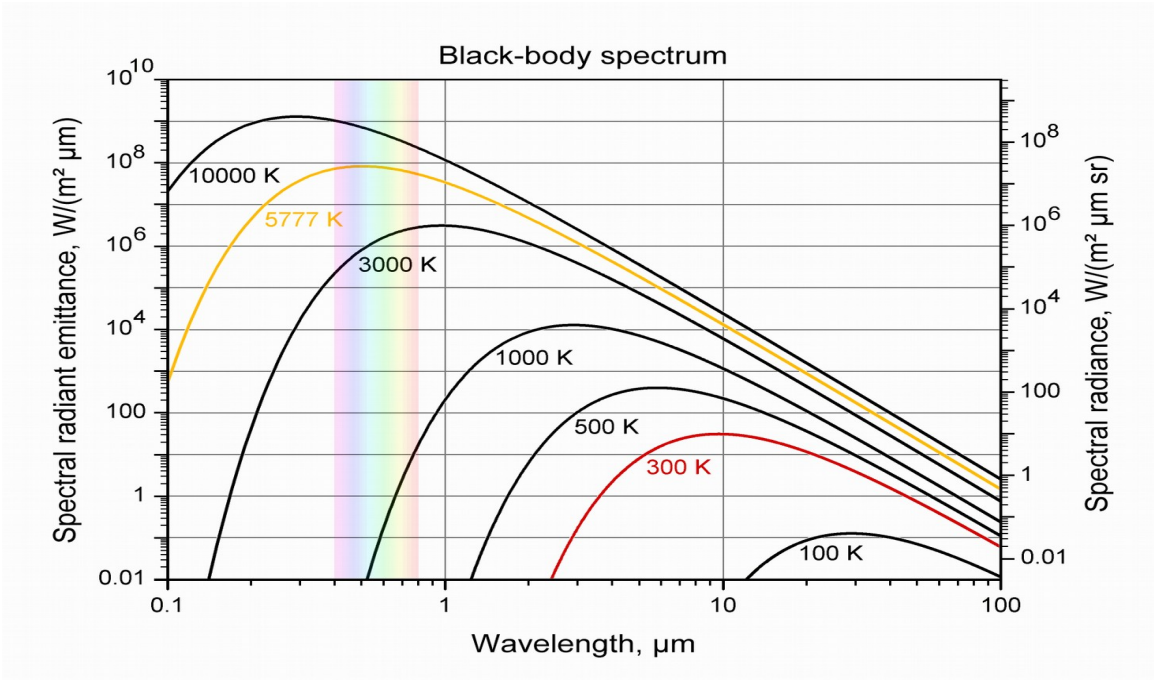

www.scienceblogs.com

Propustné oblasti a indexy lomu pro 4 μm

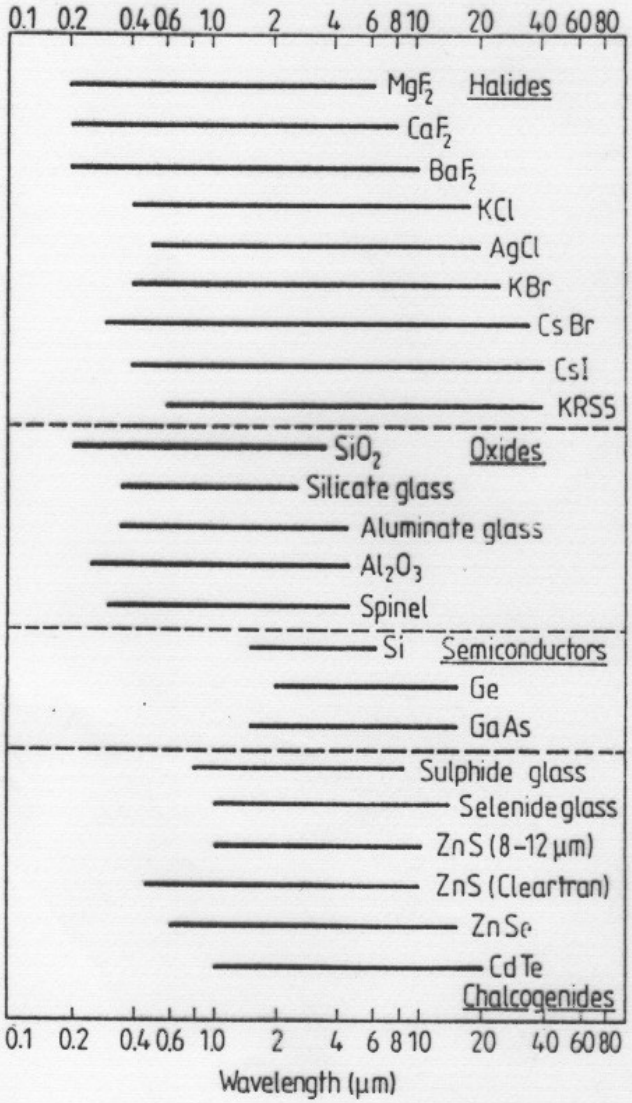

Figure 2.2 The relative transmittance ranges of some halide, oxide, semiconductor and chalcogenide materials.

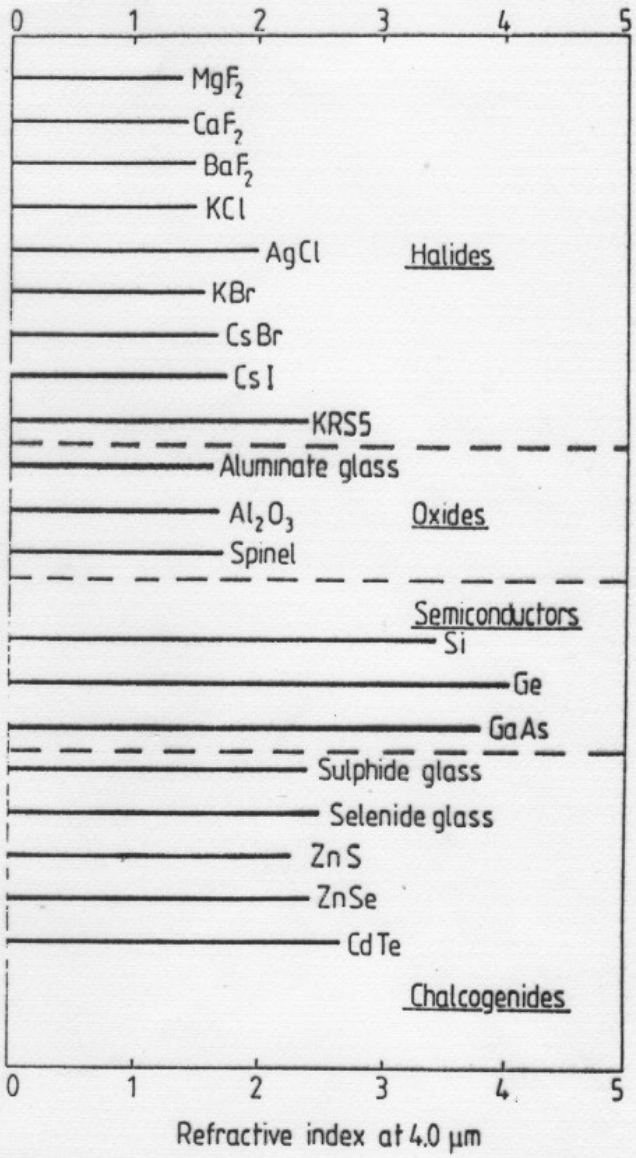

Figure 2.3 The relative refractive indices at 4.0 μm for some halide, oxide, semiconductor and chalcogenide materials.

Propustnost

Sulfidové sklo 1.9 mm
Ge 30%, S 50%, As 20%

Selenidové sklo 1.8 mm
Ge 34%, As 8%, Se 58%

Selenidové – teluridové
2.3 mm
Ge 30%, As13%, Se 27%,
Te 30%

Teluridové sklo 1.6 mm
Ge 10%, As 50%, Te 40%

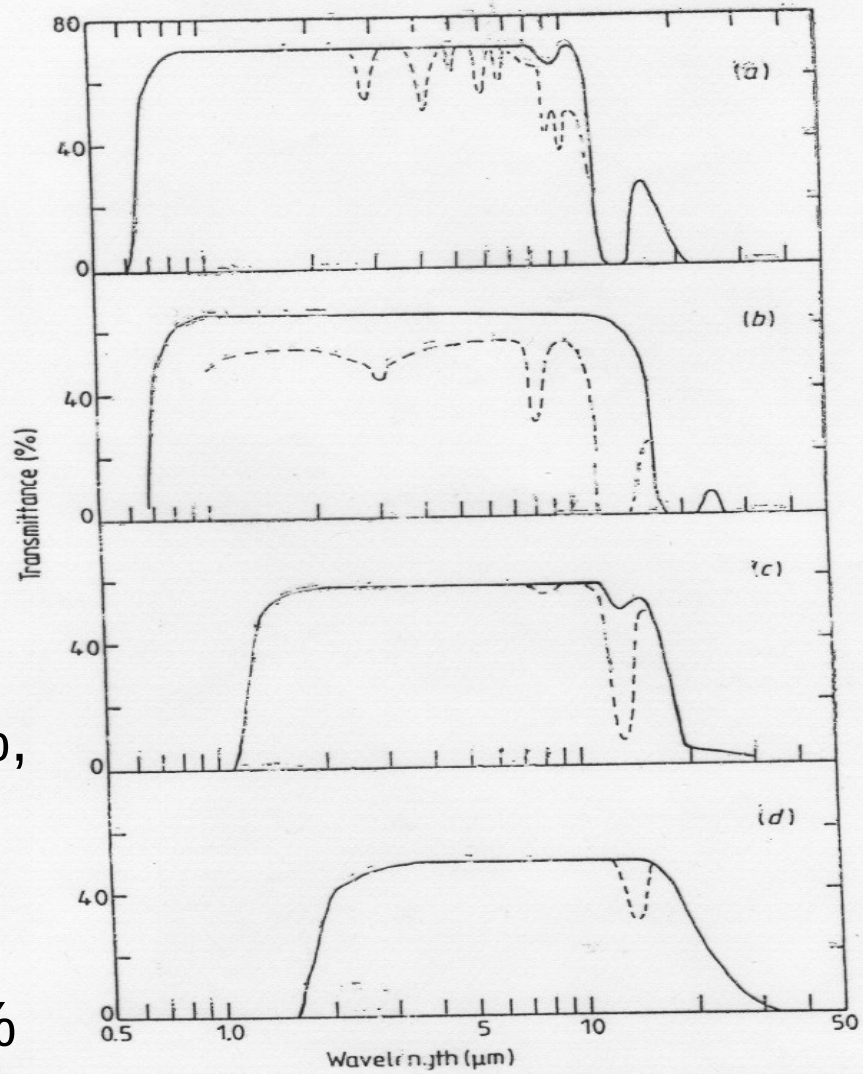

Figure 4.10 Transmittance of : (*a*) sulphide glass atomic % Ge 30, As 20, S 50, 1.9 mm thick (full curve), extrinsic impurity absorptions due to H_2O, H_2S oxide and carbon (broken curve); (*b*) selenide glass atomic % Ge 34, As 8, Se 58, 1.8 mm thick (full curve), extrinsic impurity absorptions due to oxide (broken curve); (*c*) Selenide—telluride glass atomic % Ge 30, As 13, Se 27, Te 30, 2.3 mm thick (full curve), extrinsic impurity absorptions due to oxide (broken curve); (*d*) telluride glass atomic % Ge 10, As 50, Te 40, 1.6 mm thick (full curve), extrinsic impurity absorptions due to oxide (broken curve).

Index lomu vs. disperze a propustnosti v IR

ν=(n10-1)/(n8-n12)

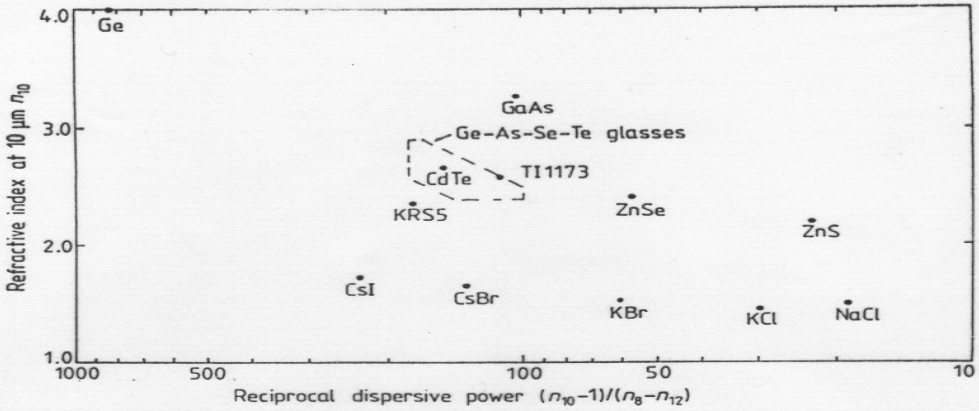

Figure 4.1 Reciprocal dispersive power $(n_{10}-1)/(n_8-n_{12})$ plotted against n_{10} at 10 μm for a number of optical materials useful in the far (8–12 μm) infrared.

Ge 3mm (A),
GaAs 3mm (B)

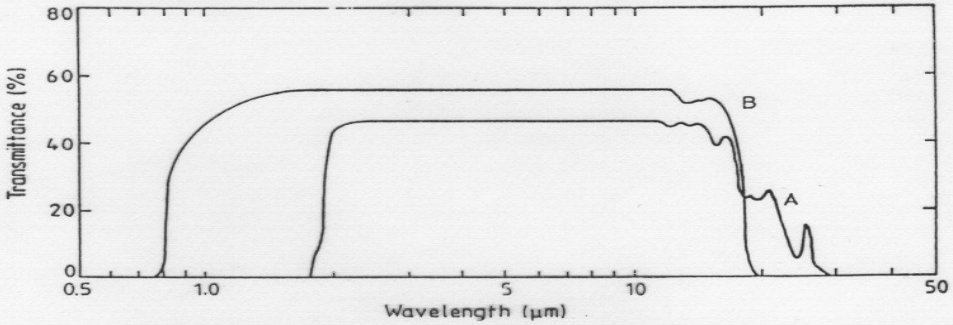

Figure 4.2 Transmittance of germanium 3 mm thick (A) and gallium arsenide 3 mm thick (B).

A) NaCl 10mm
B) Kcl 10mm
C) AgCl 1mm
D) KRS5 1mm
E) CsI 5mm

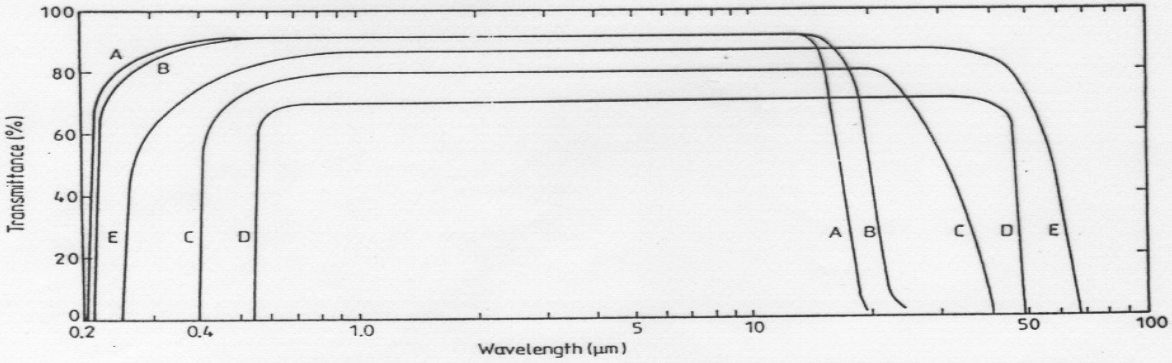

Figure 5.5 An illustration of the transmittance capability of several halides: A, NaCl 10 mm thick; B, KCl 10 mm thick; C, AgCl 1 mm thick; D, KRS5 1 mm thick; E, CsI 5 mm thick.

Tepelná roztažnost a tvrdost

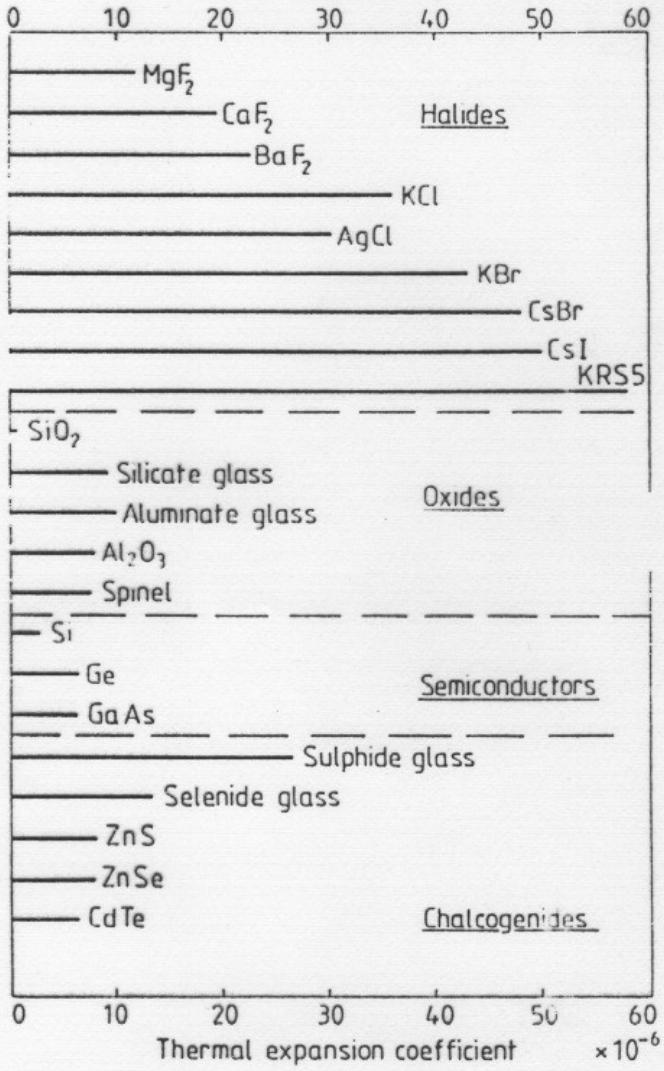

Figure 2.4 The relative thermal expansion coefficients of some halide, oxide, semiconductor and chalcogenide

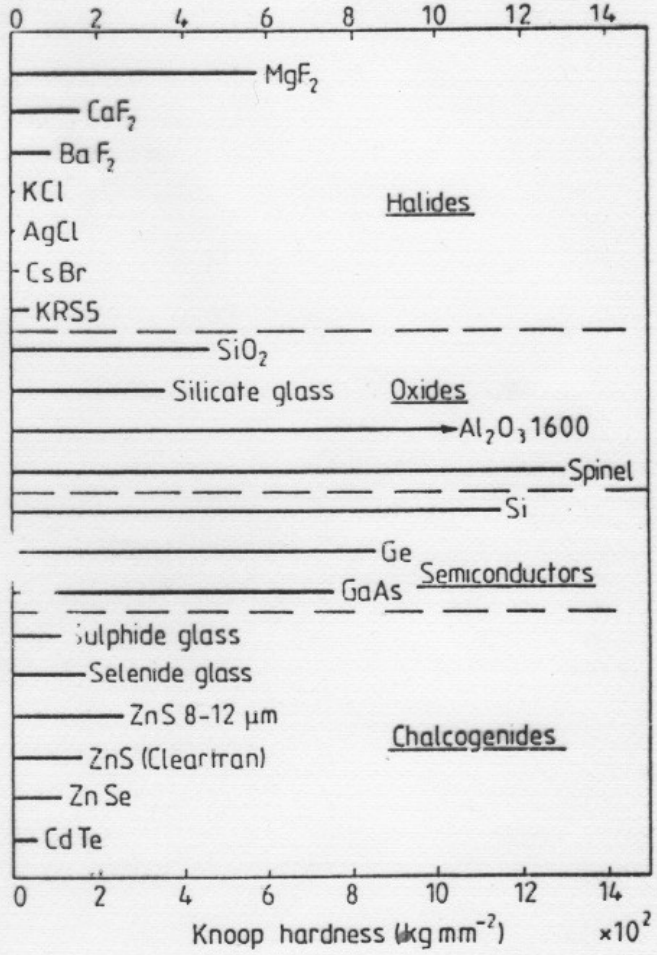

Figure 2.5 The relative hardness of some halide, oxide, semiconductor and chalcogenide materials.

Dvojlomné materiály

Table 2.1 Refractive indices of some common uniaxial crystals at 589.3 nm. After [2].

Crystal	Chemical structure	Symmetry class	type	n_o	n_e
Ice	H_2O	trigonal	positive	1.309	1.313
Quartz	SiO_2	trigonal	positive	1.544	1.553
Beryl	$Be_3Al_2(SiO_3)_6$	hexagonal	negative	1.581	1.575
Sodium nitrate	$NaNO_3$	trigonal	negative	1.584	1.336
Calcite	$CaCO_3$	trigonal	negative	1.658	1.486
Tourmaline	complex silicate	trigonal	negative	1.669	1.638
Sapphire	Al_2O_3	trigonal	negative	1.768	1.760
Zircon	$ZrSiO_4$	tetragonal	positive	1.923	1.968
Rutile	TiO_2	tetragonal	positive	2.616	2.903

M. Fox: Optical properties of solids, Oxford university press, 2001.

Rtg oblast

Dielektrická funkce (Drude):

$$\varepsilon(\omega) = 1-ne^2/[\varepsilon_0 m\omega(\omega+i/\tau)]$$

Limita vysokých frekvencí

$$\varepsilon(\omega) \simeq 1-ne^2/[\varepsilon_0 m_e\omega^2]$$

$$\varepsilon(\omega) \simeq 1-NZr_e\lambda^2/\pi < 1$$

$$r_e=e^2/[4\pi\varepsilon_0 m_e c^2]=2.8179\cdot 10^{-15}\ \mathrm{m}$$

$$n = 1-\delta+i\beta = 1-(\delta_0-i\beta_0)\rho_{rel}$$

$$\delta\simeq -NZr_e\lambda^2/\pi$$

Electron density = proton density ~ mass density

$$\delta= -N(Z+f_1)r_e\lambda^2/\pi$$

$$\beta= Nf_2r_e\lambda^2/\pi$$

Rtg oblast

$n=1-\delta+i\beta$

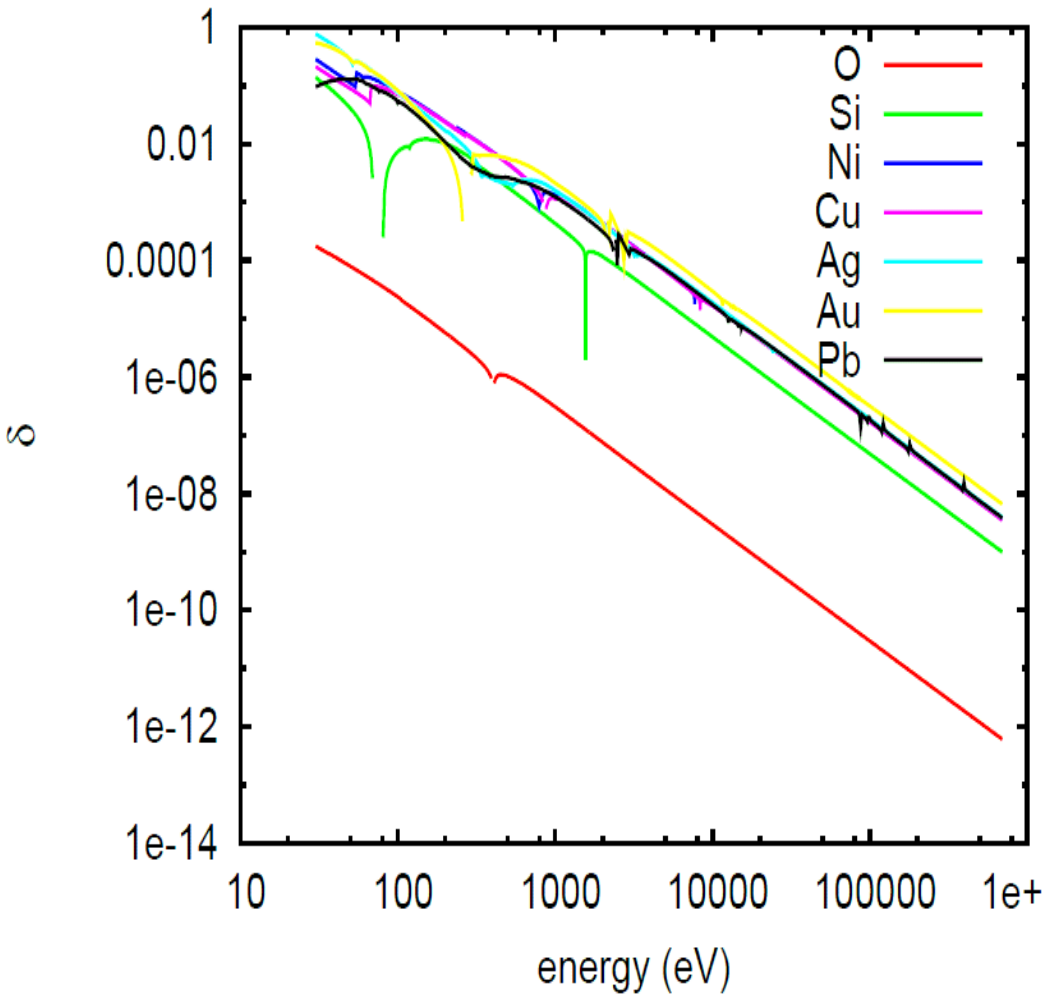

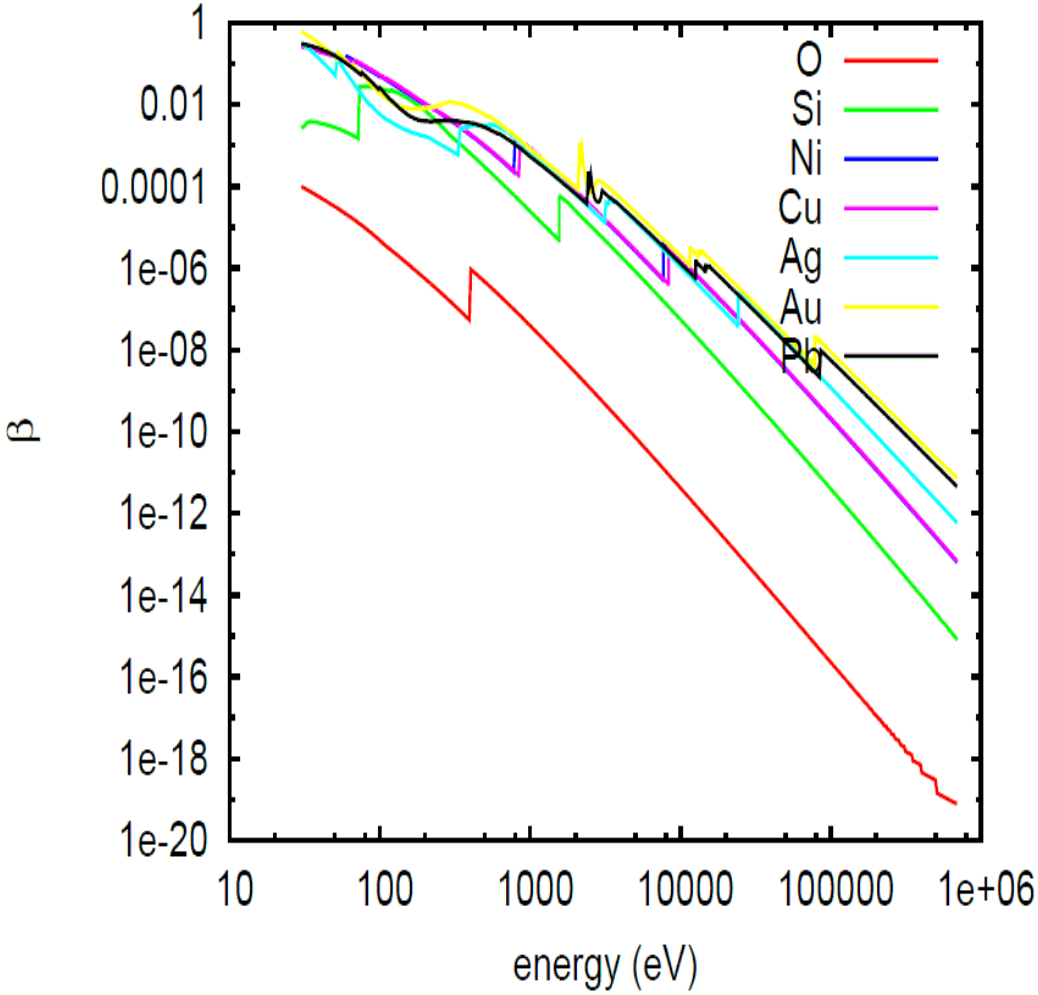

Rtg oblast

$$\varepsilon = 1 - (r_{el}\,\lambda^2/\pi)\,\Sigma\, c_j\, f_j = 1 - (r_{el}\,\lambda^2/\pi)\,\Sigma\, c_j\,(Z_j + f_{1j} - i f_{2j})$$

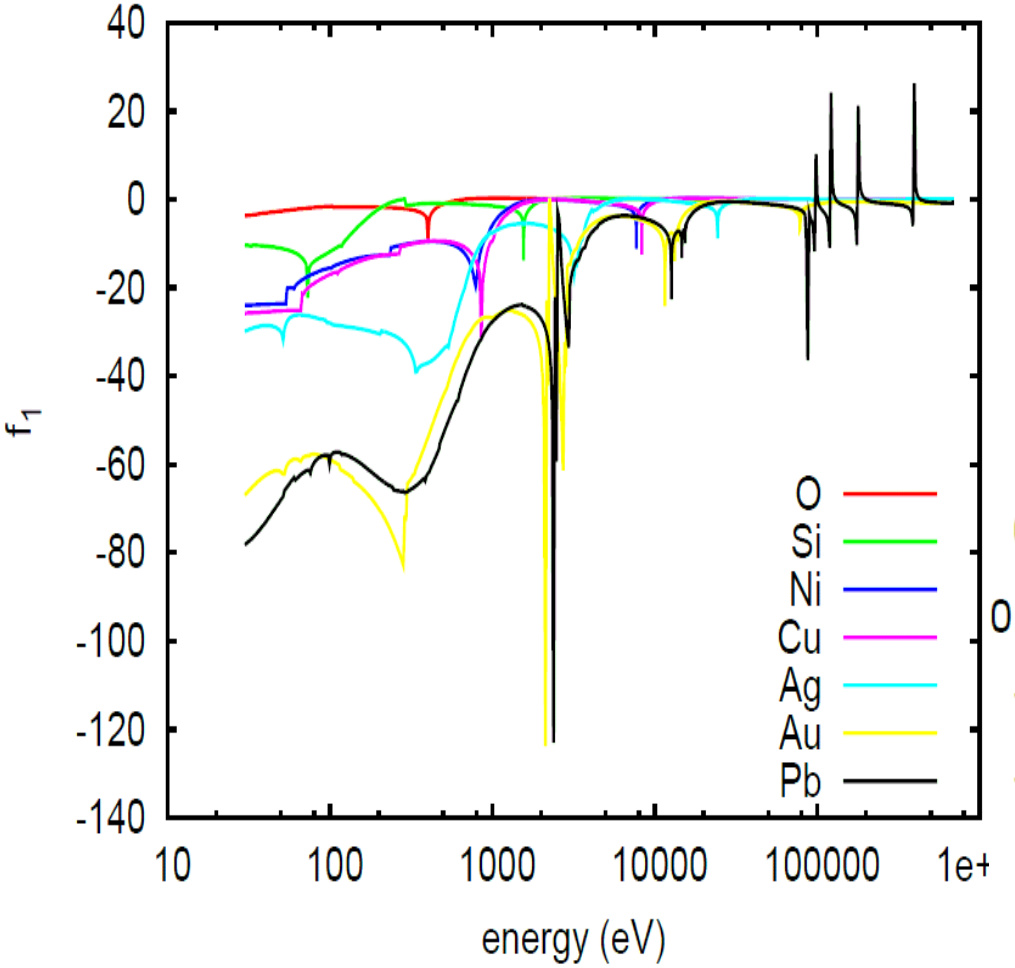

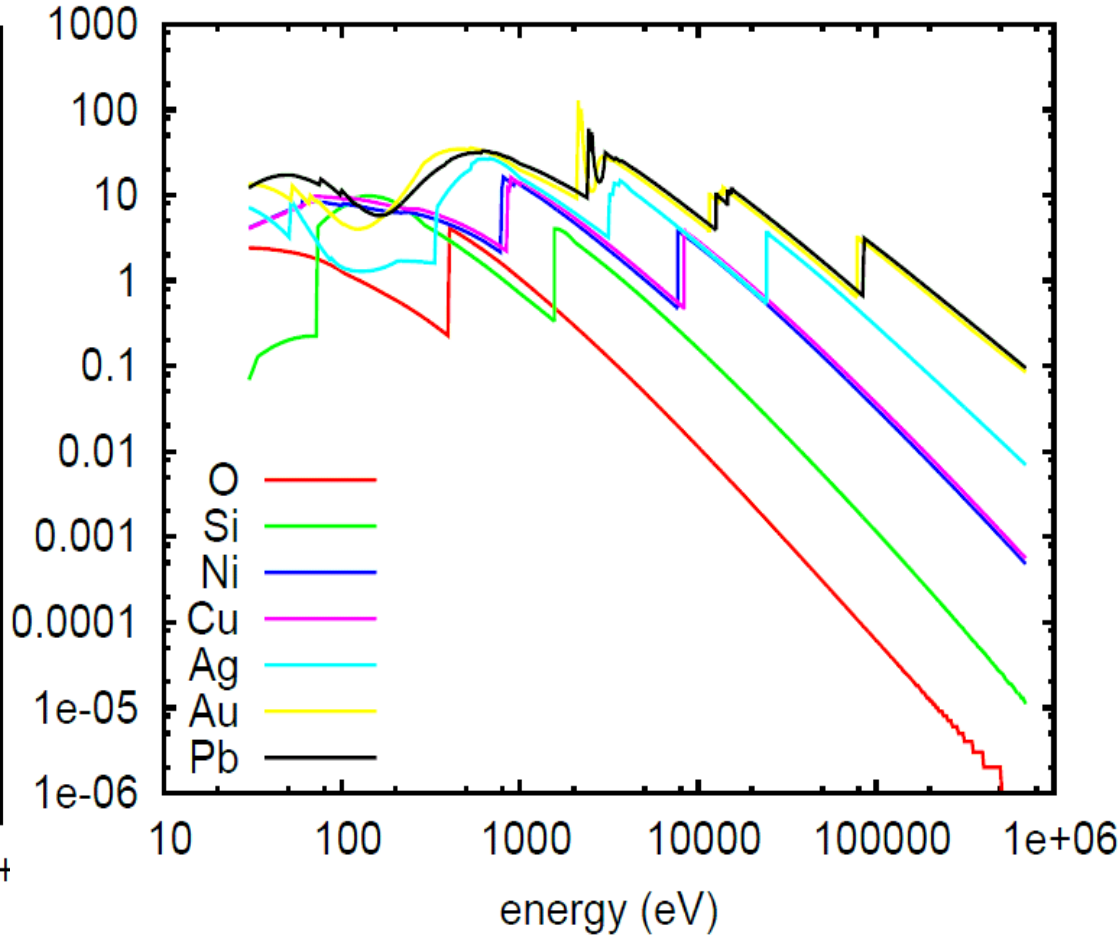

Dekrement indexu lomu $\delta(E)=1-n(E)$: závislost reálné a imaginární části na energii

Reálná část

$\delta \sim E^{-2}$

Imaginární část

$\beta \sim E^{-3}$

→ Dávka z ozáření klesá!

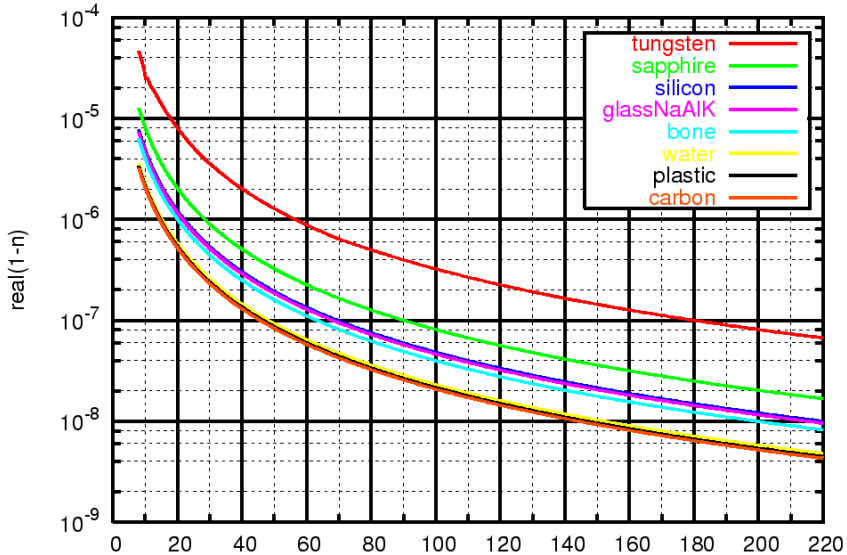

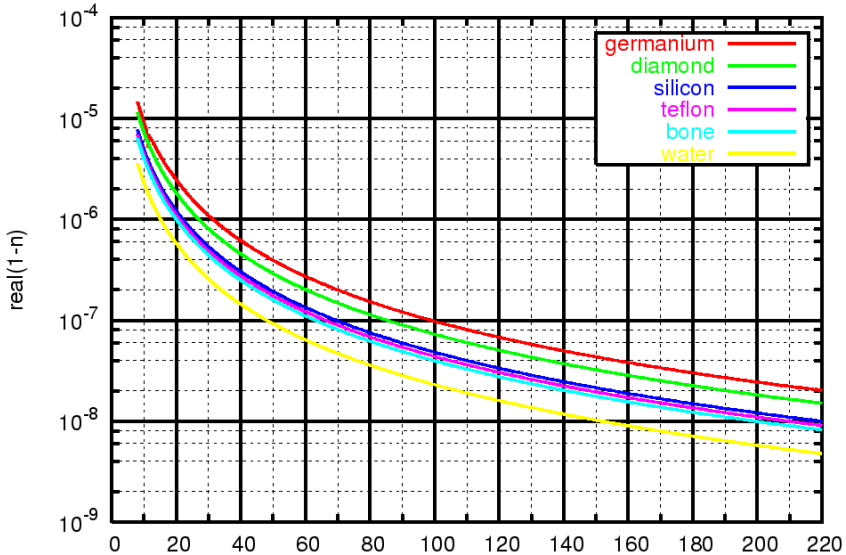

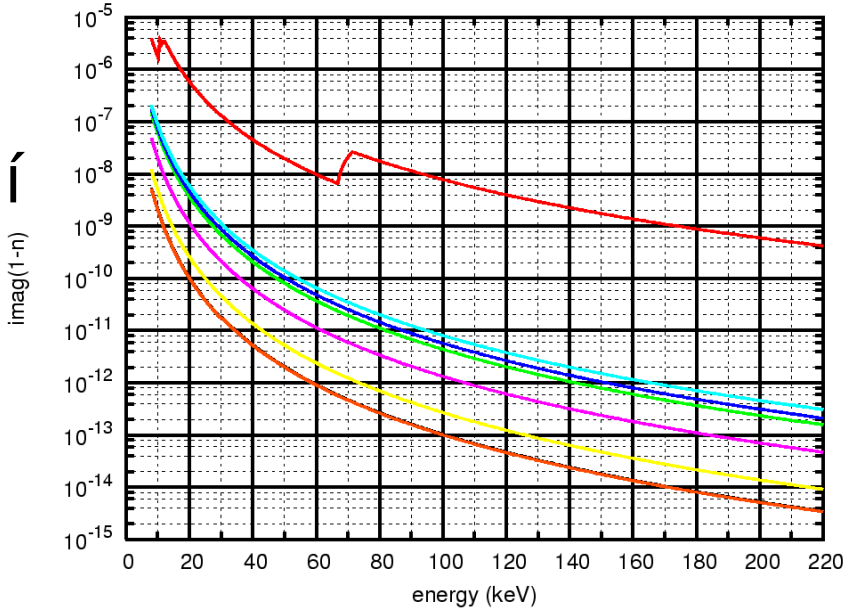

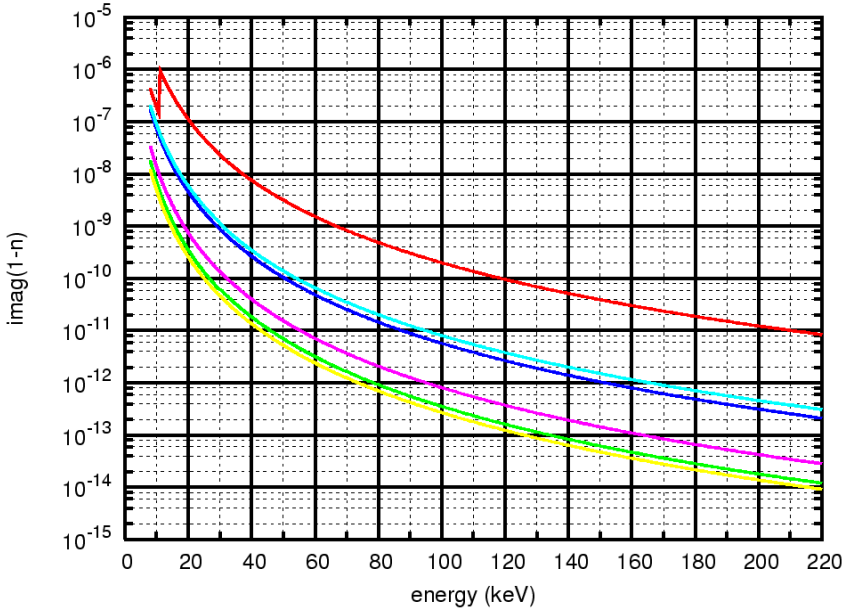

Rentgenka – laboratorní zdroj rtg záření

Lorentzův profil spektrálních čar:

$$I_R(E) = 1 / [1 + (2(E-E_0)/w)^2]$$

Cu-Kα1: 8048.06 eV = 1.54051 4.75e-4 Å rel.int. =1.0

Cu-Kα2: 8028.10 eV = 1.54433 5.20e-4 Å rel.int. = 0.497

Polohy charakteristických čar:

CoKa1=1.78896 Å

CuKa1=1.54056	CuKa2=1.54439	CuKa=1.54184	CuKb1=1.39222 Å
MoKa1=0.7093	MoKa2=0.71359	MoKa=0.711445	MoKb1=0.632288 Å
AgKa1=0.559408	AgKa2=0.563798	AgKa=0.561603	AgKb2=0.497069 Å

TaKa1=0.215947 Å

WKa1 =0.20901 Å